VILNIUS GEDIMINAS TECHNICAL UNIVERSITY

Audrius GRAINYS

MICROSECOND HIGH MAGNETIC FIELD SHAPED PULSE GENERATORS RESEARCH

DOCTORAL DISSERTATION

TECHNOLOGICAL SCIENCES,
ELECTRICAL AND ELECTRONIC ENGINEERING (01T)

Vilnius LEIDYKLA TECHNIKA 2014

Doctoral dissertation was prepared at Vilnius Gediminas Technical University in 2010–2014.

Supervisor

Prof Dr Jurij NOVICKIJ (Vilnius Gediminas Technical University, Electrical and Electronic Engineering – 01T).

The Dissertation Defense Council of Scientific Field of Electrical and Electronic Engineering of Vilnius Gediminas Technical University:

Chairman

Prof Dr Dalius NAVAKAUSKAS (Vilnius Gediminas Technical University, Electrical and Electronic Engineering – 01T).

Members:

Prof Dr Algirdas BAŠKYS (Vilnius Gediminas Technical University, Electrical and Electronic Engineering – 01T),
Dr Oliver LIEBFRIED (French-German Research Institute of Saint-Louis, Electrical and Electronic Engineering – 01T),
Prof Dr Vytautas URBANAVIČIUS (Vilnius Gediminas Technical University, Electrical and Electronic Engineering – 01T),
Prof Dr Algimantas VALINEVIČIUS (Kaunas University of Technology, Electrical and Electronic Engineering – 01T).

The dissertation will be defended at the public meeting of the Dissertation Defense Council of Electrical and Electronic Engineering in the Senate Hall of Vilnius Gediminas Technical University at 2 p. m. on 11 June 2014.

Address: Saulėtekio al. 11, LT-10223 Vilnius, Lithuania.
Tel.: +370 5 274 4956; fax +370 5 270 0112; e-mail: doktor@vgtu.lt

A notification on the intend defending of the dissertation was send on 9 May 2014.

A copy of the doctoral dissertation is available for review at the Internet website http://dspace.vgtu.lt/ and at the Library of Vilnius Gediminas Technical University (Saulėtekio al. 14, LT-10223 Vilnius, Lithuania).

VGTU leidyklos TECHNIKA 2254-M mokslo literatūros knyga

ISBN 978-609-457-684-3

audrius.grainys@vgtu.lt

VILNIAUS GEDIMINO TECHNIKOS UNIVERSITETAS

Audrius GRAINYS

MIKROSEKUNDINIŲ STIPRIŲ MAGNETINIŲ LAUKŲ FORMUOTŲ IMPULSŲ GENERATORIŲ TYRIMAS

DAKTARO DISERTACIJA

TECHNOLOGIJOS MOKSLAI,
ELEKTROS IR ELEKTRONIKOS INŽINERIJA (01T)

VGTU
LEIDYKLA
TECHNIKA
Vilnius 2014

Disertacija rengta 2010–2014 metais Vilniaus Gedimino technikos universitete.

Vadovas

prof. dr. Jurij NOVICKIJ (Vilniaus Gedimino technikos universitetas, elektros ir elektronikos inžinerija – 01T).

Vilniaus Gedimino technikos universiteto Elektros ir elektronikos inžinerijos mokslo krypties disertacijos gynimo taryba:

Pirmininkas

prof. dr. Dalius NAVAKAUSKAS (Vilniaus Gedimino technikos universitetas, elektros ir elektronikos inžinerija – 01T).

Nariai:

prof. dr. Algirdas BAŠKYS (Vilniaus Gedimino technikos universitetas, elektros ir elektronikos inžinerija – 01T),
dr. Oliver LIEBFRIED (Saint-Louiso Prancūzijos-Vokietijos tyrimų institutas, elektros ir elektronikos inžinerija – 01T),
prof. dr. Vytautas URBANAVIČIUS (Vilniaus Gedimino technikos universitetas, elektros ir elektronikos inžinerija – 01T),
prof. dr. Algimantas VALINEVIČIUS (Kauno technologijos universitetas, elektros ir elektronikos inžinerija – 01T).

Disertacija bus ginama viešame Elektros ir elektronikos mokslo krypties disertacijos gynimo tarybos posėdyje **2014 m. birželio 11 d. 14 val.** Vilniaus Gedimino technikos universiteto senato posėdžių salėje.

Adresas: Saulėtekio al. 11, LT-10223 Vilnius, Lietuva.
Tel.: (8 5) 274 4956; faksas (8 5) 270 0112; el. paštas doktor@vgtu.lt

Pranešimai apie numatomą ginti disertaciją išsiųsti 2014 m. gegužės 9 d.

Disertaciją galima peržiūrėti interneto svetainėje http://dspace.vgtu.lt/ ir Vilniaus Gedimino technikos universiteto bibliotekoje (Saulėtekio al. 14, LT-10223 Vilnius, Lietuva).

Abstract

Microsecond high magnetic field shaped pulse generators are investigated in the dissertation. High magnetic field technologies, circuit transition processes and the pulse shaping technique are analysed. Two prototypes of the high magnetic field generators are developed, one of them with asymmetric pulse shape with amplitude over 10 T, the rise time of 200 μs and decay time of 800 μs was applied for express calibration of the magnetic field sensors. Another generator generates repetitive microsecond high magnetic field square shaped pulses with amplitude up to 5 T and duration of 3–25 μs. Such generator has been applied to investigate the response of the biological objects to high-pulsed magnetic fields.

The dissertation consists of three parts including introduction, 3 chapters, conclusions and references.

The introduction reveals the investigated problem, importance of the thesis and the object of research and describes the purpose and tasks of the paper, research methodology, scientific novelty, the practical significance of results examined in the paper and defended statements. Author's publications on the subject of the dissertation and conference presentations are supplied.

Chapter 1 revises scientific articles related to the subject of the dissertation. The analysis of the magnetic field generation technology, devices used in magnetic field generators and microinductors are presented. The behaviour of the manganite and biological materials in high-pulsed magnetic fields are described. Conclusions and the tasks of dissertation are formed.

Chapter 2 describes the structure of the high magnetic field generators prototypes. High magnetic field generator, consisting from capacitor bank, crowbar circuit and SCR switch is presented. Magnetic field distribution and Joule heating in multilayer inductors are analysed. High repetitive magnetic field generator based on MOSFET switch is presented. Transient processes in generator circuits are analysed. Microinductor field distribution and Joule heating are presented. Conclusions are formed.

Chapters 3 is focused on the investigation of the magnetoresistive magnetic field sensors and the biological objects behaviour in the microsecond pulsed magnetic fields. The experimental results of the express calibration using one pulse technique of the magnetoresistive sensors and biological objects response in high magnetic fields are presented.

Research results related to the dissertation subject are published in 7 scientific articles; 5 articles – in Thomson Reuters Web of Science database journals with impact factor, 2 – in others international (IndexCopernicus and IEEE/IEE) database journals, 7 presentations on the subject have been done in the conferences at national and international level.

Reziumė

Disertacijoje nagrinėjami mikrosekundinių stiprių magnetinių laukų formuotų impulsų generatoriai. Analizuojami magnetinio lauko generatorių pereinamieji vyksmai, impulsų formavimo ir magnetinio lauko generavimo technologijos. Darbe pristatomi du mikrosekundinių stiprių magnetinių laukų formuotų impulsų generatorių prototipai. Pirmasis mikrosekundinių stiprių magnetinių laukų generatorius gali generuoti asimetrinės formos magnetinius impulsus, kurių amplitude viršija 10 T, impulso priekinis frontas siekia 200 μs, galinis frontas – 800 μs. Impulsinis stipraus magnetinio lauko generatorius naudojamas magnetorezistyvinių jutiklių kalibravimui. Antrasis pasikartojančių stačiakampės formos nuo 3 μs iki 25 μs trukmės mikrosekundinių magnetinių laukų iki 5 T generatorius yra panaudotas biologinių ląstelių savybių tyrimuose.

Pirmajame skyriuje pateikta stiprių megnetinių laukų generavimo technologijų apžvalga. Aprašyta induktorių, naudojamų stiprių magnetinių laukų generavimui analizė, mikrosekundinio stipraus magnetinio lauko įtaka manganitinėms ir biologinėms medžiagoms. Skyriaus pabaigoje suformuluoti disertacijos uždaviniai.

Antrajame skyriuje aprašyti mikrosekundinių stiprių magnetinių laukų formuotų impulsų generatorių prototipai, jų struktūra ir pagrindiniai parametrai. Pateikti magnetinio lauko generatorių kompiuteriniai modeliai, mikrosekundinės trukmės magnetinių impulsų generatorių pereinamųjų vyksmų tyrimai. Aprašyti daugiasluoksniai induktoriai magnetorezistyvinių magnetinio lauko jutiklių kalibravimo tyrimams atlikti. Pateikti magnetinio lauko pasiskirstymo ir įšilimo tyrimo rezultatai. Pateikta mikroinduktorių su integruota kiuvete sandara, magnetinio lauko pasiskirstymo skaičiavimo rezultatai.

Trečiajame skyriuje pateikti magnetorezistyvinių jutiklių kalibravimo metodika ir eksperimentiniai rezultatai. Aprašyta biologinių objektų tyrimų metodika stipriame mikrosekundiniame magnetiniame lauke ir pateikti eksperimentiniai rezultatai.

Disertacijos tema paskelbti 7 straipsniai: 5 – Thomson Reuters Web of Science duomenų bazės moksliniuose žurnaluose su citavimo indeksu, 2 – kituose recenzuojamose žurnaluose. Disertacijos tema perskaityti 7 pranešimai Lietuvos bei tarptautinėse konferencijose.

Notations

Symbols

A	–	magnetic vector potential;
A_m	–	mean radius of the solenoid;
B	–	magnetic flux density;
C	–	capacitance;
C_{ISS}	–	input capacitance of the metal-oxide semiconductor field-effect transistor;
C_m	–	specific membrane capacitance;
C_{OSS}	–	output capacitance of the metal-oxide semiconductor field-effect transistor;
C_{RSS}	–	reverse transfer capacitance of the metal-oxide semiconductor field-effect transistor;
C_T	–	heat capacitance;
D	–	diameter;
dl	–	differential length;
ds	–	differential surface;
D_W	–	wire diameter;
E	–	first order elliptic integral;
E_e	–	electric field;
F	–	frequency;
f_r	–	pulse repetition rate;

H – magnetic field strength;
I – current;
K – second order elliptic integral;
L – inductance;
L_i – length;
m – number of layers;
n – number of turns;
r – radius of the solenoid;
R – resistance;
r_1 – inner radius of the solenoid;
r_2 – outer radius of the solenoid;
r_{cell} – radius of the cell;
T – temperature;
t – time;
t_r – rise time;
U – voltage;
U_c – capacitor voltage;
V_{coil} – inductor effective volume;
δ_a – distance between centres of two layers;
Δt – pulse width;
$\Delta\Psi_m$ – transmembrane potential;
ε_e – permittivity;
μ – magnetic permeability;
μ_0 – magnetic constant;
σ_c – specific conductivity of the cell;
σ_e – electrical conductivity of the material;
σ_m – maximum allowable mechanical stress;
σ_s – specific conductivity of the extracellular medium;
τ_p – polarization time;
φ – angle of the applied electric field;
Φ – magnetic flux.

Abbreviations

ADC – analog to digital converter;
CFU – relative culture forming unit;
CFU_c – relative culture forming unit of the controle;
CFU_t – relative culture forming unit after treatment;

CPPS – capacitive storage pulse power systems;
DC – direct current;
EMI – electromagnetic interference;
FCG – flux compression generator;
FEM – finite element analysis;
FTMC – center for physical sciences and technology;
GTO – gate turn-off thyristor;
HV – high voltage;
IGBT – insulated-gate bipolar transistor;
JFET – junction gate field-effect transistor;
MACD – majority carrier devices;
MFASG – magnetic field asymmetric shaped pulse generator;
MICD – minority carrier devices;
MOSFET – metal-oxide semiconductor field-effect transistor;
PPS – pulsed power systems;
SCR – silicon-controlled rectifier.

Contents

[1]The annexes are supplied in the enclosed compact disc

Introduction

The Investigated Problem

In last few decades the interest in high magnetic field application in science, medicine and military technologies increased dramatically. The investigations of the various semiconductor materials or biological objects in magnetic fields become very relevant in these days. Usually the magnetic fields with amplitudes over 10 T are required. The magnetic field facilities over the world can generate magnetic fields with amplitude up to 100 T. Such facilities are unique and very expensive they require high-energy network and cryogenic cooling. The magnet operates only stationary and the incorporation of the new facilities become problematic. Therefore, compact high magnetic field facilities able for transportation and flexible integration into the new infrastructure are welcome. In most cases the compact shaped pulse high magnetic field systems can replace the complex, expensive and sizable magnetic field generators if the actual volume of the experimentation is limited up to 1 cm^3. Pulse energy capacitor banks, semiconductor switches and microinductors can be used for such applications. High magnetic field shaped pulse generation is novel for electrical engineering and applied sciences. Varying pulse shape new properties can be tuned. Nevertheless the development of the shaped pulse high magnetic field generators is complex interdisciplinary task, which has to deal with the solution

of the high magnetic field distributions, field homogeneity evaluation, transient processes in the circuit and Joule heating effects and mechanical overloads in pulsed inductors. High magnetic fields are powerful experimental tool for novel material investigations. Last decade magnetoresistive B–scalar sensors are invented and applied for high power applications. Magnetoresistive sensors are sensitive to technological conditions, material structure and temperature. High magnetic field shaped pulses can be applied for express calibration. In other hand biotechnology has become potential area for high magnetic field applications. Contactless technology allows to avoid contamination of the investigated biological objects. The impact of the magnetic fields to biological objects strongly depends on pulse shape, amplitude and repetition frequency. New experimental methodology should be developed and investigated.

Importance of the Thesis

The generation of high magnetic fields requires a lot of energy, expensive cooling devices. High magnetic field shaped pulse generation is complex and interdisciplinary task. Due to this fact the experiments can be carried out only in one place because the transportation of these devices is not available and incorporation in to the other already equipped infrastructure is not possible. The volume of such systems increases dramatically increasing required magnetic field. Therefore the development of the compact high magnetic field shaped pulse generators very important for the interdisciplinary collaboration and new material and technologies investigations.

Magnetoresistive sensors are sensitive to technological conditions, material structure and temperature. Due to high temperature sensitivity sensors should be calibrated by one pulse with different rise and decay times. Therefore the development of the microsecond shaped pulse magnetic field generator with asymmetric pulses can be powerful investigation tool for the calibration of the magnetoresistive sensors.

High magnetic pulse technology allows contactless treatment and the contamination of the investigated biological objects can be avoided. The impact of the magnetic fields to biological objects strongly depends on pulse shape, amplitude and repetition frequency. The development of the microsecond shaped pulse magnetic field generator for contactless investigation of biological objects is obligatory. The generator, which can generate repetitive square shaped pulse magnetic field up to 5 T can be incorporated to sterile biotechnological or biomedical infrastructure and new experimental results of the biological objects in high pulsed magnetic fields can be carried out.

The Object of Research

Microsecond high magnetic field shaped pulse generators for the calibration of the magnetoresistive sensors and biological object treatment in high magnetic fields.

The Goal of the Thesis

The goal of the scientific work is the development and the research of the microsecond high magnetic field shaped pulse generators applicable to express calibration test of magnetoresistive sensors and the investigation of the biological objects in high magnetic fields.

The Tasks of the Thesis

The following tasks have to be solved to achieve the aim of the work:

1. To develop the prototypes of the microsecond high magnetic field shaped pulse generators and to investigate transient processes in the generators circuits.
2. To develop multilayer and planar microinductors and to investigate magnetic field distribution and Joule heating.
3. To investigate the express calibration of the magnetoresistive sensors using 10 T microsecond asymmetric shaped pulse magnetic field generator.
4. To investigate biological objects in pulsed magnetic fields using microsecond 5 T high magnetic field repetitive square shaped pulse generator.

Research Methodology

The analytical, numerical and experimental methods were applied in this work. The numerical methods were applied to investigate transient processes of the microsecond shaped pulse magnetic field generator using PSPICE program package, using COMSOL program package the analysis of the inductors heating and generated magnetic fields using finite element method were done. All verification of developed systems was carried out with experimental methods.

Importance of Scientific Novelty

The scientific novelty of research is demonstrated by the following results:

1. Developed compact high microsecond magnetic field asymmetric shaped pulse generator generates pulses with amplitude over 10 T and the rise time of 200 μs and the decay time of 800 μs is applicable of express calibration test of the magnetoresistive magnetic field sensors. The calibration methodology is single pulse, which allows to avoid Joule heating influence on sensor parameters.
2. Developed pulsed inductor enables to generate magnetic fields above 10 T with less then 1% inhomogeneity of the magnetic field in the volume of 50 mm^3, which is acceptable for the express calibration with total error of ±10% of the magnetic field magnetoresistive sensors.
3. Developed high microsecond shaped pulse magnetic field generator with controlled magnetic field amplitude up to 5 T is applicable for contactless investigation of the biological objects in high-pulsed magnetic fields. The controllable pulse width from 3 μs to 25 μs and pulse repetition rate from 1 Hz to 35 Hz allows the wide range experiment possibility.
4. Developed microinductor with integrated cuvette ensure the contactless investigation of the biological objects avoiding the contamination problems. The behaviour of the biological objects in pulse magnetic field strongly depends on treatment intensity.

Practical Significance of Achieved Results

The developed millisecond pulse magnetic field generator consisting from SCR switch and crowbar circuit allows to generate asymmetrical pulses with amplitude of 10 T is acceptable for the express calibration of the magnetoresistive magnetic field sensors in pulsed magnetic field. The generator was successfully applied for manganite sensor calibrations in the project "Magnetic sensor development for electric power systems" Nr. 31V–149 funded by Lithuanian Agency for Science, Innovation and Technology (MITA).

The developed microsecond high magnetic field square shaped pulse generator with MOSFET switch is carried out fully controlled output parameters such as pulse width, amplitude and pulse repetition time is applicable for wide range contactless investigation of the reversible and irreversible behaviour of the biological object in pulsed magnetic field. Developed generator is applied in

interdisciplinary experiments with pathogenic fungi in Nature Research Centre Vilnius, Lithuania.

The Defended Statements

1. The pulsed magnetic field facility consisting of capacitor bank, SCR thyristor switch and multilayer inductor connected in parallel with crowbar circuit is capable to generate asymmetric magnetic field pulses over 10 T with axial field inhomogeneity less than 1%, which is acceptable for calibration of magnetic field magnetoresistive sensors
2. Magnetoresistive sensors calibration by application of asymmetric pulses of rise time of 200 μs, decay time of 800 μs and amplitude of 10 T allow the express calibration of magnetoresistive sensors with error of 10% by one pulse registration avoiding sensor overheating.
3. The pulsed magnetic field facilities consisting of capacitor bank, MOSFET switch and microinductor with integrated cuvette generates repetitive up to 35 Hz and up to 5 T amplitude square shaped pulses and insure contactless biotechnological experimentation.
4. Depending on repetition rate microsecond 3–25 μs in duration and amplitude of 5 T pulsed magnetic field pulses are capable to initiate reversible and irreversible changes of biological object structure.

Approval of the Results

Research results are published in 7 scientific articles; 5 articles – in Thomson Reuters Web of Science database journals with impact factor, 2 – in others international (IndexCopernicus and IEEE/IEE) databases journals, 7 presentations on the subject have been done in the conferences at national and international level:

- International scientific conference *"Electronics 2011"*. 2011. Kaunas, Lithuania;
- Scientific conference *"Science – future of Lithuania: electronics and electrical engineering*". 2011. Vilnius, Lithuania;
- International conference *"MIKON – 2012"*. 2012. Warsaw, Poland.
- Scientific conference *"Science – future of Lithuania: electronics and electrical engineering*". 2012. Vilnius, Lithuania;

- 9th International Conference on Measurement, "*Measurement 2013"*. Smolenice castle, Slovakia;
- Scientific conference *"Science – future of Lithuania: electronics and electrical engineering"*. 2013. Vilnius, Lithuania;
- 2nd international scientific conference on Thermal Analysis and Calorimetry *"CEEC-TAC2"*. 2013. Vilnius, Lithuania.

Dissertation Structure

The thesis is comprised of an introduction, three chapters, general conclusions, references, a list of the author's publications on the subject of the thesis and a summary in Lithuanian. The volume of the thesis – 111 pages; the text of the thesis contains 28 formulas, 52 figures, 8 tables and 97 references.

Acknowledgements

I would like to thank my supervisor Prof Dr Jurij Novickij, I had not started and finished a PhD without his education, encouragement and support during these years.

I would like to thank all my colleagues Dr Sonata Tolvaišienė and Vitalij Novickij from the Institute of High Magnetic Fields of Vilnius Gediminas technical university for their constant support and encouragement.

Also I would like to thank Prof Habil Dr Saulius Balevičius, Prof Dr Nerija Žurauskienė, Dr Voitech Stankevič and Prof Dr Vygaudas Kvedaras for the education and valuable discussions.

I like to thank Dr Volker Zorngiebel, Dr Lothar Gernandt and Dr Caroline Gauthier-Blumand from the French-German Research Institute of Saint-Louis for the valuable discussion and the possibility to make the internship in French-German Research Institute of Saint-Louis.

Especially I would like to thank my family and my fiancée Lina for understanding, support and encouragement during these years.

1

Review of High Power Pulsed Magnetic Field Generation

The chapter revises scientific articles related to the subject of the dissertation. The analysis of the magnetic field generation technology, devices used in magnetic field generators and inductors presented. The behaviour of the magnetoresistive and biological materials in high-pulsed magnetic fields are described.

1.1. High Pulsed Magnetic Field Generation

In last few decades the interest in high magnetic field application in science, medicine and military technologies increased dramatically (Committee to Assess the Current Status and Future Direction of High Magnetic Field Science in the United States 2013; Herlach 2006; Idehara 2006; Levy 2002; Paul 2006). The required magnetic field amplitudes in such areas often exceed the amplitudes of 10 T (Akiyama 2007; Herlach, Miura 2001; Narsetti 2005). The high magnetic field generation technologies has been highly improved during few years as the interest of application of the magnetic fields with amplitudes over 10 T increased. The progress of the magnetic field generation mostly depends on the development of the new semiconductor switches or material properties as well

as the non-destructive inductors, which are needed to create high magnetic fields (Buttram 2002; Peng 2006). Nevertheless still the main role acts the engineers that overcome technological problems to create more stable, reliable, safe and economically useful magnetic field generation systems.

The technology challenges can thus be grouped into advancing specific aspects of magnet materials properties, and by applying engineering design innovations and manufacturing process. All magnets must simultaneously satisfy a number of competing electrical, structural, thermal and economic issues (Devaux 2012; Witte 2006). High magnetic field generation systems can be categorized in three main categories: using resistive, superconductive or hybrid inductors for generation high magnetic fields (Herlach 1985; Herlach, Miura 2001). Also these three categories must be divided in two main groups: steady state magnetic field or pulse magnetic field generation systems. These two groups mainly depend on used energy source (Ribeiro 2001).

All of these inductors can be used for generating steady and pulsed magnetic fields. Though the generation of the steady state magnetic field and its application is very attractive in many application areas, nevertheless the generation of these fields is expensive and highly complex (Campbell 1996; Miller 1994). The main difficulty of creation static and quasi-static magnetic fields is Joule heating and the energy consumptions (Ding 2012; Liu, Herlach 2011; Novickij 2004; Peng 2006; Praeg 1970; Schillig 1994; Vanacken, Li, Liu 2006). Which appears due to high current flow in the inductor. For the systems that can generate homogeneous magnetic fields over 10 T the highly complex cooling system are required (Bae 2014). Due to this fact the volume of the whole system increases dramatically. The main advantage of pulsed magnetic field generators is that long term stored energy is discharged through the inductor thus the energy is compressed in time and space, which in comparison with static magnetic field generation technology gives huge economical advantage (Novickij 2004). One of the pulsed magnetic field generation benefits are relatively small costs of the inductor cooling system as in some experiments if ultra fast magnetic fields are generated the use of the expensive cooling systems is not necessary (Committee to Assess the Current Status and Future Direction of High Magnetic Field Science in the United States 2013). Upon unloading a large amount of energy in a very short time from few microseconds to several tens of seconds, thermal transition process is adiabatic, thus the heat inertia in the inductive load fails to heat up. Necessary energy required to generate high-pulsed magnetic fields can be stored in capacitors, inductors and even in chemical energy tanks, which is one more benefit of the pulse power technology (Novickij, Kačianauskas 2004). Also the volume of the whole pulsed magnetic field generation system, compared to steady state magnets is one of the main

benefits. As it can be easily transported, which provides more flexibility for application in certain fields.

To produce magnetic fields with amplitudes over 10 T tens of kA must be applied into the inductive load. Depending on the pulse shape, pulse width and amplitude the powerful spark gap, thyratron, insulated–gate bipolar transistor (IGBT), metal–oxide semiconductor field effect transistor (MOSFET), silicon-controlled rectifier (SCR) thyristors are used as a switch in pulsed power system (PPS) circuits (Castagno 2006; Goussev 2012; Podlesak 2005; Zorngiebel 2011; Zorngiebel, Spahn 2008; Welleman 2003). For some application where magnetic field amplitudes up to 1000 T are required, even the explosives can be used to generate pulsed magnetic fields (Altgilbers 2010). The Figure 1.1 shows the fundamental working principle of all pulsed power technologies. As it is represented in the Figure 1.1 the main idea is to compress low power long lasting input energy into high power short lasting output pulse. The basic diagram representing fundamental working principal of pulsed power technologies can be seen in Figure 1.1.

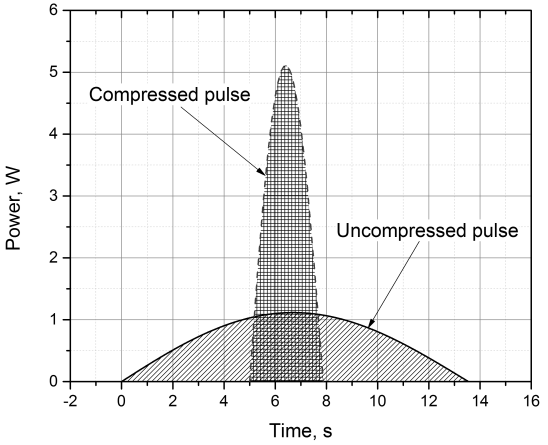

Fig. 1.1. Working principle of pulsed power technology

The typical pulsed power system can be seen on Figure 1.2 consists from these main parts. The pulsed inductor, as a load. Power supply, which transforms input voltage into required high DC voltage. Energy storage device depending on application area and output characteristics can be capacitance, inductance and in some cases explosives or rotation energy storage devices known as flywheel. One of the most important parts of pulsed power system is a switch. Which can be spark gaps, reed switches, relays or solid-state switches depending on required output characteristics and pulse repetition rate.

Pulsed power systems (PPS) based on energy storage device technology can be divided into main two categories which are capacitive storage pulsed power systems and inductive storage systems. (Mitra 2012; Shirong 2013; Bluhm 2006) The inductive storage pulse power systems can store up to 30 times more energy density but compared to capacitive storage PPS the topology requires highly complex opening switches, which compared with relatively simpler closing switches are extremely expensive moreover high power current sources are required (Bluhm 2006).

Capacitive storage pulsed power systems (CPPS) are one of the simplest and as a rule most often used in PPS where high currents are required. In the simplest design as shown in Figure 1.2 the system consists from high voltage (HV) DC power supply, charging resistor R1, capacitor C1 as an energy storage device, MOSFET semiconductor switch and inductive load L1. The energy stored in the high voltage capacitor banks is discharged through the inductive load by closing the semiconductor switch.

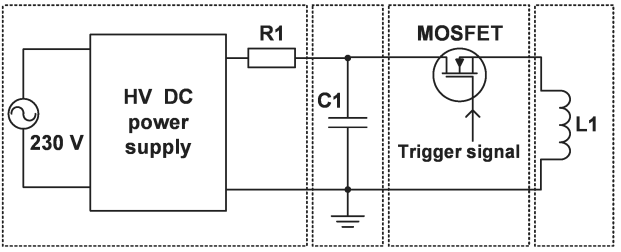

Fig. 1.2. Basic schematics of the capacitive storage pulsed power system

The Table 1.1 presents the capacitor-driven non-destructive magnets in the main high magnetic field laboratories working with high magnetic field generation (Aubert 2006).

Table 1.1. Highest magnetic fields generated with capacitor-driven non-destructive magnets (Han 208)

Facility	Generated field, T
NHMFL (Los Almos, USA)	50–70
Tuluse	30–80
Dresden	94
Nicholas Kurti Magnetic Field Laboratory	50–60
VMC (Vilnius, Lithuania)	40

Where magnetic fields with amplitude up to 1000 T are required are so called magnetic flux compressor generator can be used (FCG) (Bluhm 2006). The magnetic flux compression generator is an explosive driven device that transforms chemical energy stored in the explosives into electromagnetic energy. As a result of the huge energy which can be stored in explosives and capability to generate ultra strong pulsed magnetic fields, the flux compressor generators can be used in wide application areas, especially where weight and area of the whole pulsed power system are limited. The principal diagram and working principal of the magnetic flux compression generator is shown on Figure 1.3.

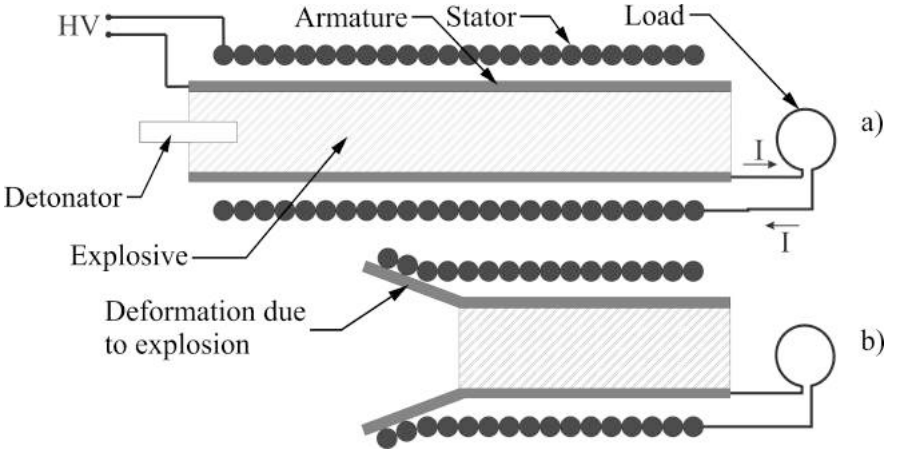

Fig. 1.3. Working principle of spiral magnetic flux compressor:
a) before detonation and b) after detonation

As it can be seen the spiral magnetic flux compressor consist of the spiral inductor called stator, and the armature with loaded explosives. The generator is connected to the primary HV source, which creates initial magnetic flux in the load. In fact, the FCG generator uses explosives as a secondary power supply to compress initial long lasting and small amplitude magnetic field density in time. When explosives are detonated the expanded armature is moving with explosive detonation velocity. The explosion is timed so the initial current amplitude I_0 in the load will be maximal. The primary HV source is safely disconnected from the generator (Fowler 2003; Neuber 2004). The stator – is not moving part of the generator. Stator and inductive load have initial inductance inductive load is $L_{T(0)}$. After the explosion the expanded armature keeps moving with explosive velocity by making contact with spiral winded stator wires. In such way the generator inductance total initial inductance from $L_{T(0)}$ to total final inductance

$L_{T(\tau)}$. The initial magnetic field energy E_0 and total final current I_T with total final energy $E_{(\tau)}$ can be expressed by Equation (1.1) – (1.3) (Fowler 2003):

$$E_0 = \frac{1}{2} L_{T0} I_0^2, \tag{1.1}$$

$$I_T = I_0 \left[\frac{L_{T0}}{L_{T(\tau)}} \right]^{1-R_\tau/L_0}, \tag{1.2}$$

$$E_{(\tau)} = E_0 \frac{L}{L+L_s} \left[\frac{L_{T0}}{L_{T(\tau)}} \right]^{1-2R_\tau/L_0}, \tag{1.3}$$

where I_0 – initial current, I_T – total final current, $L_{T(0)}$ – total initial inductance, $L_{T(\tau)}$ – total final inductance, E_0 – initial magnetic field energy and $E_{(\tau)}$ – final magnetic field energy.

The main advantages of such pulsed magnetic field generator are extremely small size compared to generated ultra strong magnetic field pulses, which can exceed 1000 T (Herlach, Knoepfel 1965). Nevertheless the main disadvantage of such pulsed magnetic field generation method is the dangerous working area for operators as well as for expensive measurement devices. The application of the FCG systems requires special training of the operators and working area specially designed for such applications. In addition, the expensive inductors and investigation objects are destroyed after the pulse. Which requires a lot of time and resources to prepare for each experiment.

1.2. Switches Used in Pulsed Power Generation Systems

From the first look the switch is the simplest element of the pulsed magnetic field generator, as it only closes the circuit and the current flowing in it depends only on the electric components connected in series. But there is no ideal switch as it was described. For each pulsed power application the certain switch with different parameters must be carefully selected to ensure the required characteristics of the generated pulse. Selecting the most appropriate device for a given application is not an easy task because it requires knowledge about the device characteristics, their unique features, innovation, and engineering design experience. High power pulse switches, such as thyratrons, ignitrons, and spark gaps have been used for pulsed power generators (Yun 2012; Sanders 2004; Winands 2005). Recently, various semiconductor switches, which can handle

high voltage and high current, are researched and developed for pulse power applications and they are expected to replace conventional discharge switches due to the fact that the semiconductors have advantages of long lifetime, high reliability, high switching frequency capability and small size. (Ramezani 1997; Ramezani, Spahn 1994; Sanders 2004; Welleman 1999; Zhang 2011).

Semiconductor devices have made dramatic progress in power handling over the last decade. Today's technology and production capabilities make it possible to produce devices with high blocking voltage combined with very high current handling (Das 2011; Hartmann 2013, Lopez 2012; Molloy 2011). Depending on the design and the device structure, also very high current rise rates in the range of up to several tenths of kA/μs are possible. Especially for single pulse or medium pulse repetition rates semiconductor devices are getting more and more competitive in comparison to conventional technologies like thyratrons, ignitrons, spark-gaps and mechanical switches. The main advantages are the reliability, lifetime, and almost no maintenance of the semiconductor switches. The type of semiconductor used and the rating of the device are extremely important for a reliable operation and need an in-depth know-how of the application and the switching device (Baliga 2008).

The classification of the semiconductor switches can be done in three different ways. The switches can be classified by the number of terminals, by the type of charge caries they use and by the control factor. In the first classification, the switches can be divided into two groups depending on number of the terminals. The Figure 1.4 presents block diagram of classification of the semiconductor devices used in pulsed power electronics.

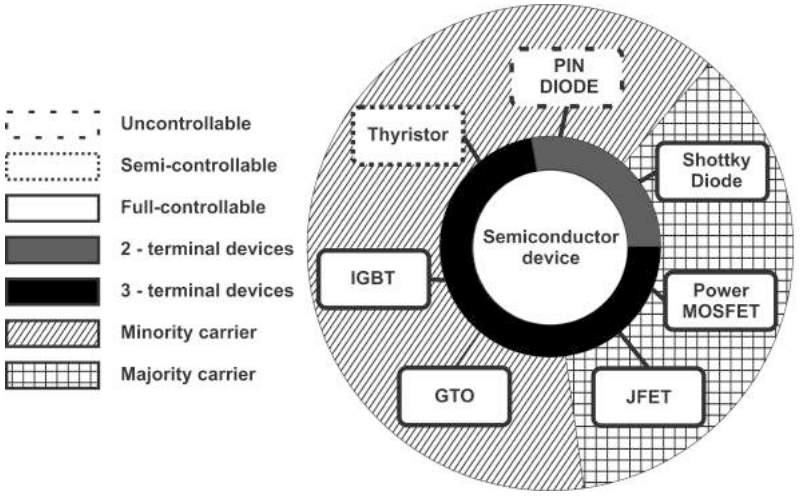

Fig. 1.4. Classification of semiconductor switches

The state of the two terminal devices such as diodes and Shottky diodes depends only on the power circuit were they are connected. The three terminal devices acts different, their state depends not only on external power circuit they are connected to, but also on the external driving signal which must be applied to their driving terminals: gate or base. By second classification switches also can be divided in to groups: ones which uses only one type of charge carries such as holes or electrons this group is called majority carrier devices (MACD) and those who uses both holes and electrons are called minority carrier devices (MICD). Third classification divides semiconductor switches into three groups: uncontrollable, semi-controllable and fully controllable semiconductor devices.

1.2.1. Spark gap

Historically the first switches in pulsed power application was spark gaps, which ensures capability to withstand high voltage and currents with relatively low pulse repetition frequency up to several hundreds of Hz. The spark gap switch often use air as dielectric between contacts but it also can be filled with other gases or liquids. By changing dielectric properties the threshold voltage and other characteristics of the switch can be changed (Mankowski 2000). The spark gap can be triggered using external electrode or laser beam in order to force the switch to close even if the threshold voltage is not exceeded (Larsson 2013). Spark gaps are very durable and the threshold voltage can be easily changed in some configurations, which is very relevant in pulsed power applications. The drawback of the spark gap is the limited repetition rate and electrode electrical corrosion, which limits electrode lifetime. As well as the big electrical noise occurs in the circuit during the spark, which can interfere measurement results (Lee, Huang 2011). The electrodes are usually shaped like Rogowski coils in order to produce the highest electric field where the spark is wanted. There are spark gaps with several series connected electrodes called spark peakers. These multi electrode spark gaps can be used as pre pulse suppressors or load voltage rise time enhancers.

1.2.2. Thyratron

The thyratron resembles a spark gap but the gas inside the thyratron is hydrogen. Low gas pressure gives the tube a higher voltage hold-off capability and decreases recovery time. High gas pressure gives better rates of rise of current, but lowers the hold-off voltage and increases the tube recovery time. Thyratrons are fast acting high voltage switches suitable for a variety of applications including radar, laser and scientific use (Stokes 1992). A plasma forms in the grid-cathode region from electrons when a positive triggering pulse is applied to

the grid. The plasma passes through the apertures of the grid structure and causes electrical breakdown in the high-voltage region between the grid and the anode. This is also called commutation. Once the commutation interval has ended, a typical hydrogen thyratron will conduct with nearly constant voltage drop on the order of 100 V regardless of the current. Thyratrons open (recover) via diffusion of ions to the tube inner walls and electrode surfaces, where the ions can recombine with electrons. This process takes from 30 s to 150 s depending on the tube type, fill pressure, and gas (hydrogen or deuterium). Like a spark gaps the main disadvantages of these switches are reduced lifetime by electrical corrosion and incapability to generate high frequency pulses. The theoretical maximum pulse repetition rate is inversely proportional to the recovery time.

1.2.3. Thyristors

The thyristors are one of the most attractive switching technologies in the market where the switch-off capability is not required. Due to their capability to withstand voltages up to several tens of kV and currents of several tens of kA they have found have place in pulse power application area. There are many different thyristor switches in the market, but all of them are solid-state switches, which act as open circuits capable of withstanding the rated voltage until triggered (Dongdong 2012). The thyristors can be turned on when positive gate current is applied. When thyristor switch is triggered, the switch become low impedance current paths and remain in that condition until the current either stops or drops below a minimum value called the holding level, due to the influence of the circuit elements connected in series. Once a thyristor has been triggered, the trigger current can be removed without turning off the device. Which makes thyristor triggering technology relatively simple compared to other semiconductor switches. Silicon controlled rectifiers (SCR) is one of the member of the thyristor family. An SCR thyristors switch is designed to switch load current in one direction. The load is applied across the multiple junctions and the trigger current is injected at one of them. The trigger current allows the load current to flow through the device, setting up a regenerative action that keeps the current flowing even after the trigger is removed. These characteristics made SCR thyristors extremely popular in pulsed power applications where huge currents and voltages must be applied. The SCR thyristors are characterised by their capability to withstand forward and reverse voltages also on-state currents. Thyristor (SCR) technology is a well-proven solution, which is used for high currents, relatively long pulses, and low current rise rates in capacitor discharge applications. For higher voltage devices can be stacked in series connection. (Bongseong 2011; Tsunoda 2001). The Table 1.2 shows the

new generation power SCR thyristor switch voltage and surge current handling capabilities.

As it can be seen the thyristors switches are capable to withstand surge currents over 80 kA and voltages over 8 kV. In comparison of the thyristors switches between the MOSFET or IGBT switches, the thyristors are the best choice if large currents and voltages must to be applied into the load. The main drawback of the thyristors there is no possibility to turn-off the switch and the current rise time *dI/dt* is relativity low. Which leads to the next problem: the pulse repetition time is also limited as the switch turns-off if the current drops below holding level.

Table 1.2. Silicon controlled rectifier thyristor voltage and surge current handling capabilities

Silicon controlled rectifier switch	Surge current, kA	Voltage, V
DCR3980H50	59.58	8500
DCR4100WK2	83.5	4200
DCR45840H42	53.5	4200

1.2.4. Metal Oxide Semiconductor Field-Effect Transistors

Metal oxide semiconductor field effect transistor (MOSFET) device belongs to the unipolar device family, because it uses only the majority carriers in the conduction (Baliga 2010). The development of metal oxide-semiconductor (MOS) technology for microelectronic circuits opened the way for development of the power MOSFET device in 1975 (Muhammad 2011). The power MOSFET's are fastest switching device in over all semiconductor switches for pulsed power application. The turn on/off time of the power MOSFET is only several tens of ns. The switch can work with switching frequency in the range MHz, and with voltage power ratings up to several of kV and surge current rating as high as several hundreds of amps. The Table 1.3 represents the most powerful MOSFET switches in the market and their voltage and current handling capabilities. As it can be see from the Table 1.3, the power MOSFET's are incomparable switching device in pulse power application if the switching speed is required. The commercial solid-state switches are available only with maximum voltage of 1200 V and maximum surge current handling capability over 450 A. Which cannot compete with powerful thyristor or IGBT switches, which can withstand voltages of several kV. Nevertheless the MOSFET are easy to connect in parallel and in series, which gives opportunity to enlarge current and voltage capabilities of the pulsed power system and expand the application area of the MOSFET devices.

Table 1.3. Power metal oxide semiconductor field-effect transistor voltage and surge current handling capabilities

Power metal oxide semiconductor field-effect transistor switch	Surge current, A	Voltage, V
CCS050M12CM2	250	1200
BSM120D12P2C005	240	1200
BSM180D12P2C101	360	1200
CAS100H12AM1	400	1200
APTM120U10SAG	464	1200

The Power MOSFET is the most popular device for applications where high switching frequencies are required but operating voltages and currents are relatively are low.

1.2.5. Insulated-Gate Bipolar Transistors

The Insulated-Gate Bipolar Transistor (IGBT) is a minority caring device with high impedance and able to withstand large currents. The IGBT can be described as a device with MOSFET input characteristics and bipolar junction transistor (BJT) output characteristics. Actually the IGBT semiconductor switches are integrated MOSFET and bipolar junction transistor (BJT) switches in one monolithic form. This combination gives us the best attributes of these two semiconductor switches what gives as optimal devices characteristics of both semiconductor switch technology. In comparison to the Power MOSFET semiconductor switches IGBT's have some advantages and disadvantages. The main advantages of these switches can be described as follow:

- The IGBT switch has a very low on-state voltage drop due to conductivity modulation and has superior on-state current density. So smaller chip size is possible and the cost can be reduced.
- Low driving power and a simple drive circuit due to the input MOS gate structure. It can be easily controlled as compared to current controlled devices (thyristor, BJT) in high voltage and high current applications.
- It has superior current conduction capability compared with the bipolar transistor. It also has excellent forward and reverse blocking capabilities.

Nevertheless the IGBT switches serious disadvantages compared to the MOSFET semiconductor switches. The main drawbacks can be described as follow:

- Switching speed is slower to that of a Power MOSFET because of the collector current tailing due to the minority carrier, which causes the

turn-off speed to be slow. If the switching speed is the main parameter of the developed circuit, the IGBT switch is not the best choice.

- There is a possibility of latchup due to the internal PNPN thyristor structure.
- Connection in parallel is always a complex task and can lead to destruction of the semiconductor switch.

Table 1.4. The main power insulated-gate bipolar transistor switch characteristics

Power insulated-gate bipolar transistor switch	Surge current, A	Voltage, V
FZ750R65KE3	1500	6500
DIM2400ESM17A	7200	1700
CM600HG-130H	1200	6500
T9S0083403DH	35000	800
FZ3600R17HP4-B2	7200	1700

The most powerful IGBT switches in the market and their current and voltage handling capabilities are presented in Table 1.4. As it can be seen from the table the power IGBT switches can withstand voltages up to 6.5 kV and surge currents up to 1.5 kA. These parameters give superiority to IGBT technology over the power MOSFET's. If the switching speed is not the most important parameter and the turn on/off semiconductor switch is required the IGBT switches are the best choice for the pulse power application.

1.2.6. Protection Circuits from Overvoltage and Currents

In pulsed power applications the high voltage and currents must be used to generate magnetic fields with amplitudes up to several tens of T. The semiconductor switches, used in such technologies are capable to commutate high currents and voltages over the few tens of kV and tens of kA (Carroll 1999; Rashid 2006). Nevertheless, semiconductor switches are very sensitive if operation values are beyond safe operation conditions, which may lead to their failure of the device. Semiconductor device acts as a capacitor with its in-built junction capacitance when the reverse voltage starts to build up during turn-off time. To ensure safe and reliable work of the switch the circuits to reduce current and voltage spikes during turn off/on procedures must be applied. The protective circuits are placed across the semiconductor switches are so called snubbers (Naayagi 2001). Also crowbar circuits are used in pulsed power technologies in parallel connection with the load, to ensure the safe work of the

capacitors bank. There are number of different snubber circuits but the most common used in pulsed power applications are the resistor – capacitor (RC) and resistor – capacitor – diode (RCD) snubber circuits. The mane tasks of such circuits can be described as follows:

- Reduce or eliminate voltage and current spikes.
- Limit the *dI/dt* or *dU/dt* of the pulse during the turn on/off time.
- Shape the pulse on the load to keep it in safe operation area.
- Transfer power dissipation from the switch to the load.
- Reduce total losses due to switching.

In application of the power MOSFET as a switch in the high power application, the RC turn of snubber circuits must be applied to prevent voltage spikes and oscillations over MOSFET during the turn-off. Usually the turn-on snubber circuit is not required, as the MOSFET semiconductor switches can handle large current spikes and the current rise time *dI/dt* can be easily controlled by controlling the gate current. Also in generation of the high magnetic fields the RLC circuits usually are over damped due to large inductive load in the circuit. Due to this the turn on snubber circuits are not required in the pulsed magnetic field generation technology. The Figure 1.5 shows typical RC snubber circuit for control of the *dU/dt* during the turn-off time.

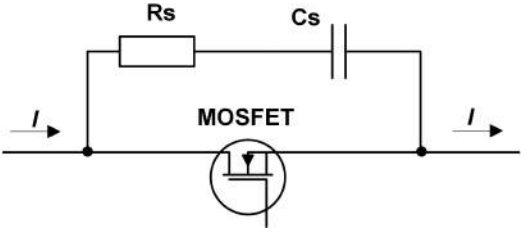

Fig. 1.5. Snubber circuit for the power metal oxide semiconductor field-effect transistor controls *dU/dt* during turn-off

In case in use of the thyristors in pulse power application, the switch needs to be protected during turn-on from *dI/dt* and during turn-off from *dU/dt*. The turn-on and turn-off snubber circuit configuration for the SCR thyristor switch can be seen in Figure 1.6. As it can be seen the inductor *Ls* controls *dI/dt* and the series *Rs* and *Cs* connection controls overvoltage's during the turn-off.

It is common approach to build high voltage pulse generators with semiconductor switches stacked in series to multiply the voltage and in parallel to increase current handling capabilities. The parallel connection of the MOSFET and IGBT's semiconductor switches in parallel due to their positive

temperature coefficient, the connection in series is more complex task, which can lead to the destruction of the switch.

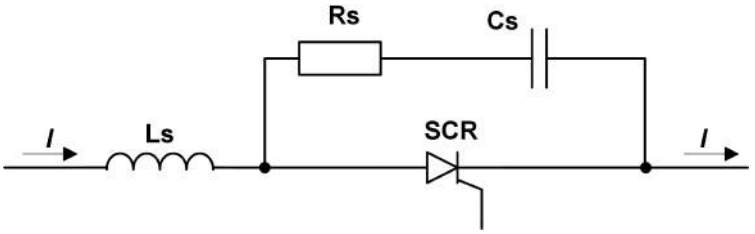

Fig. 1.6. Turn-off and turn-on snubber circuits for silicon-controlled rectifier thyristors switch

The complexity of the series connection of the switches comes from the differences of the semiconductor characteristics and their gate drive circuits. A complex monitoring and synchronization of each switch gate is required, in order to maintain a good dynamic voltage sharing of the switches and prevent their damage. Furthermore, the system has to be able to handle the failure of one of the switches without destroying the whole assembly as well as an over-current emergency turn-off (Jang, Ahn 2010).

1.3. Inductors for Magnetic Field Generation

The pulsed inductors for high pulse magnetic field generation are widely used in all high magnetic field generation facilities around the world and are one of the main components for high magnetic field generation (Ling, Cheng 2012).

For each application the pulsed power inductors for the desired magnetic field generation must be created, as the selected inductor configuration and its inductance can easily change the high magnetic field pulse parameters such as pulse duration, pulse amplitude and rise and decay time. The main pulsed inductor geometries for the high more then 2 T magnetic field generation can be described as follow (Ortenberg 1996; Sterzelmeier 2008; Werst 1994):

- The toroidal inductors.
- The solenoids, which can be multiple or single turn.
- Pancake coils or planar inductors.

The main parameters, which represent the inductors for high magnetic field generation is their inductance L and internal resistance R_L, created magnetic field B and the magnetic energy stored in the inductor (Garcia, 2001).

The single layer multi turn inductor inductance can be expressed as follow (Grover 2004):

$$L=\frac{\mu_0 n^2}{3}D\left(\sqrt{1+\left(\frac{l}{D}\right)^2}\times\right.$$
$$\left.\times\left(\left(\left(\frac{D}{l}\right)^2-1\right)E\left(\frac{1}{1+\left(\frac{l}{D}\right)^2}\right)+K\left(\frac{1}{1+\left(\frac{l}{D}\right)^2}\right)\right)-\left(\frac{D}{l}\right)^2\right). \quad (1.4)$$

The simplified equation can be written as (Grover 2004):

$$L=\frac{\mu_0 n^2}{4}\frac{\pi D^2}{\sqrt{l^2+D^2}}, \quad (1.5)$$

where E and K are the elliptic integrals, n – number of turns, l – length of the inductor, D – diameter of the inductor and μ_0 – magnetic constant.

The maximal generated magnetic field amplitude can be expressed by this Equation (1.6) (Kazimierczuk 2009):

$$B=\mu_0\mu H, \quad (1.6)$$

where μ – magnetic permeability.

The single turn inductors are used in generation of ultra strong magnetic fields more then 100 T. The disadvantage of such circuit that during the application of the voltages over 50 kV and currents over several hundreds of kA. The single turn inductors are destroyed. The special experimental area as well as the special training of the personal is required.

The generated magnetic field in multiturn inductors can be expressed by Equation (1.7), (1.8) (Kazimierczuk 2009):

$$B=\mu_0\frac{nl}{r_1}\left(\frac{F(\alpha,\beta)}{2\beta(\alpha-1)}\right), \quad (1.7)$$

$$F(\alpha,\beta)=\beta\ln\frac{\alpha+\sqrt{\alpha^2+\beta^2}}{1+\sqrt{1+\beta^2}}, \quad (1.8)$$

where I – current in the inductor, n – number of turns, $\alpha = r_2/r_1$, $\beta = l/2r_1$ – relative sizes, r_1 and r_2 – inner and outer radius of the inductor.

The inductance of the multi layer solenoid can be expressed by Equation (1.9) (Grover 2004):

$$L = 4\pi^2 n^2 m\left(\frac{2a_0^4 + a_0^2 l^2}{\sqrt{4a_0^2 + l^2}} - \frac{8a_0^3}{3\pi}\right) + \\ +8\pi^2 n^2 \left(\begin{array}{l} \left((m-1)a_1^2 + (m-2)a_2^2 + ...\right)\left(\sqrt{a_1^2 + l^2} - \frac{7a_1}{8}\right) + \\ +\frac{1}{2}\left(m(m-1)a_1^2 + (m-1)(m-1)a_2^2 + ...\right)\left(\frac{a_1\delta_a}{\sqrt{a_1^2 + l^2}} - \delta_a\right) - \\ -\frac{1}{2}\left(m(m-1)a_1^2 + (m-2)(m-3)a_2^2 + ...\right)\frac{\delta_a}{8} \end{array}\right), \quad (1.9)$$

where n – number of turns of the solenoid, m – number of layers, l – length of the inductor, a_0 – the mean radius of the solenoid, a_1, a_2, …a_m – mean radius of the various layers of the solenoid and δ_a – distance between centres of any two consecutive layers.

The simplified equation for the inductance calculation of the multilayer turn solenoid can be expressed by Wheeler's approximation (1.10) (Grover 2004):

$$L = \frac{31.6 \cdot r l^2 \cdot n^2}{6rl + 9l + 10(r_2 - r_1)}, \quad (1.10)$$

where r – radius of the solenoid, r_1 and r_2 the inside and outside radius of the inductor respectively.

One of the most common problem in the high magnetic field generation technology is the temperature increase in the inductors due to Joule heating effect. The temperature increase in the inductor can be expressed by Equation (1.11) (Batti 2008):

$$\rho_m C \frac{\partial T}{\partial t} = k\nabla^2 T + \frac{\left(\nabla\left(\frac{1}{\mu}\nabla A\right) + \sigma_e \frac{\partial A}{\partial t}\right)^2}{\sigma_e}, \quad (1.11)$$

where μ – the magnetic permeability, ε – permittivity, σ_e – electrical conductivity of the material, $\boldsymbol{A}$ – magnetic vector potential, C – heat capacitance.

By generating high more then 10 T magnetic fields the magnetic pressure or Lorenz force must be taken into consideration. The inductors should have reinforced layer between the windings, to ensure safe operation of the inductor.

For the first approximation the equation of the maximum available magnetic field inside the inductor can be calculated with Equation (1.12):

$$B = \sqrt{2}\left(1 - \frac{1}{r_1 - r_2}\right)\sqrt{2\mu_0\sigma_m}, \tag{1.12}$$

where the μ_0 – magnetic permeability of the free space, σ_m – maximal allowable mechanical stress.

1.4. Magnetoresistive Magnetic Field Sensors

The measurement of the generated magnetic field in high magnetic field applications is relevant. For high magnetic field measurements the well-known magnetic field sensing technologies such as Hall, B-dot and magneto-optical sensors are widely used (Lenz 2006). All these magnetic field sensing devices have the same disadvantage for the pulse magnetic field measurements. Using these sensors the magnetic field direction must be known in advance or several sensors must be used in the experiment (Ripka 2001; Lenz 2006). In some cases, such as measurement of magnetic field in liner electromagnetic motors or in electromagnetic rail guns where the generated magnetic field can't be known in advance or the direction of magnetic field, during measuring can change. Due to this fact the B-scalar magnetic field sensing devices are welcome (Liebfried 2009).

Recently the CMR-B-Scalar high magnetic field sensors, based on colossal magnetoresistance (CMR) were invented. They are able to measure the absolute magnitude of the magnetic field independently on the direction of it (Žurauskienė, Balevičius 2010). The CMR-B-Scalar magnetoresistive sensors working principle is based on the negative CMR effect in the manganite films. It means that the resistance of the manganite films decreases at applying of magnetic field.

The Figure 1.7 shows the principal structure of the CMR-B-Scalar magnetic field sensor. The sensor consists of these main parts: thin manganite (La-Sr-Mn-O) film, temperature sensor and shielding. All active sensor parts are covered with polyurethane to avoid damage of the sensor. Due to the small size, which can vary from ~2 to 10 mm^3 the sensing device can be used to investigate

magnetic fields in rail or coil gun systems where magnetic field direction amplitude and homogeneity changes very fast.

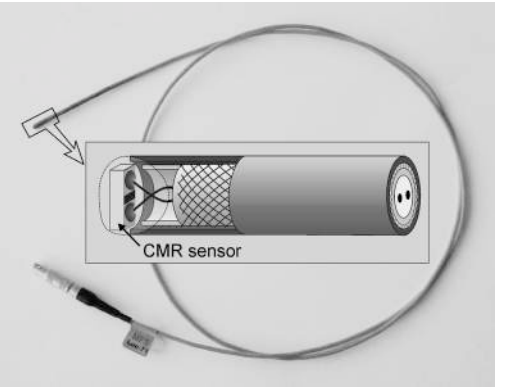

Fig. 1.7. Picture and schematic 3D cross section of the CMR-B-scalar sensor with cable (Stankevic 2014)

In these application areas the electromagnetic interference can be very high and induced voltage accrues in the cables used to supply it with DC current. The Figure 1.7 shows the installed protection measures from the electromagnetic interference (EMI). The specially twisted pair cables are putted to a Teflon tube, the flexible metallic shielding was put on it and the flexible isolated tube covers all the cable. All these protection measures ensure the protection against high-frequency electromagnetic noise, which can occur during the fast *dB/dt* high magnetic field generation.

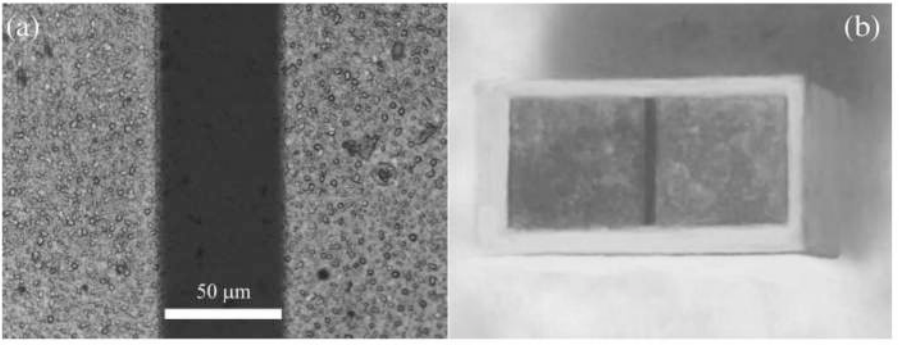

Fig. 1.8. Outside view of the Ag electrodes (a) and the picture of the magnetoresistive sensor after lithography (b) (Stankevic 2011)

The Figure 1.8 shows the picture of the magnetoresistive sensor after standard photolithography (b) and the etched area between the Ag electrodes (a). The magnetoresistive sensors are fabricated using a conventional integrated circuit processing technique. The rectangular-shaped areas of the manganite film with are formed from the film plate by using standard photolithography and by etching down to the substrate. The electrical contacts were prepared by the thermal deposition of silver (Ag) through the following way. The layers of Ag having a width of 0.4 mm were deposited onto the plate along the formed manganite film areas separated by a distance of 50 μm. As a result, the layers of silver covered partially the manganite film and partially the substrate at the etched places. The contacts were annealed in an argon atmosphere at 420 °C for 40 min. Therefore, the active volume of each sensor was only 400 μm × 50 μm × 0.4 μm. The substrate was cut into 0.5 mm long and 1 mm wide pieces. Then, the samples were soldered to wires bifilarly twisted in the direction perpendicular to the surface of the films. After that, the active surface of the sensor and the soldered area with the contacts were covered by special thermoglue (Liebfried 2009).

The physical properties of the magnetoresistive sensors strongly depend on technological conditions, temperature and material structure. The Figure 1.9 shows the resistance dependence on the applied temperature, when three different temperatures 650 °C, 700 °C and 750 °C were used in the sensor fabrication stage.

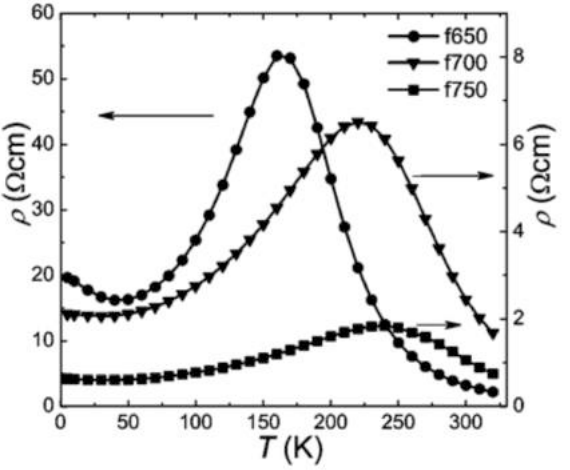

Fig. 1.9. The resistance dependence on the applied temperature with three different fabrication temperatures 650 °C, 700 °C and 750 °C (Žurauskienė, Balevičius 2010)

As it can be seen on Figure 1.9 the resistance of the sensor increases in the low temperature range and starts to decreasing in high temperature ranges >170 K and it also depends on the fabrication temperature. The Figure 1.10 shows the resistance of the magnetoresistive sensor dependence from the temperature with applied magnetic field *B* from 0 T to 20 T. As it can be seen the resistivity also depends on the applied magnetic field strength in different temperature ranges. The nonlinear dependence of the applied magnetic field can be observed in lower magnetic fields. Therefore the resistivity dependence on the temperature more or les is linear in the high magnetic field ranges >10 T. Due to this fact the magnetoresistive magnetic field sensors must be calibrated in different temperature ranges.

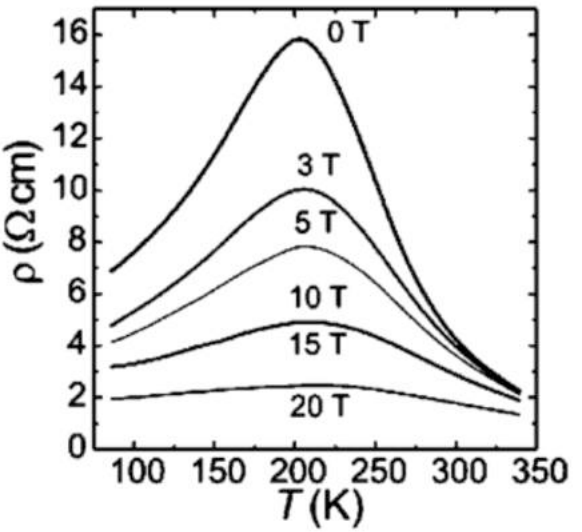

Fig. 1.10. The resistance dependence on the applied temperature when different magnetic field *B* is applied (Balevičius 2010)

The sensors measurement technology is based on the magnetoresistance effect of the manganite sensors. The magnetoresistance of the CMR-B-Scalar magnetic field sensors can be calculated using the Equation (1.13) (Žurauskienė 2009):

$$MR = \frac{R_B - R_{B=0}}{R_{B=0}}, \tag{1.13}$$

where $R_{B=0}$ – the film resistance when no magnetic field is applied, R_B – the film resistance when magnetic field B is applied.

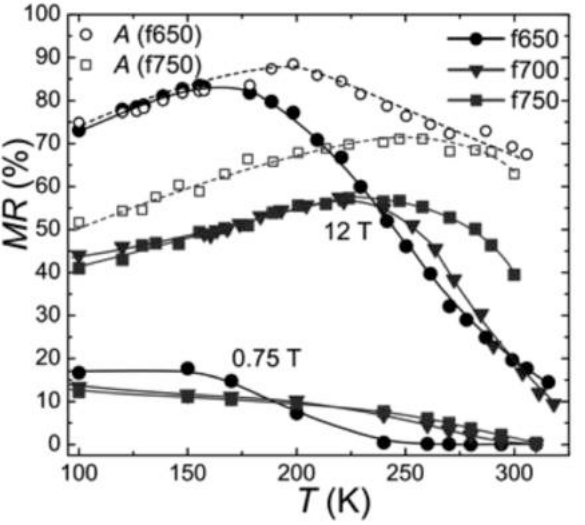

Fig. 1.11. The magnetoresistance dependence on the applied temperature (Žurauskienė, Balevičius 2010)

The Figure 1.11 shows the manganite sensor magnetoresistance dependence on the applied temperature in different magnetic fields of 12 T and 0.75 T.

The Figure 1.12 shows the magnetoresistance of the manganite sensor dependence on the applied magnetic field strength. The nonlinear dependence can be observed in lower magnetic field ranges up to 6 T. The sensors output is more or less linearly dependant in the higher magnetic field ranges. As it can be seen from the Figure 1.12 the magnetoresistance of the manganite sensors also depends on the material structure. Due to the fact that the nonlinear magnetoresitance dependence on the applied magnetic field occurs in lower fields, the precise calibration of the manganite sensors must be done in lower ranges of the magnetic field <6 T.

Nevertheless the manganite sensors must be calibrated using single high magnetic field pulse (express calibration) to ensure the constant temperature during the calibration and avoid temperature dependence effect. Even more, during the express calibration the sensor must be calibrated in high and low magnetic fields simultaneously. It follows that the amplitude of the magnetic field for the express calibration must be high >10 T to calibrate sensor in high magnetic fields and the change of the magnetic field *dB/dt* in lower magnetic

field regions <6T should be as low as possible to make precise calibration in low magnetic fields.

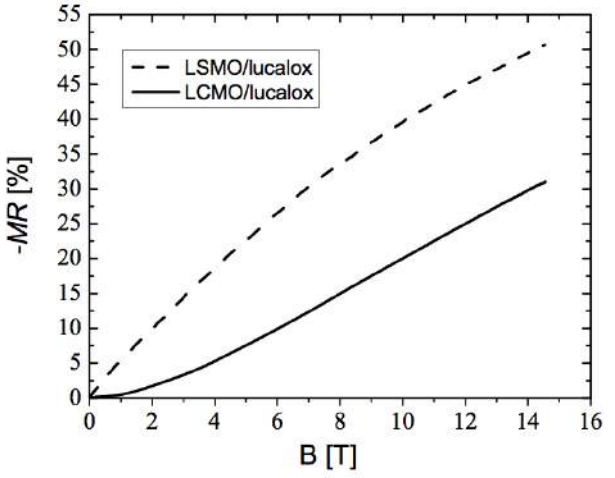

Fig. 1.12. The magnetoresistance of the manganite sensor with different material structure dependence on the applied magnetic field strength (Schneider 2007)

The size of the CMR-B-Scalar magnetic field sensor varies from 2 to 10 mm^3. Therefore to ensure the precise calibration of the CMR-B-Scalar magnetic field sensors the sensor must be placed in homogeneous high-pulsed magnetic field with inhomogeneity less then 1% in the area of >10 mm^3 together with calibrated loop sensor that acts as an etalon.

1.5. Effects of Pulsed Fields on Biological Objects

Electroporation is a technique based on polarisation of the dielectric membrane of the biological cells by application of pulsed electric fields resulting in the occurrence of temporary nanometre pores in the membrane (Kotnik 2012; Ivorra 2010). The method has found application in biomedicine and in the field of drug delivery technologies as a tool for transportation of chemicals inside and outside the cell (Dev, Rabussay 2000; Lee, Demirci 2009). Increase of the treatment intensity results in the severe irreversible damage of the membrane following by the death of the cells. The effect is known as irreversible electroporation, which has found application as a cancer treatment technique (Maor 2008). It should be noted that, as a rule electroporation involves application of the metal electrodes that are in direct contact with the cell medium, which causes several limitations

for the technique. First, it may cause possible contamination issues, which influence the experimental results. Second, the presence of accidental air bubbles in the medium between the electrodes results in the discrepancy of the medium conductivity and affects the pulse form (Arena 2011). Such factors limit the use of the technique in the environmental sciences and in biotechnology and in order to eliminate these issues contactless facilities of cell treatment should be developed. One of the solutions could be application of pulsed magnetic fields, which could allow contactless treatment. However, the effects caused by magnetic fields in biological objects must be investigated.

Presently, the area of magnetic field treatment of biological objects is poorly studied and the research is performed mostly in the field of low power applications such as transcranial magnetic stimulation (Williams 2001, Tatarov 2011). The purpose, methodology and the generation facilities for such techniques are not applicable for membrane permeabilisation applications where high power is required.

In the traditional electroporation when the high voltage between the electrodes is applied the voltage potential between the inside and the outside of the cell membrane changes because of the polarization effects (Washizu 2008; Washizu 2008). When the transmembrane potential is high enough temporary nanometer pores start to appear in the dielectric lipid membrane and transportation of drugs or other chemicals becomes possible (Cahill 2010). The transmembrane potential in high frequency oscillating fields according to Schwan Equation (1.14) (Marszalek 1990):

$$\Delta\Psi_m = \frac{3Er_{cell}\cos\varphi}{2\sqrt{1+\left(\omega\tau_p\right)^2}}, \tag{1.14}$$

where E – amplitude of the electric field, r_{cell} – the radius of the cell, τ_p – the polarization time, φ – the angle of the applied field with respect to the cell poles, and $\omega = 2\pi f$, where f is the frequency of the applied field.

The potential should be above 200 mV for electroporation to happen (Teissie 2005). From Equation (1.14) it can be seen that the success of the technique strongly depends on the amplitude of the applied field and the size of the cell. In case of irreversible cell membrane permeabization the electric field of hundreds of kV/m is required, which implies that the transmembrane potential should be even higher (Davalos 2005).

The other important parameter in the evaluation of transmembrane potential is the time required for the polarization to happen, which is defined as Equation (1.15) (Ramos 2006):

$$\tau_p = C_m r\left(\frac{1}{\sigma_c}+\frac{1}{2\sigma_m}\right), \tag{1.15}$$

where r – cell radius, C_m – specific membrane capacitance, σ_c, σ_m are the specific conductivities of the cell and the extracellular medium, respectively.

Thus, the time required for polarization is specific for different kinds of cells. In case of electroporation the cells are subjected to the electric field, however it should be noted that in the case of magnetic field treatment the cells are subjected both to magnetic and induced electric fields. Therefore, it should be mentioned that it is appropriate to maximize the effect of both electric and magnetic field treatment components.

As it was mentioned above the transmembrane potential depends on the amplitude of the electric field. Therefore, in case of magnetoporation the induced electric field should be also estimated. According to Faraday's law the changing magnetic field induces the electric field:

$$\oint_L E \cdot dl = -\frac{d}{dl}\iint B \cdot ds, \tag{1.16}$$

where B – the magnetic flux density, t – the time, ds and dl are the differential surface and length, respectively.

According to Biot-Savart's law the magnetic field B at a position r due to segment dl of current I could be expressed by Equation (1.17):

$$dB = \frac{\mu_0 I}{4\pi}\frac{dl \cdot r}{r^3}, \tag{1.17}$$

where μ_0 is the magnetic constant.

In case of a solenoid the resultant magnetic field is calculated as a superposition of segments of current I thus the induced electric field inside the inductor could be defined as Equation (1.18):

$$E = -\frac{r}{2}\frac{dB}{dt} \sim \frac{dI}{dt}, \tag{1.18}$$

where r is the distance from the centre of the inductor, which implies that the strongest effect will be near the walls of the inductor.

According to Equations (1.16) – (1.18) the voltage potential occurring due to induced electric field on the membrane of a biological object during magnetoporation could be rewritten as function of current derivative:

$$\Delta\Psi_{\mathrm{m}} = f\left(\frac{dI}{dt}\right). \tag{1.19}$$

Also the peak values of the magnetic and induced electric fields are proportional to the peak current through the inductor, therefore it is appropriate to maximize the current value and therefore the energy of the pulse.

However, the current is limited by the heat generated in the inductor due to the Joule heating, which is proportional to the square of the current amplitude:

$$Q_{\mathrm{J}}(t) = \int_0^t I^2(t) R dt, \tag{1.20}$$

where R – the resistance of the wire.

The increase in temperature may couse death of biological objects. Therefore, Joule heating must be minimized and a balance between the pulse energy and the generated heat should be found. Also from Equation (1.20) it can be seen that the generated heat is proportional to the pulse length. However, based on Equation (1.19) it is not appropriate to use long magnetic field pulses because the induced electric field is dependent on the change of the magnetic field flux. Therefore, in order to increase the treatment intensity the application of series of pulses is required.

1.6. Conclusions for the Chapter 1 and the formulation of the thesis tasks

1. The application of the pulsed power magnetic field in science, medicine, industry and military areas increased dramatically in last few decades, therefore the investigation and development of the high-pulsed magnetic field generation systems are important and relevant.
2. Properties of the investigation objects depend on the magnetic field pulse shape and amplitude. The compact flexibly integrated into laboratory facilities high magnetic field pulse generation systems are in high demand.
3. Manganites physical properties highly depend on fabrication conditions, material structure and operation temperature. Therefore magnetoresistive sensors should be calibrated in high pulse magnetic field to avoid heating influence on calibration accuracy.
4. Biological objects response to high pulse magnetic field is purely investigated. Induced by pulsed magnetic field electric field is one of

factors influenced on biological object behaviour. Therefore special shaped pulse generators applicable for biotechnological purposes should be developed.

5. Biological objects are very sensitive for sensors and electrode invasions. Contactless facilities integrated into biotechnological equipment should be developed to avoid the contamination problems.

The following tasks have to be solved to achieve the aim of the work:

1. To develop the prototypes of the microsecond high magnetic field shaped pulse generators and to investigate transient processes in the generators circuits.
2. To develop multilayer and planar microinductors and to investigate magnetic field distribution and Joule heating.
3. To investigate the express calibration of the magnetoresistive sensors using 10 T microsecond asymmetric shaped pulse magnetic field generator.
4. To investigate biological objects in pulsed magnetic fields using microsecond 5 T high magnetic field repetitive square shaped pulse generator.

2

Development and Investigation of Microsecond High Magnetic Field Shaped Pulse Generators

The developed two microsecond high magnetic field shaped pulse generators are presented and analysed in this section. The computer simulation models of the developed shaped pulse generators are created and presented. The analysis of the transient processes of the generators is presented. The developed multilayer inductor for the express calibration of the magnetoresistive sensors as well as the multilayer microinductor and planar inductor for the investigation of the biological objects are presented. The magnetic field distribution as well as the Joule heating effect in the inductors are analysed.

Four scientific publications were published on the section topic (Grainys 2012; Grainys *et al.* 2013, Grainys 2010; Grainys, Novickij 2011, Grainys, Novickij 2013).

2.1. High Magnetic Field Asymmetric Shaped Pulse Generator

In this section the compact 43×35×100 cm microsecond high magnetic field asymmetric shaped pulse generator, capable to generate high more then 10 T magnetic fields with rise time of 200 μs and the decay time of 800 μs, using the 15.5 μH multilayer inductor designed and developed for the express calibration of the magnetoresistive sensors is presented and analysed.

The manganite sensors have nonlinear characteristics in weak (<6 T) magnetic fields. In high (>6 T) magnetic fields the magnetoresistance dependence on the applied magnetic field amplitude varies linearly (see Figure 1.12). More other the magnetoresistance of the manganite sensors strongly depends on the temperature (see Figure 1.11). Therefore, when the pulsed magnetic field is used for calibration of sensors it is important for the *dB/dt* to be as low as possible in the low (<6 T) magnetic field region, to ensure the sensitivity of the calibration and to avoid calibration errors. Netherless the calibration curves must be done and in the high magnetic field regions. So the peak amplitude and the back front of the pulse will be used as in the front time the *dB/dt* is high and the errors in calibration experiments can occur.

The system is specially designed for the magnetoresistive magnetic field sensor express calibration using one pulse methodology. The main requirements for the pulsed magnetic field generator to be used for magnetoresistive magnetic field sensor calibration is mobility, safety, capable to generate magnetic field pulse amplitude over 10 T with inhomogeneity of less then 1% in a 50 mm^3 volume. To ensure low slow *dB/dt* in low magnetic field regions the pulse must be shaped to asymmetric form with high-rise time and low decay time. In order to match the magnetic field pulse requirements currents up to 50 kA should be supported and high energy up to 40 kJ accumulations is required.

During the pulse the sensitive parts of the high magnetic field asymmetric shaped pulse generator (MFASG) can be damaged due to high voltage and current spikes in the circuit. The computer simulation model of the MFASG circuit must be created to investigate transient processes to avoid the damage to the high power system.

2.1.1. Computer Simulations of the Microsecond High magnetic Field Asymmetric Shaped Pulse Generator

In order to determine the characteristics and the influence of the high voltage components to microsecond high field asymmetric shaped pulse generator the computer simulation model and the analysis of the transient processes must be made.

Using the PSPICE simulation package the computer model of the MFASG circuit was created. The main circuit parameters used in the simulation model are presented in the Table 2.1.

Table 2.1. The main circuit parameters used in the PSPICE simulation model

Parameter	Denotation	Circuit parameters
Inductance	L, H	$15.5 \cdot 10^{-6}$
Initial capacitor voltage	U_c, V	570
Capacitance	C1, F	$5.4 \cdot 10^{-3}$
Crowbar resistance	R1, Ω	from 0.05 to 1
Simulation time	t, s	$5 \cdot 10^{-3}$

The created MFASG generator computer model using the PSPICE simulation package is shown in the Figure 2.1.

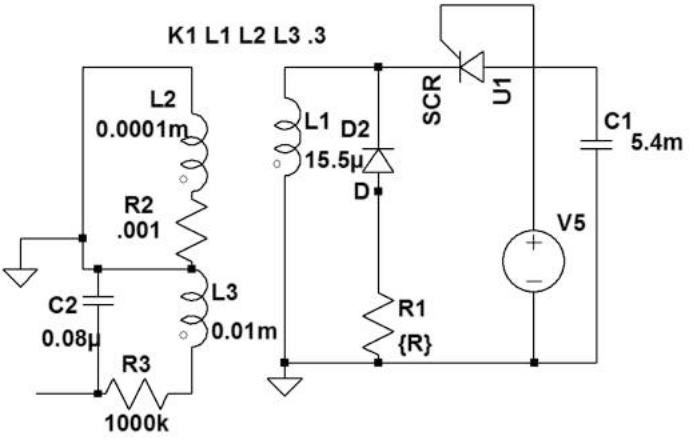

Fig. 2.1. Computer simulation model of microsecond magnetic field asymmetric shaped pulse generator

As it can be seen from the Figure 2.1 the computer model of the created microsecond magnetic field asymmetric shaped pulse generator consists of these main parts: 5.4 mF capacitor C1, SCR thyristor switch, crowbar circuit consisting from crowbar diode D2 and crowbar resistor R1, pulsed inductor L1 as a load and magnetic field sensor simulation circuit.

The initial conditions of the initial voltage of the capacitor bank C1 was set tot 570 V. The capacitor bank was discharged through the inductive load

L1, which represents the multilayer inductor. During the pulse the reverse voltage on the capacitor bank appears. The reverse voltage strongly effects the lifetime of the capacitor banks. The crowbar circuit is implemented into the system to minimize reverse voltage effect to the 5.4 mF capacitor banks. The reverse voltage on the capacitor bank dependence on the crowbar resistance is shown on the Figure 2.2.

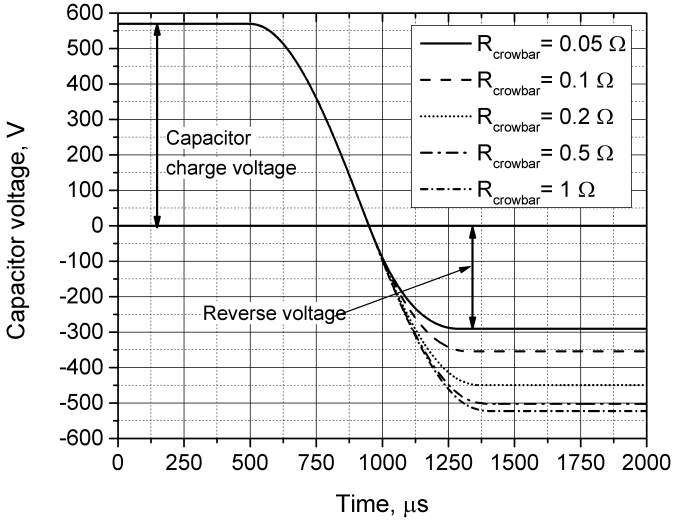

Fig. 2.2. Voltage on the 5.4 mF capacitor bank dependence on crowbar resistance

As it can be seen from the Figure 2.2 the reverse voltage on the capacitor bank is almost 90% of the initial charged voltage if no crowbar circuit is implemented into the system. Which leads to the fact that the capacitor banks for one pulse generation are twice charged and discharge, which twice shortens the lifetime of the capacitor bank. As the capacitor have limited charge discharge procedure number the minimization of the reverse voltage should be done. In order to investigate crowbar circuit effect on the reverse voltage the circuit was simulated using resistors from 0.05 Ω to 1 Ω. As it can be seen from the Figure 2.2 by reducing the crowbar resistance the reverse voltage can be minimized from 525 to 325 V using crowbar resistance of 0.1 Ω and to 290 V using 0.05 Ω crowbar resistor. From the given results the minimization of the crowbar resistance should be taken into account.

Nevertheless the crowbar resistance cannot be minimized to zero as it is also used to limit the transient currents in the crowbar diode. The elimination of

the crowbar resistance from the circuit can lead to the destruction of the crowbar diode. The current in the crowbar diode dependence on the crowbar resistance is shown on the Figure 2.3.

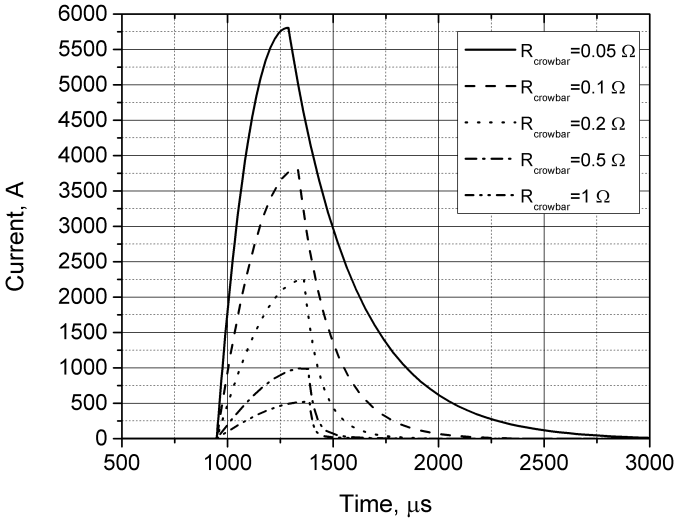

Fig. 2.3. Current in the crowbar diode dependence on the crowbar resistance R6

As it can be seen from the Figure 2.3, the current in the crowbar diode increases in the crowbar diode during the pulse with minimizing the crowbar resistance. The current in the crowbar diode increase from 500 A using 1 Ω crowbar resistor to 6 kA using 0.05 crowbar resistance when the capacitor was charged to 570 V. Therefore the crowbar resistance cant be minimized to zero as it limits the current in the crowbar diode.

The simulated current pulse in the inductive load L1, inductance of 15.5 μH and its dependence on the crowbar resistance is presented in the Figure 2.4.

As it can be seen in Figure 2.4 the crowbar circuit acts as a pulse-shaping device. By implementing the crowbar circuit into the generator the decay time of the generated pulse can be changed. By minimizing the crowbar resistance the decay time of the generated magnetic field pulse can be prolonged. The decay time increase from 300 μs using 1 Ω crowbar resistance to 900 μs with crowbar resistance of the 0.05 Ω can be observed in the Figure 2.4. This leads to decrease of the current change rate *dI/dt* of the generated pulse from $1.8 \cdot 10^6$ A/s to $0.51 \cdot 10^6$ A/s respectively. This particular influence of the crowbar

circuit can be used in the express calibration of the magnetoresistive sensors using the one pulse methodology.

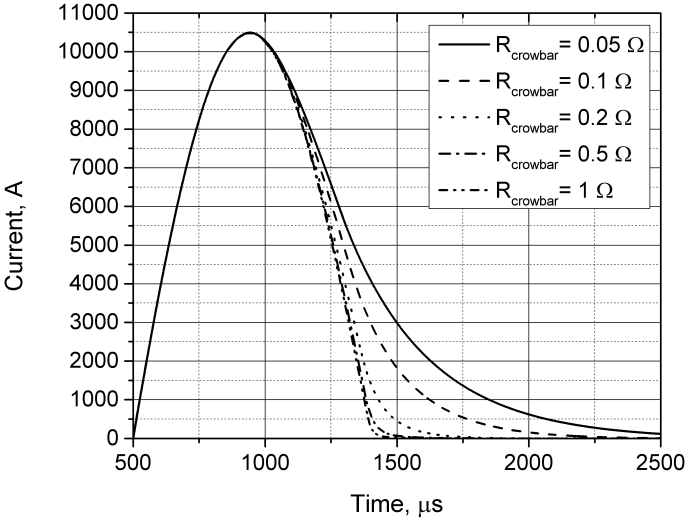

Fig. 2.4. Current changes in the 15.5 μH inductive load by changing crowbar resistance R6

Due to high voltage capacitor bank discharge through the inductive load L1. The reverse voltage on the SCR thyristor switch occurs. The reverse voltage on the SCR thyristor switch during the pulse and its dependence on the crowbar resistance is shown on the Figure 2.5.

As it can be seen in Figure 2.5 the negative voltage on the SCR thyristor using 1 Ω crowbar resistor is equal to the initial charge voltage. Using the 0.05 Ω resistor the negative voltage can be minimized to 50 % of the initial charged voltage. To minimize the reverse voltage effect on the thyristor switch the crowbar resistance must be as low as possible.

Nevertheless the limitation of the current in the crowbar diode, reverse voltage on the capacitor banks and required magnetic field pulse shape must be taken into account and the optimal crowbar resistance must be selected.

To ensure all these parameters the crowbar resistance of 0.2 Ω was selected and implemented into the developed high magnetic field asymmetric shaped pulse generator. The selected crowbar resistance ensures safe work of the developed high power system and allows the express calibration of the magnetoresistive sensors with one pulse methodology.

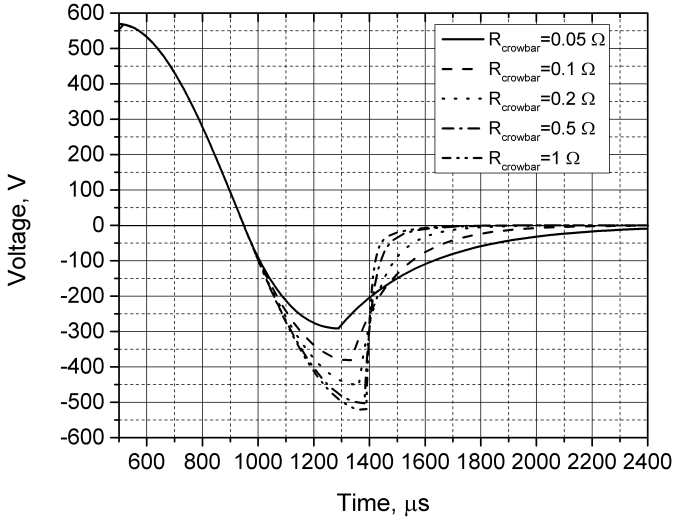

Fig. 2.5. Negative voltage on the SCR thyristor switch during the pulse

The Figure 2.6 shows the generated inductor current pulse dependence on the load inductance L1.

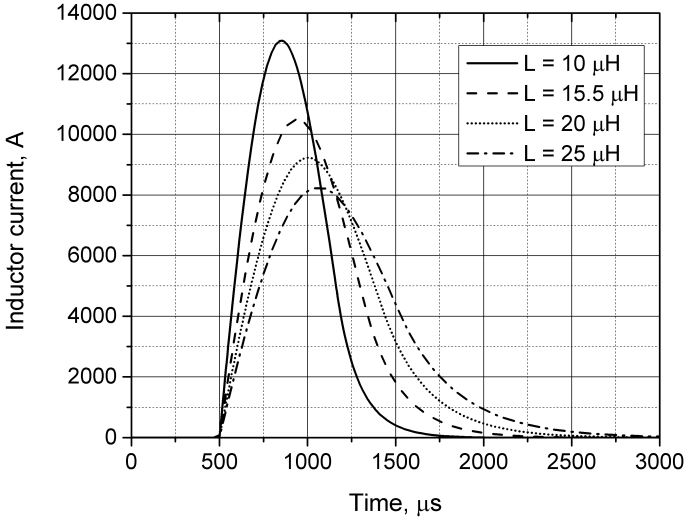

Fig. 2.6. Current dependence on the load inductance L1

As it can be seen the resultant current pulse width and pulse amplitude can be changed by changing load inductance L1. The pulse width increase from 700 μs (inductive load 10 μH) to 2 ms (inductive load 25 μH).

2.1.2. Technical Parameters of the Microsecond High Magnetic Field Asymmetric Shaped Pulse Generator

The developed microsecond high magnetic field asymmetric shaped pulse generators picture with remote control unit for safety applications is presented in the Figure 2.7.

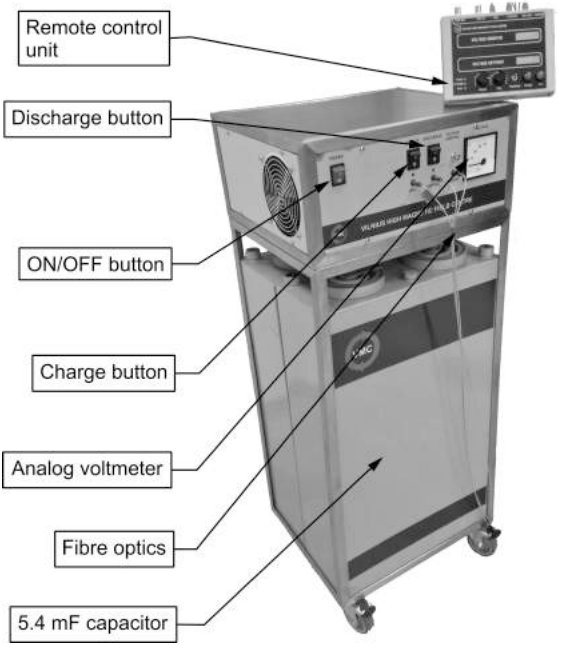

Fig. 2.7. Picture of the developed microsecond magnetic field asymmetric shaped pulse generator

As it can be seen, the created system is mobile and can be easily transported to any laboratory and integrated into already existing laboratory equipment. The total weight of the developed high power facility is 200 kg. The integration possibility of the generator allows to provide interdisciplinary experiments in high-pulsed magnetic fields. The remote control unit also shown on Figure 2.7 ensures safety requirements for the operator as it allows to control developed high power system from the distance of 20 m.

The simplified block diagram of the developed microsecond magnetic field generator with asymmetric pulse shape is presented in Figure 2.8.

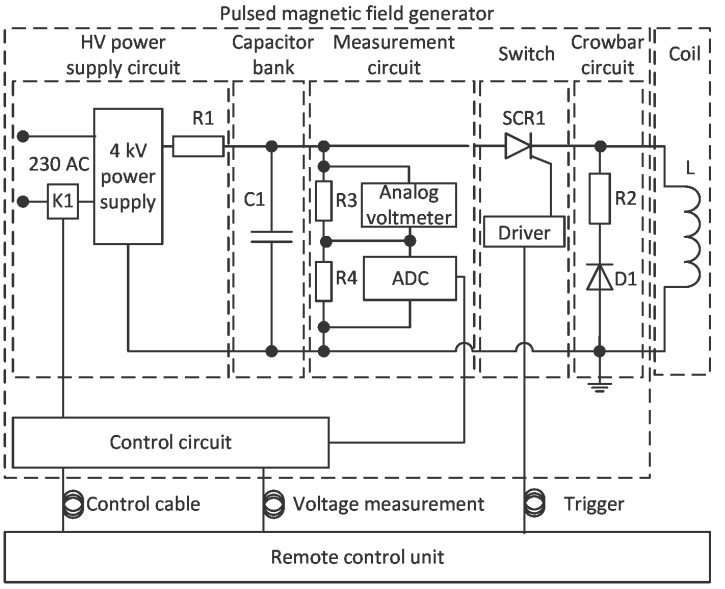

Fig. 2.8. The simplified schematic of the microsecond high magnetic field asymmetric shaped pulse generator

As it can be seen in the Figure 2.8 the developed high magnetic field asymmetric shaped pulse generator consist of these main parts: 4.3 kV power supply, two high voltage 4.3 kV and 2.7 mF paper oil capacitor banks connected in parallel, high power 53 kA and 4.2 kV SCR semiconductor switch with control circuits, crowbar circuit, consisting from the 83 kA and 4 kV crowbar diode with series connected 0.2 Ω crowbar resistor, pulsed 15.5 μH inductor, and the remote control unit to ensure safety of the operator.

The developed high magnetic field with asymmetric shaped generator uses two 4.3 kV and 2.7 mF capacitor banks connected in parallel, as an energy storage device. The total capacitance of both capacitors is 5.4 mF. The step up 2.9 kV and 170 mA transformer with implemented full-wave rectification circuit was chosen as a power source for the charging of the 5.4 mF capacitor banks. To ensure safe and reliable voltage charging operation, so called “time control” method was chosen to charge high voltage capacitor banks to required voltage. For this purpose the high voltage relay K1 and 220 V relay K2 was implemented into the circuit, which through high power 100 W and 10 kΩ resistors provides safe and reliable capacitor bank charging and discharging operations.

Using voltage dividers and analogue to digital converters (ADC), the voltage on the capacitor banks is converted to digital signal and transmitted to remote control unit via 20 m fibre optic cable. The measured voltage is displayed on the remote control unit. Also for safety applications the analogue voltmeter was implemented into the front panel of the pulsed generator to ensure reliable and uninterruptable voltage measurement in case of the failure of the control circuit.

During the high magnetic field generation, the high voltage capacitor banks are charged by reverse voltage. To ensure safe work of the high magnetic field generator, the reverse voltage must be minimized. The cheapest capacitor banks in the market are electrolytic capacitors, but the application of these capacitors in the pulsed power technologies are limited due to incapability to withstand reverse bias voltages during the pulse. It should be mentioned that capability to withstand negative voltage and current pulses is one of the most important factor in choosing the capacitor banks. For this purpose the two 2.7 mF and 4.3 kV oil and paper capacitor banks where chosen as a high voltage energy source. Despite that oil and paper capacitors are one of the most attractive energy storage devices in pulse power application, the reverse bias voltage can reduce capacitors lifetime. To investigate reverse bias voltages during the pulse the mathematical simulation (see Figure 2.2) and experimental measurements were done. The measured revers bias voltage on the capacitor is shown on Figure 2.9.

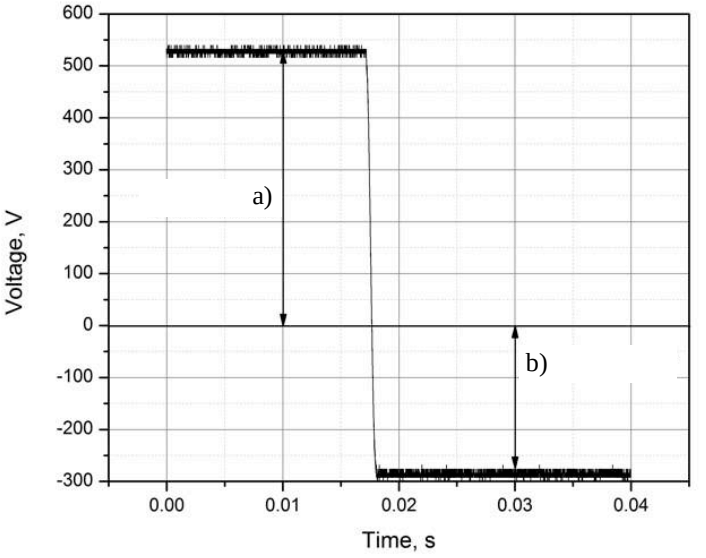

Fig. 2.9. Measured capacitor voltage: a) charged voltage and b) reverse voltage on the capacitor banks during the pulse

As it can be seen from Figure 2.9 after the implementation of the crowbar circuit with crowbar resistance of the 0.2 Ω the reverse voltage b) on the capacitors are reduced by 40% and it is equal to half of the charge voltage a).

Generation the high magnetic fields with amplitudes >10 T the currents of several tens of kA must be applied into the inductive load. To match these requirements high power, fast semiconductor switches must be used. Also the capability to withstand over currents and over voltages which can appear during turn–on and turn–of operation of the switch. Given the fact that created magnetic field generators magnetic field pulse must be shaped asymmetrically, the use of MOSFET or IGBT semiconductor switches is optional. Taking into account all the given parameters of the created magnetic field generator, the power SCR semiconductor switch, capable to commutate non-repetitive 53 kA currents with *dI/dt* of 400 A/μs and withstand voltages up to 4.2 kV, was selected and implemented into the circuit.

The control of the high power SCR thyristor switch S1 was realized by implementation of the factory driver circuit into the developed high power system. The factory driver circuit is controlled via fibre optics only from the remote control unit to ensure safe work for the operator. For the safety operation the trigger circuit is isolated with fibre optic cables to prevent electrical breakdown between power and control circuits, while protecting damaging expensive SCR thyristors. The digital trigger signal of the SCR thyristor is formed in remote control unit, converted into an optical signal and sent to the factory SCR trigger module.

The generated magnetic field pulse using 15.5 μH inductor is presented in the Figure 2.10.

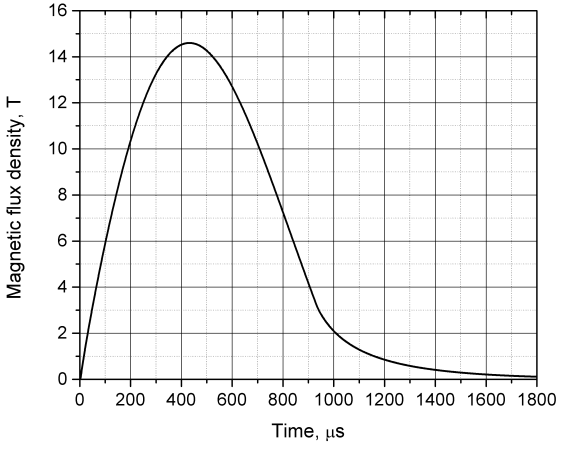

Fig. 2.10. The asymmetric pulse shape of the generated high magnetic field

As it can be seen in the Figure 2.10 the generated 14.5 T magnetic field pulse is asymmetrically shaped due to implemented crowbar circuit, which allows the express calibration of the magnetoresistive magnetic field sensors in high and low magnetic field ranges.

2.1.3. The Remote Control Unit for Safety Applications

Due to the fact that the created high-pulsed magnetic field generator uses the currents up to 50 kA one of the main objectives to the high-pulsed magnetic field generator design was safety to the operator of the facility. For that purpose the remote control unit capable to perform operations such as “Fire”, “Charge”, “Discharge”, voltage set and voltage indication on the capacitor banks, was created. The connection between the main control circuit and remote control unit was established with 20 m fibre optic cable. In such way any interaction between generator and operator of the facility was eliminated.

The simplified block diagram of the main control unit is presented in the Figure 2.12. The main control unit performs all control operations of the high-pulsed power generator. The remote control unit acts like a trigger and information analyser for main control circuit, which ensure safety protocols. The simplified schematic of the remote control unit is shown in the Figure 2.11. As it can be seen from the Figure 2.11 the remote control unit consist of these main parts: microcontroller, comparator, two displays, voltage set encoders, and control buttons.

The remote control receives the capacitor banks voltage measurements from main control circuit. Measurements are converted in optic converter and sent to the comparator. The measurement readings are compared with the set ones. To ensure safety the “Fire” operation can be performed only on the remote control unit.

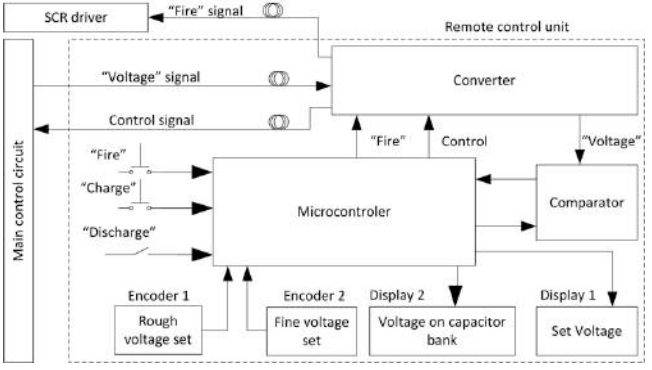

Fig. 2.11. Remote control unit of the pulsed magnetic field generator

The Figure 2.12 represents the simplified diagram of the main control circuit. The main control unit consist from these main parts: ADC converter, microcontroller, relay K2 and the fibre optics converter. The main control circuit is responsible for the control of the whole system except the “Fire” operation, which can be performed only in remote control unit.

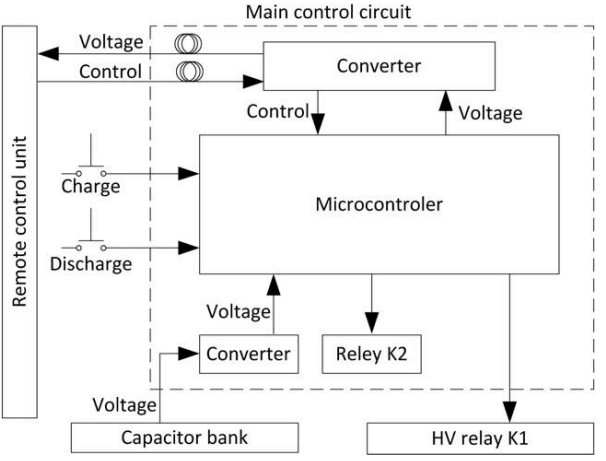

Fig. 2.12. Main control circuit

To ensure safe work of the facility, the discharge operation will be implemented in cases of lose of power or if the generator is turned off.

2.2. Microsecond High Magnetic Field Square Shaped Pulse Generator

In this section the developed portable microsecond pulse magnetic field generator capable to generate square shape magnetic field pulses with amplitudes up to 5 T and the pulse duration from 3 μs to 25 μs will be presented. The computer simulation model using the PSPICE software package was developed to investigate the transient processes in the electrical circuit of the microsecond high magnetic field square shaped pulse generator. The computer simulation model and the analysis of the transient processes is presented. The designed prototype of the microsecond magnetic field square shaped pulse generator is used to investigate the biological objects in the microsecond high-pulsed magnetic fields. For this application, magnetic field pulses with amplitudes up to 5 T are required. The rise and fall time of the generated pulse

should be as fast as possible to induce as high as possible electric field inside the cuvette (see Equation (1.18)). For these reason the magnetic field generator capable to generate microsecond magnetic field repetitive square pulses with amplitude up to 5 T, rise time of 2 μs, controllable pulse width from 3 μs to 25 μs and adjustable pulse repetition rate from 1 Hz to 35 Hz was designed and developed.

2.2.1. Computer Simulations of the High Magnetic Field Square Shaped Pulse Generator

To investigate the transient processes the computer simulation model, using the PSPICE simulation package, of the developed microsecond high magnetic field repetitive square shaped pulse generator is created and presented in this section. The analyses of the transient processes in the developed circuit are presented as well. The created PSPICE computer simulation model of the developed microsecond high magnetic square shaped pulse generator is shown in the Figure 2.13. As it can be seen the simplified simulation model consists of 4 MOSFET switches U100–U400, connected in series and in parallel, 200 μF capacitor bank C10, 2 kV power source, 4.1 μH inductor L1 as a load, ballast resistor R1, crowbar diode D2, crowbar resistor R2 and RC snubber circuits, which are connected in parallel to the MOSFET switches.

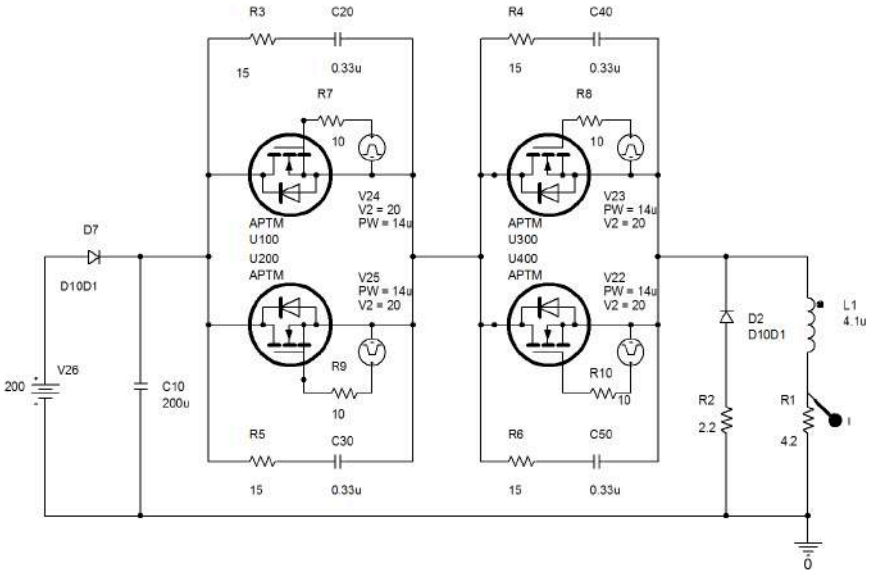

Fig. 2.13. Simulation model of the microsecond pulsed magnetic field generator

As it can be seen from the Figure 2.13, to protect the MOSFET switches from the reverse voltage and the overcurrent spikes during the pulse generation, the snubber and the crowbar circuits was implemented into the PSPICE simulation model. Also the ballast resistor R1, which acts like a pulse-forming device in the circuit and in the same time protects the MOSFET switches from the reverse voltage during the pulse was implemented into the circuit. To ensure safe work of the developed circuit these main protection and pulse forming components must be analysed.

The Figure 2.14 shows the simulated magnetic field dependence on the crowbar resistance R2 using the 4.1 μH inductor. As it can be seen the rise time of the pulse doesn't depend on the crowbar circuit.

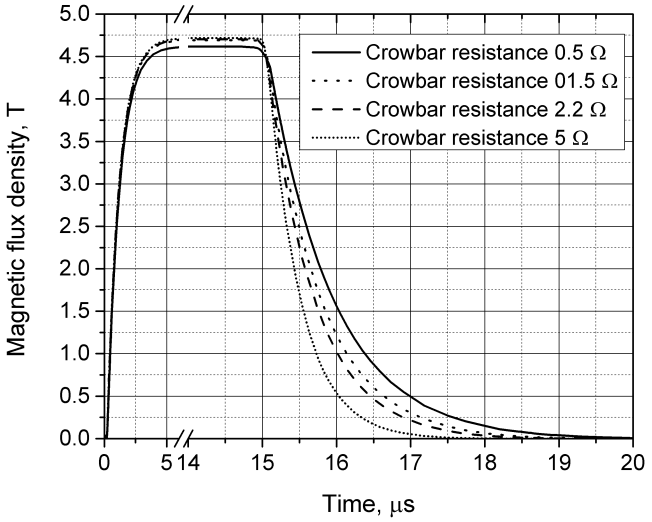

Fig. 2.14. Simulated magnetic field pulse dependence on the crowbar resistance R2

As it can be seen from the Figure 2.14 the decay time of the magnetic field pulse in the 4.1 μH inductor strongly depends on the crowbar resistance. The fall time measuring from 90% to 10% of the pulse, increases form 1 us using the 5 Ω crowbar resistance to 2.5 μs using the resistance of 0.5 Ω. For the investigation of the biological objects in the pulsed magnetic fields the rise and fall times must be as fast as possible. Therefore the resistance of the crowbar circuit must be selected as big as possible

Nevertheless the crowbar circuit protects capacitor banks and semiconductor switches from reverse voltage and overcurrent spikes during the pulse. The Figure 2.15 shows simulated current pulse in the 4.1 μH inductive

load with and without crowbar circuit. As it can be seen the current spikes can be eliminated by implementing the crowbar circuit.

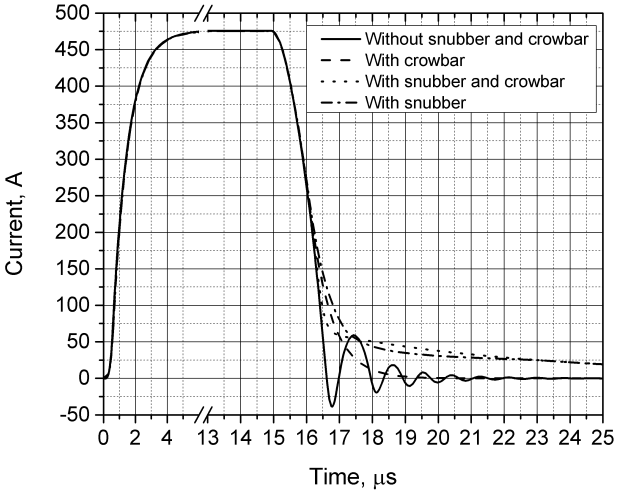

Fig. 2.15. Simulated current pulse on 4.1 μH inductive load with and without crowbar and snubber circuits

The Figure 2.16 shows the voltage drop on the MOSFET switches during the pulse dependence with and without crowbar circuit.

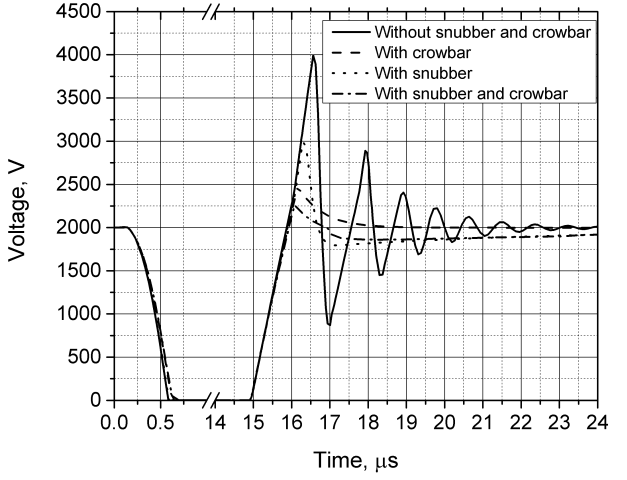

Fig. 2.16. Simulated voltage drop on the MOSFET switch using 4.1 μH pulsed inductor as a load with and without snubber and crowbar circuits

The revers voltage on the MOSFET switches with amplitude of the 4 kV can be observed if no crowbar circuit is implemented into the system. As it can be seen the crowbar circuit eliminates the overcurrent's on the MOSFET switch. The resistance of the crowbar circuit must be as low as possible to ensure protection of the MOSFET switches. As it can be seen in the Figure 2.16 using 4.1 μH inductive load the MOSFET switches without snubber circuit are exposed to reverse voltage with amplitude of 500 V, which can damage the switch. With the proposed snubber circuit configuration the voltage spikes on the MOSFET switches are minimized from the 500 V to 250 V, which together with crowbar circuit ensure safe operation of the developed microsecond high magnetic field square shaped pulse generator.

The Figure 2.17 shows the reverse voltage dependence on the ballast resistor R1 using the 4.1 μH inductive load.

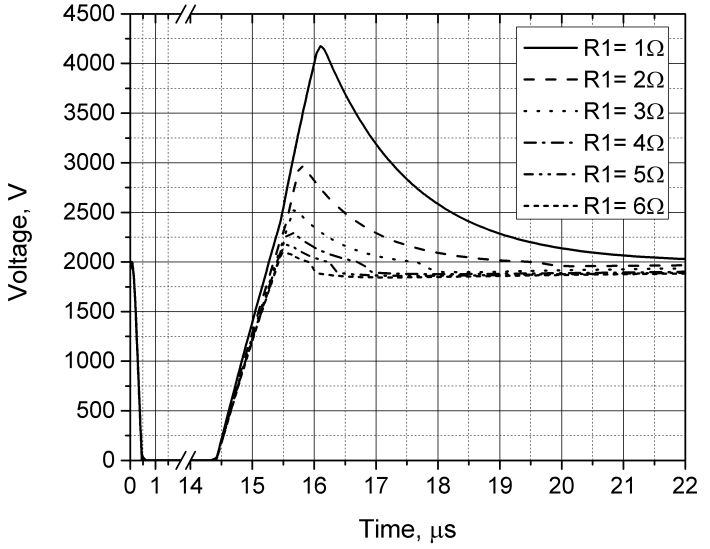

Fig. 2.17. Simulated voltage drop on the MOSFET switch using 4.1 μH inductor dependence on the ballast resistor R1

As it can be seen in the Figure 2.17 by implementing the ballast resistor to the developed circuit the influence of the inductive load to the MOSFET switch can be minimized by increasing the resistors R1 value. Nevertheless the R1 resistor acts as a pulse-forming device in the circuit and defines the maximal value of the current pulse in the inductive load.

The Figure 2.18 shows the current in the 4.1 μH inductor dependence on the ballast resistor value.

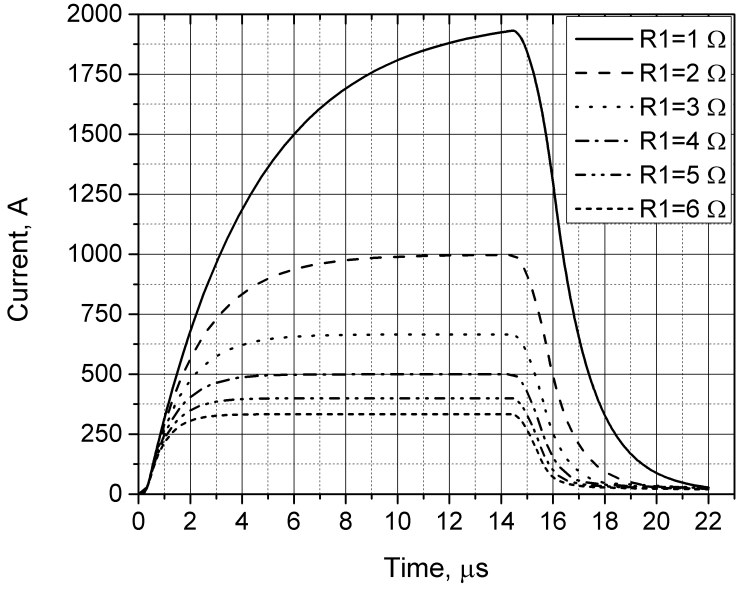

Fig. 2.18. Simulated current pulse in the 4.1 μH inductor dependence on the ballast resistor R1

To generate square shaped pulse magnetic field with fast rise and decay time in the multilayer inductor, the influence of the inductive load must be minimized to minimum. As it can be seen in the Figure 2.18 the by increasing the value of the ballast resistor R1, the RLC circuit changes from critical damped to underdamped circuit. To generate square magnetic field pulses with fast rise and decay time the ballast resistor value must be as high as possible. Nevertheless the current value in the inductor must be high enough to generate required magnetic field strength of 5 T.

Also to protect high power MOSFET switches the snubber circuit was implemented in to the system. As it can be seen from the Figure 2.13 the RC snubber circuit topology was chosen for the MOSFET switch protection during the turn–of procedure. For snubbert circuit consisting from resistor R3–R6 with resistance of 15 Ω and capacitors C10–C50 with capacitance of 0.33 μF. Snubber circuits are connected in parallel to the MOSFET switches.

The Figure 2.19 shows the generated magnetic flux dependence on the snubber resistance.

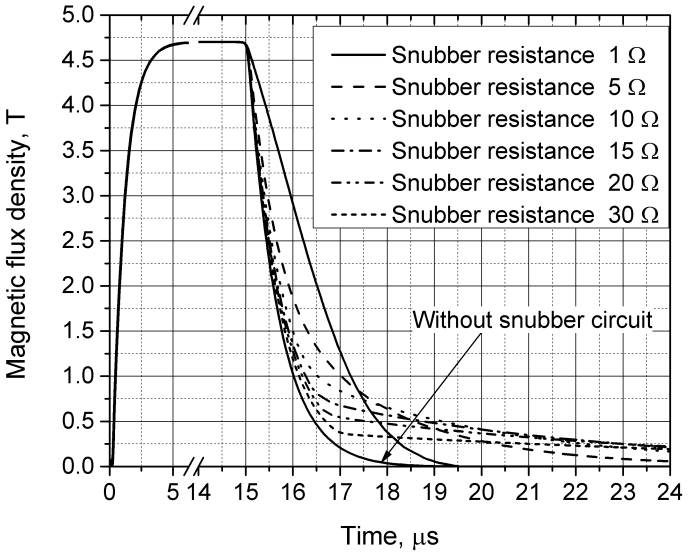

Fig. 2.19. Simulated magnetic field pulse using 2.1 μH pulsed inductor as a load

As it can be seen from Figure 2.19 the rise and fall time of the generated pulse are 2 μs and 2.5 μs respectively, during the simulation capacitor voltage was set to 1.6 kV, ballast resistor 4.2 Ω and the 2.1 μH and 4.1 μH pulsed inductors was chosen for the further investigation.

2.2.2. Developed Microsecond Magnetic Field Square Shaped Pulse Generator

The simplified diagram of the developed microsecond high magnetic field square shaped pulse generator is presented in the Figure 2.20. The designed prototype consist of these main parts: 1) specially designed and developed 2 kV and 20 mA high voltage power source, based on flyback converter topology, 2) two energy storage banks, which consists from five 4.7 mF and 400 V electrolytic capacitor banks connected in series and two 1 kV and 1 mF polypropylene capacitor banks connected in series as well, two energy storage banks are connected in parallel, 3) voltage measurement part, 4) high power switching part, which consist of four fast *dI/dt* = 68 ns, high voltage 1.2 kV and high surge current with amplitude of 463 A MOSFET switches connected in series and parallel, 5) crowbar and snubber circuit for capacitor and semiconductor switch protection, 6) specially designed pulsed inductor with ballast resistor, 7) specially designed control circuit for MOSFET triggering

operation, voltage measurement, capacitor bank charge and high voltage power supply control operation and of the human interface.

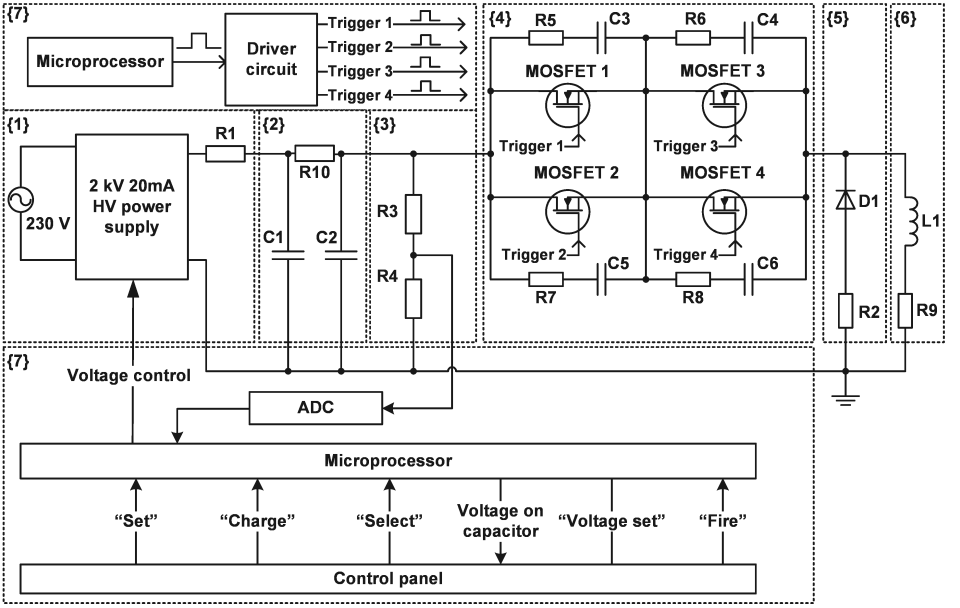

Fig. 2.20. Simplified diagram of microsecond high magnetic field square shaped pulsed generator

The developed high magnetic field square shaped pulse generator will be used to investigate high up to 5 T square shaped pulse magnetic field influence to the biological cells. For these applications square magnetic fields pulses with amplitude up to 5 T, fast magnetic field rise and fall time and controllable pulse width from 3 μs to 25 μs, amplitude and pulse repetition time from 1 Hz to 35 Hz must be developed. To reach such high magnetic field square shaped pulses is complicated and challenging task. As it was mentioned before, the fastest controllable semiconductor switches are MOSFETs. Due to this fact four MOSFET switches with (1.2 kV) and high surge current 463 A were selected and implemented into the circuit. As it can be seen on Figure 2.20, switches are connected in series to enhance voltage and in parallel to increase current commutation capability. The high powers MOSFETS (APTM120U10SAG) with series and parallel power diodes with fast recovery time (265 ns) were selected. The switches must be triggered simultaneously to ensure capability of commutation of 2 kV and 900 A pulses. In worst case

scenario trigger delay can cause irreversible damage to one or even all MOSFET switches.

The image of the developed microsecond high magnetic field square shaped pulse generator is shown on Figure 2.21.

Fig. 2.21. Picture of developed microsecond pulsed high magnetic field generator

To reach such high magnetic field square shaped pulses is complicated and challenging task. As it was mentioned before, the fastest controllable semiconductor switches are MOSFETs. Due to this fact four MOSFET switches with (1.2 kV) and high surge current 463 A were selected and implemented into the circuit. As it can be seen on Figure 2.20, switches are connected in series to enhance voltage and in parallel to increase current commutation capability. The high powers MOSFETS (APTM120U10SAG) with series and parallel power diodes with fast recovery time (265 ns) were selected. The switches must be triggered simultaneously to ensure capability of commutation of 2 kV and 900 A pulses. In worst case scenario trigger delay can cause irreversible damage to one or even all MOSFET switches. Due to this fact, the designed and developed high power MOSFET driver circuit that can be seen on Figure 2.22 was implemented into the developed high magnetic field generator circuit. Proposed driver circuit ensures synchronous and galvanically isolated triggering operation. As it can be see from Figure 2.22, the trigger circuit consists of three high speed (rise and fall time 3 ns) galvanically isolated dual channel 4 A MOSFET drivers and ATXmega microprocessor. When the "FIRE" button is pushed the ATXmega generates selected pulse width, amplitude and frequency common control pulse to the galvanically separated dual input and output MOSFET driver DR1. The driver DR1 as implemented to the circuit to establish synchronous input signals to driver DR2 and DR3 in addition DR1 ensures isolation of high voltage circuit from control circuit. DR1 has the same

output ground as ATXmega circuit as it is no need of galvanic isolation. Drivers DR2 and DR3 have four galvanic isolated outputs as it is necessary to control series connected semiconductor switches.

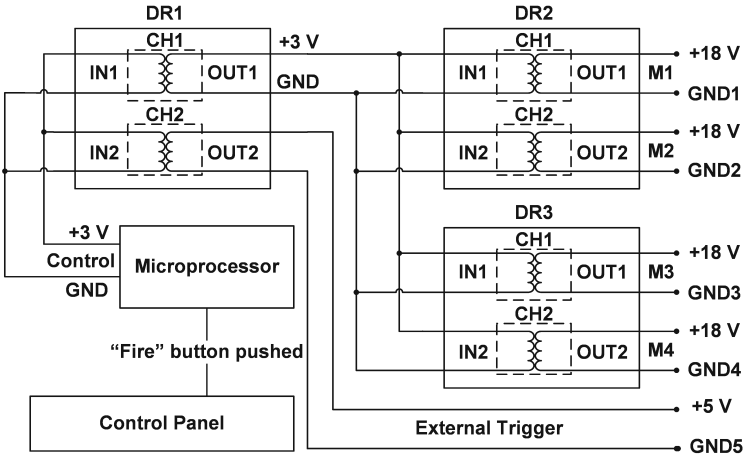

Fig. 2.22. High power MOSFET driver circuit

The Figure 2.23 represents the output signal of the developed driver for high power MOSFET switches.

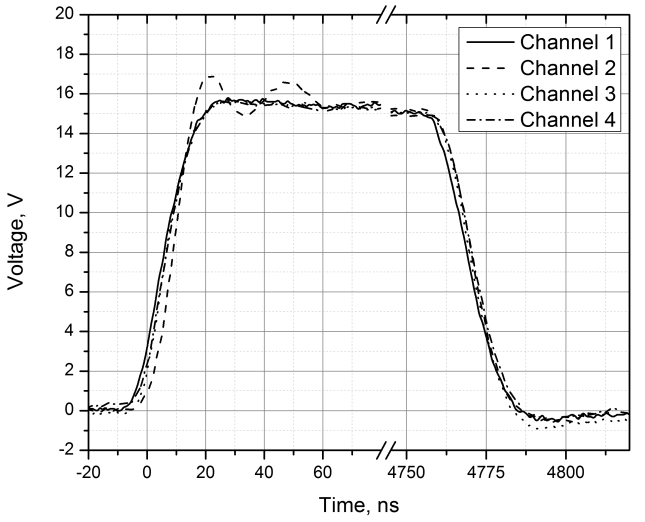

Fig. 2.23. Driver output signal

The MOSFET switches are triggered by 15 V and 3.5 A signal which length is proportional to control signal generated by the ATXmega microprocessor.

As it can be seen the four channel driving circuit generates simultaneous trigger signals with no delay. The rise and fall time of 20 ns ensures no influence to the generated pulse as the power MOSFET opening time is 265 ns.

To ensure synchronous measurement or experiment capability of the developed pulsed power generator the external output trigger signal (EXT.T) was implemented to the circuit. The external galvanically isolated 5 V output signal is formed in driver DR1 which pulse width is equal to the output signal. To ensure safe work of the generator the control and power circuits were galvanically isolated. The galvanic isolation between all outputs and inputs is equal to 5 kV.

The developed pulsed power generator is capable to generate 5 T magnetic field pulses with pulse width up to 25 μs and the pulse repetition rate of 35 Hz. For this operation, huge amount of energy is required. Due to this fact dual energy storage bank were implemented into the circuit. Energy storage bank consists of two different types of the capacitor banks. First capacitor bank is responsible for energy storage and it consists from five 4.7 mF and 400 V electrolytic capacitors connected in series which total makes 2 kV and 940 μF.

The electrolytic capacitors are ideal for high power storage but it can't be used for pulsed power application due to their high self-inductance and incapability to withstand high surge currents. For this purpose the 2 kV and 100 μF fast, low self inductance polypropylene capacitor bank was implemented to the circuit. The polypropylene capacitor banks ensure fast rise time of the generated magnetic field pulse. The polypropylene capacitor banks are fed from electrolytic capacitors that brings perfect ration of energy and fast discharge. The proposed energy storage system ensures the 5 T magnetic field square shaped pulse generation with pulse repetition time of 35 Hz and less then 10% decline of the pulse amplitude, which gives us the possibility to investigate object of interest in high *dB/dt* and in queasy stationary magnetic fields simultaneously.

To investigate crowbar and snubber circuit influence the two microinductors with inductance of 1.6 μH and 4.1 μH were selected. The 15 μs magnetic field pulses with amplitude from 3.1 T to 4.3 T were generated. The generated magnetic field pulse with and without crowbar circuit with different inductors can be seen on Figure 2.24. As it can be seen the rise time of the generated magnetic field pulse is 2.5 μs with 1.6 μH inductive load and 5 μs with 4.1 μH inductive load. The fall time of the pulse is 5 μs and 10 μs respectively.

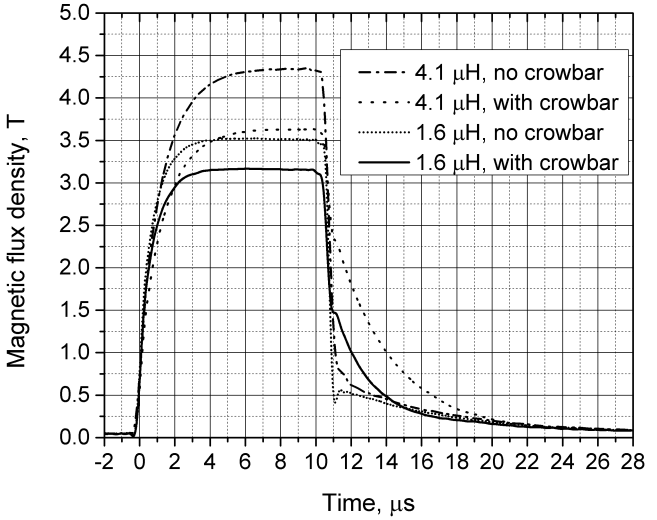

Fig. 2.24. Generated 15 μs magnetic field pulse using 1.6 μH and 4.1 μH inductive loads with and without crowbar circuit.

As it can be seen from the figure, the fall time of the pulse is strongly dependant on the crowbar and snubber circuits. The fall time with both loads with no crowbar and snubber circuit will be less then 1.5 μs. As wee can see the influence of the both circuits starts in 16 μs and in this time the *dB/dt* from $6.8 \cdot 10^5$ T/s decreases to $2.75 \cdot 10^5$ T/s.

To ensure uninterruptable power supply to energy storage bank the high voltage DC power supply was created and implemented into the system. Proposed power supply can generate voltages from 0 to 2 kV with output current maximum of 20 mA. Created voltage supply is based on the flyback converter topology. The simplified schematic diagram of high voltage power supply can be seen on Figure 2.25. As it can be seen the created power supply consist of main 7 parts: 12 volts 3 A DC voltage power supply, two high power MOSFET switches M1 and M2, dual output MOSFET driver with galvanic isolation up to 6 kV, pulse width modulator, two high voltage pulse transformers T1 and T2, two high voltage capacitor banks C1, C2 and shunt resistor R.

The presented HV power supply is based on flyback converter topologies. Each pulse transformer, which is implemented into the circuit, can produce voltage up to 1 KV. To ensure uninterruptable 2 kV voltage the two flyback converters were connected in parallel. In the output of the pulse transformers the voltage doubler circuit consisting of two 1.6 μF and 1.35 kV capacitor banks were implemented.

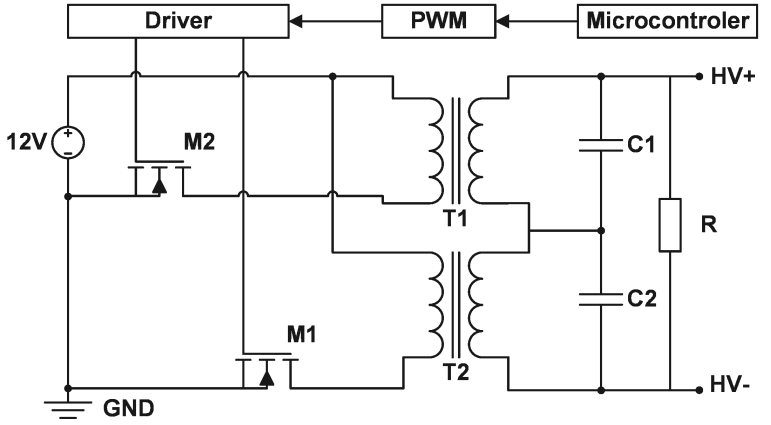

Fig. 2.25. Simplified diagram of created 2 kV 20 mA power supply

To ensure safe work of the whole system the 50 W and 84 kΩ shunt resistor R were implemented into the circuit.

2.3. Non-Destructive Microinductors for High-Pulsed Magnetic Field Generation

It is important to evaluate technical possibility to generate high up to 10 T microsecond magnetic field pulses with inductors driven by SCR thyristors and microinductors driven by MOSFET transistors and to specify the structure of prototype for further experimental investigations. The design of the inductors involves many degrees of freedom. In most pulsed power applications multilayer inductors are used and the inner, outer radiuses, length of winding, pulse duration, peak magnetic field are the basic parameters for further calculations. A lot of parameters and steps of further optimization define the final configuration of the inductor. The development of pulsed inductor used in pulsed power application is expensive and long lasting work. To avoid expensive and long lasting experiments the numerical calculations or computer simulations must be done. In general case magnetic field can be calculated using Biot-Savart Law application to each current loop. A current loop with radius R located in x–y plane centred at the origin and carried a current I in cylindrical coordinate system creates a magnetic field H that can be defined by Equation (2.1).

$$H = \begin{bmatrix} \frac{I}{2\pi}\frac{l}{r\sqrt{\left(R+r\right)^2+l}}\left(-K\left(k^2\right)\right)+\frac{R^2+r^2+l^2}{\left(R-r\right)^2+l}E\left(k^2\right) \\ \frac{I}{2\pi}\frac{l}{r\sqrt{\left(R+r\right)^2+l}}\left(+K\left(k^2\right)\right)+\frac{R^2-r^2-l^2}{\left(R-r\right)^2+l}E\left(k^2\right) \end{bmatrix}, \quad (2.1)$$

where H – magnetic field strength; l, r – axial and radial distances between the centre of a loop and the point of measurements; $K(k^2)$, $E(k^2)$ – complete elliptic integrals of the first and the second kind when

$$k^2 = \frac{4Rr}{\left(R+r\right)^2+l^2}. \quad (2.2)$$

Magnetic field components H_x, H_y, H_z can be calculated using the Equation (2.3):

$$H = \begin{bmatrix} \frac{x}{r}\frac{I}{2\pi}\frac{l}{r\sqrt{\left(R+r\right)^2+l}}\left(-K\left(k^2\right)\right)+\frac{R^2+r^2+l^2}{\left(R-r\right)^2+l}E\left(k^2\right) \\ \frac{y}{r}\frac{I}{2\pi}\frac{l}{r\sqrt{\left(R+r\right)^2+l}}\left(-K\left(k^2\right)\right)+\frac{R^2+r^2+l^2}{\left(R-r\right)^2+l}E\left(k^2\right) \\ \frac{I}{2\pi}\frac{l}{r\sqrt{\left(R+r\right)^2+l}}\left(+K\left(k^2\right)\right)+\frac{R^2-r^2-l^2}{\left(R-r\right)^2+l}E\left(k^2\right) \end{bmatrix}. \quad (2.3)$$

In case of multilayer inductor construction with n turns the magnitude of the resulting magnetic field strength is defined as superposition of n magnetic loops as it shown in Equation (2.4):

$$\left|H\right| = \sqrt{\left(\sum_{m=1}^{n} H_{m,x}\right)^2+\left(\sum_{m=1}^{n} H_{m,y}\right)^2+\left(\sum_{m=1}^{n} H_{m,z}\right)^2}. \quad (2.4)$$

However such, approximation does not include wire diameter, thickness of insulation and other important parameters that are present in the real inductors. Analytical evaluation of all these parameters becomes very complex and for this purpose the finite element method (FEM) could be applied for evaluation of the more explicit inductor model with defined designed features.

Also the proposed analytical approximations are applicable for widely spread inductors of cylindrical shape, however, it will introduce errors in estimation results of the planar inductors, where the structure is typically orthogonal due to the microfabrication limitations and process cost. Typical arrangement of windings of the planar inductors is shown in Figure 2.6.

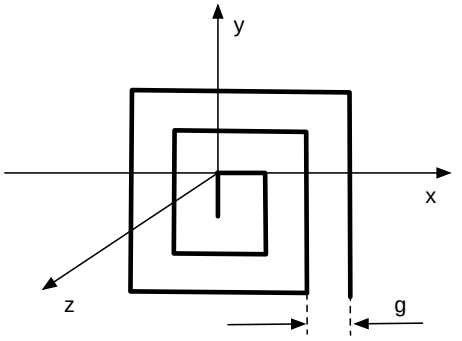

Fig. 2.26. Typical arrangement of windings of the planar inductor (Novickij V., Grainys, Novickij J. 2013)*

As it can be seen in Fig. 2.26 four wire segments form a turn. Respectively, the superposition of the magnetic field of each wire segment must be evaluated. Magnetic field components H_x, H_y, H_z will take form as shown if Equation (2.5), (2.6), (2.7):

$$H_x = \frac{zI}{4\pi\left((a-x)^2+z\right)}\left(\frac{L-y}{\sqrt{(L-y)^2+(a-x)^2+z^2}}+\frac{L+x}{\sqrt{(L+y)^2+(a-x)^2+z^2}}\right), \quad (2.5)$$

$$H_y = -\frac{zI}{4\pi\left((a-y)^2+z\right)}\left(\frac{L-x}{\sqrt{(L-x)^2+(a-y)^2+z^2}}+\frac{L+x}{\sqrt{(L+x)^2+(a-y)^2+z^2}}\right), \quad (2.6)$$

*The reference is given in the list of publications by the author on the topic of the dissertation

$$H_z = -\frac{(a-y)I}{4\pi\left((a-y)^2+z\right)}\left(\frac{L-x}{\sqrt{(L-x)^2+(a-y)^2+z^2}}+\frac{L+x}{\sqrt{(L+x)^2+(a-y)^2+z^2}}\right), \quad (2.7)$$

where *x, y, z* are the Cartesian coordinates of the point where the magnetic field is calculated, *I* is the current, *a* is the distance of the wire from the *x* – *z* plane, *L* is the half length of the wire segment.

If the magnetic field is calculated near the conductor the expression could be further simplified and take form Equation (2.8):

$$H_z = -\frac{I}{4\pi y}\left(\frac{L-x}{\sqrt{x^2+y^2+L^2-2Lx}}+\frac{L+x}{\sqrt{x^2+y^2+L^2+2Lx}}\right). \quad (2.8)$$

The amount of influencing factors is big, therefore, numerical methods such FEM was chosen for more accurate estimation of the parameters.

2.3.1. Simulation of the Inductors

One of the main components of the high-pulsed magnetic fields generators are the pulsed inductors, where magnetic field is generated. Inductors directly influence the characteristics such as peak amplitude, rise and fall times also the total pulse length of the generated magnetic field pulse. As it was mentioned before the inductors must be fabricated for each experiment specifically. The fabrication of the non-destructive inductors for the pulsed power application is expensive and takes a long time. For this purpose the mathematical calculation on the inductors must be done to evaluate the main generated pulse characteristics in advance and to avoid expensive and long lasting fabrication processes. For this purpose the finite element analysis using COMSOL software package was performed. The microinductors for investigation of biological effects of pulsed magnetic fields on biological cells (Inductor “A” and Inductor “B”) and the inductor for the calibration experiments of the CMR-B-Scalar magnetic field sensor (Inductor “C”) have been simulated. The structure of the inductors is shown in Figure 2.27.

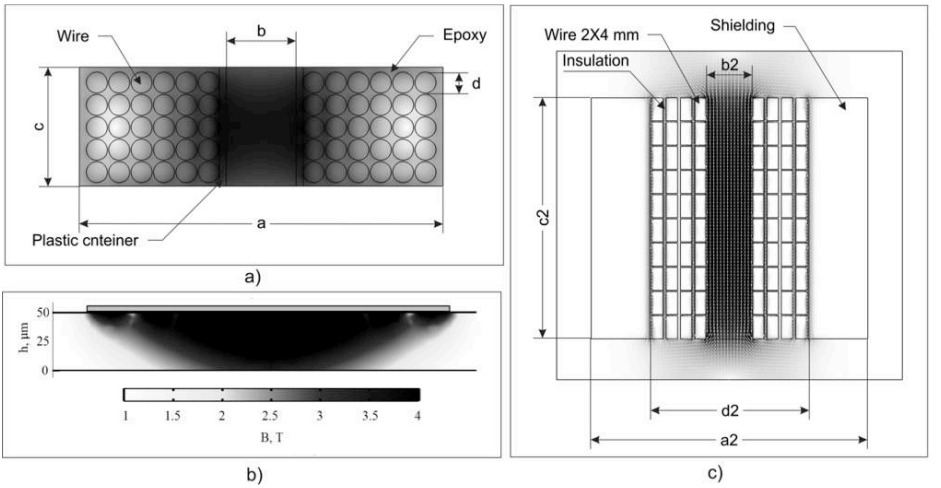

Fig. 2.27. The geometry of inductors used in simulations a) multilayer microinductor "A" used for biological experiments b) planar microinductor "B" for biological experiments (Novickij V., Grainys, Novickij J. 2013)* c) multilayer inductor "C" for CMR-B-Scalar sensor calibration

As it can be seen from the Figure 2.27 a) the inductor "A" has 5 windings and 6 layers. The copper wire of the diameter d = 0.4 mm was chosen. The copper wire is covered with enamelled insulation with breakdown voltage of >7 kV. To maintain the Lorenz force and avoid voltage breakdown each layer of the inductor is filled with epoxy. The effective inner volume is protected with plastic container – cuvette, where the objects of the investigation can be placed. The plastic container also helps to avoid the contamination of the investigation objects due to the interaction with the inductor wires. The inner effective volume of the inductor is 3 µl. The inner diameter b = 2 mm, the height of the inductor c = 2.5 mm and the outer diameter of the inductor a = 6 mm.

The inductor "B" is a planar pancake inductor that was also developed for the investigation of the biological objects in pulsed magnetic fields. The geometrical parameters of the planar inductor also can be seen in the Figure 2.27 b). In this case an orthogonal structure was proposed with the maximum length of the wire segment equal to 400 µm. The thickness of the conductor layer is usually limited by the microfabrication process. The thickness of 10 µm has been chosen in the simulation.

*The reference is given in the list of publications by the author on the topic of the dissertation

The geometry of the inductor "C" which will be used for the calibration of the CMR-B-Scalar magnetic field sensors is shown in the Figure 2.27 (c). As it can be seen the inner radius of the inductor is b2 and equal to 12 mm, outer radius d2 – 30 mm and the height c2 of the pulsed inductor is 40 mm. The inductor was wound using the copper wire with cross-section dimensions of 4×2 mm. The wire is covered with enamelled insulation with breakdown voltage of >7 kV. Each layer was covered with epoxy. The developed inductor consists from 10 windings and 4 layers, which ensures generation of magnetic fields with amplitudes >10 T with inhomogeneity of <1% in the volume of 50 mm^3. One of the main parameters for the calibration of the sensors is to ensure inhomogeneity of the generated magnetic field to be below 1%.

The main parameters of the created microinductors for the investigation of the biological effects of the magnetic field as well as inductor developed for the calibration experiments of the CMR-B-Scalar magnetoresistive magnetic field sensors are shown in Table 2.2.

Table 2.2. Values of the parameters used in simulation of the microinductors

Parameter	Denotation	Values of the Inductor "A"	Values of the Inductor "B"	Values of the Inductor "C"
Number of windings	N	5	1	10
Number of layers	L	6	3	4
Inductance	L, H	$2.3 \cdot 10^{-6}$	0.01	$15.5 \cdot 10^{-6}$
Wire diameter	D_w, mm	0.4	10 µm x 100 µm	4x2
Wire material		Copper	Copper	Copper
Insulation	U, V	>7 kV	–	>7 kV
Insulation material	–	Enamelled, Epoxy	PDMS	Enamelled, Epoxy
Inner radius	r_i, mm	0.7	0	1
Outer radius	r_o, mm	2.5	0.20	3.5
Inner surrounding	–	Water	PDMS	Air
Outer surrounding	–	Air	Cell medium	Air
Current	I, A	550	220	11000
Generated magnetic field	B, T	5	4	12

All simulations were performed using following methodology:

- All simulations were held using AC/DC package, transient time dependent analysis.

- Using built-in COMSOL CAD system, geometrical model of the microinductor was created. (The 2D axisymmetric space dimension was chosen for geometrical model construction, as it is not necessary to use 3D dimension to investigate axial magnetic field in the center of the inductor. More over the 2D simulation requires less computation time and computer resources.
- The materials of the separate microinductor parts were set. (To ensure real environmental simulation conditions all parts of the microinductors was implemented into the model. The outer boundary was set to the air, wire is made from copper, inductors "A" effective volume – water, inductors "B" effective volume – glass, "C" – air and the plastic container to isolate effective volume from the inductor).
- The "Magnetic Fields (mf)" physics and "Coil Group" domain was selected for simulation of multilayer inductive inductor. (Coil Group domain describes each winding of the inductor as a separate inductor. This implements the influence of the gaps between the windings into simulation. By approximation that in all inductors the same amplitude and shape current pulse is generated. The initial simulation temperature was set to room temperature 21 °C. The currents amplitude and pulse waveform was determined in global definitions.)
- Using global definition, the current pulse waveform and amplitude was set. (The current pulse and amplitude was set considering the current pulse shape and amplitude in developed microsecond pulse generator. Current amplitudes are given in Table 2.2).
- The mesh of the developed microinductor was created. (To ensure best precision in the areas of interest, the "User-define" mesh was chosen. The "Free Triangular" mesh structure was selected as it is flexible to model complex geometries and their boundaries. For inductors "A" and "C" the element size differs from 0.2 μm in the middle of the inductor, where the precision is required to 50 μm in the outer boundaries. For inductor "B" the mesh size differs from 0.1 μm to 20 μm.
- The finite element calculations were made using time dependent study model. (The time range of the time dependent study was set from 3 μs to 900 μs considering the current pulse width set in global definitions.

The inductor "A" structure is limited by the effective inner volume requirement and the need for the highest magnetic field generation capability with the minimum current supplied. Due to this fact the geometry of 5 layers and 6 windings with inner diameter of 2 mm was selected. The created inductive inductors 3D model and the generated magnetic field flux density in the inductor can be seen on Figure 2.28. The 5 T magnetic field was generated in the centre

of the inductor. To generate magnetic fields with amplitudes in the range of 5 T in the effective volume of 2–3 μl the pulse current with amplitude of the 550 A must be applied into inductive load.

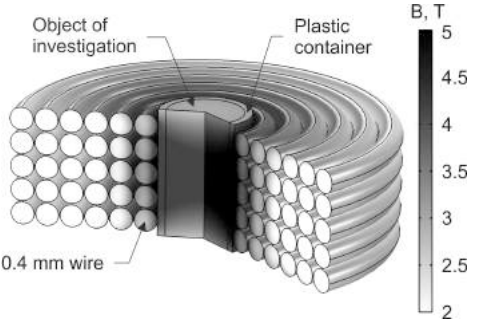

Fig. 2.28. 3D projection of the developed microinductor "A" and the simulated magnetic flux density

It should be noted that the peak current is also limited by the generated Joule heat inside the windings of the inductor, which should also be taken into account.

The simulated magnetic flux density of the "Inductor B" can be seen on Figure 2.29. As it can be seen from the figure the maximal value of magnetic flux density with amplitude up to 4 T was created. The current in the inductor during the simulations was set to 220 A. A dual structure or the Helmholtz construction of inductor "B" could be also implemented to improve the homogeneity by driving the microinductor with separate switches. The pancake or orthogonal planar inductor construction is very promising in experiments with biological cells, however issues with biological objects handling may occur.

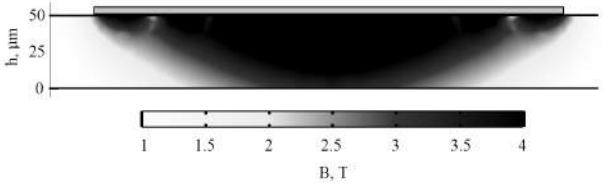

Fig. 2.29. The simulated magnetic flux density in inductor "B" (Novickij V., Grainys, Novickij J. 2013) [*]

[*]The reference is given in the list of publications by the author on the topic of the dissertation

Coupled with the microfabrication challenges and the cost of photolithography masks the inductor "B" features major drawbacks, therefore the inductor "A" was assumed to be a more advantageous structure for treatment of biological objects.

For calibration of the sensors the inductor with high effective volume must be developed. The inductor geometry and the generated magnetic flux density with maximal amplitude up to 12 T are shown in the Figure 2.30. To ensure high accuracy of calibration of the magnetic field sensor the inhomogeneity of the generated magnetic flux density of 1% in the area of 8 mm^3 must be ensured. To fulfil such objectives the construction of the 4 layer and the 10 windings inductor was chosen. As it can be seen from the Figure 2.30 (a) the inhomogeneity of the generated magnetic field in Z axis doesn't exceed 1% in the volume of the 50 mm^3. The simulation results show that the selected inductors geometry equipped with created microsecond high magnetic field asymmetric shaped pulse generator based on the SCR thyristors switches can be used in the calibration experiments of the CMR-B-Scalar magnetoresistive sensors.

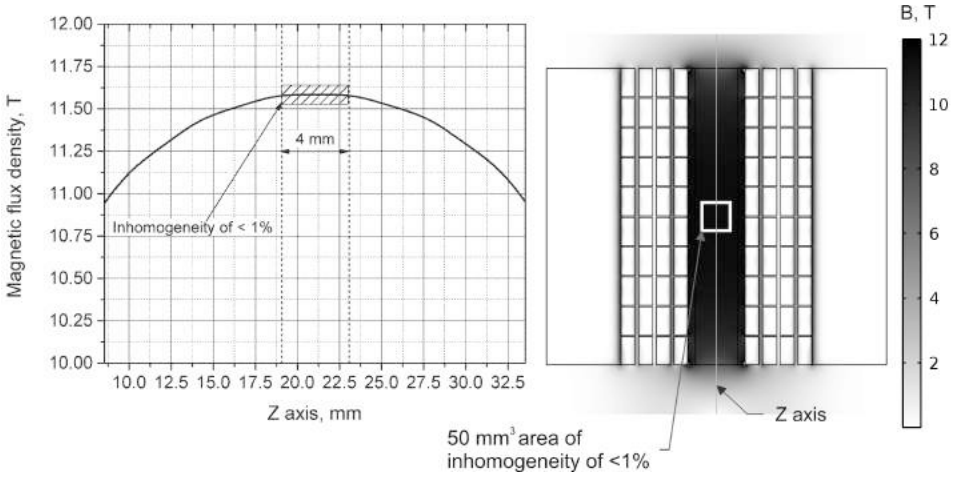

Fig. 2.30. The inductor geometry and the simulated magnetic flux density with maximal amplitude up to 12 T

2.3.2. Simulated Joule Heating

One of the side effects of the generating high magnetic fields with amplitudes over 1 T is the Joule heating effect occurring in the windings of the inductor, due to the high currents flowing threw the inductive load. The temperature rise due to Joule heating can reach temperatures over 100 °C and affect the objects of the

investigation. For biological experiments the estimation of the best balance between maximum possible pulse repetition frequency, and the minimum resultant Joule heating, while the effective volume and the generated magnetic field pulse must be kept constant. The FEM simulation with inductor "A" has been performed. Different simulations were done with various *N/L* (*N* – number of windings, *L* – the length of the inductor) ratio of the inductor "A" as well as different current amplitude. The pulse width for all simulations was set to 3 µs. The resultant simulated temperature increase in the medium after maximum of 400 pulses with pulse repetition of the 35 Hz is presented in the Figure 2.31. It should be mentioned that the temperature increase over 40 °C can cause the death of the biological cells.

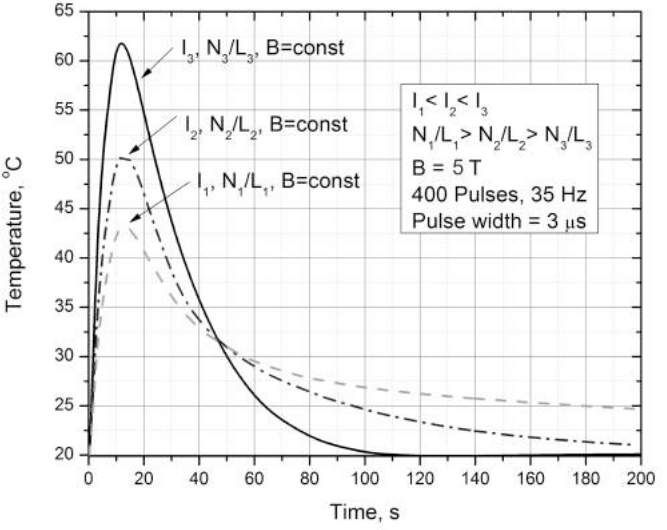

Fig. 2.31. Simulated temperature increase due Joule heating (Grainys, Novickij, Švedienė 2014) *

As it can be seen from the Figure 2.31 it is possible to achieve the constant magnetic flux density with amplitude of the 5 T by alternating the ratio *N/L* and the maximum current amplitude *I*. The application of higher currents (I_3) results in generation of massive amount of heat in the inductor. However, it should be noted that the inductor is cooled faster and the inductance is lower due to smaller amount of windings and layers, therefore the rise and fall time of the pulse will be lower. On the contrary increase of the amount of windings and layers and the

*The reference is given in the list of publications by the author on the topic of the dissertation

reduction of the current amplitude results in lower heat generation. The cooling of the inductor and the cuvette medium takes longer and the rise and fall times will be increased due to inductance increase. Based on the simulation data it has been decided to fabricate 6 layers 5 windings representing marginal case and investigate the thermal influence on the vitality of the biological objects.

It can be noted that at the time of 0.03 s, which corresponds to the frequency of 33 Hz the temperature increase is in the range of 0.03 °C. Taking into account all the approximations specified it was determined that 250 magnetic field pulses can be shot with repetitive frequency of 35 Hz and the resultant medium temperature will be still ≤ 30 °C and the influence of the Joule heating to the objects of the investigation can be neglected. However the temperature rise due to Joule heating must be taken into the account if the geometrical changes of the inductive inductors appears.

2.4. Conclusions for the Chapter 2

1. The structures of pulsed magnetic field generator and transient processes in electrical circuits have been investigated. The pulsed magnetic field facility consisting of pulsed capacitor bank, high power SCR thyristor switch and crowbar circuit connected in parallel with pulsed inductor is capable to generate magnetic field asymmetric shaped pulses over 10 T.
2. The distribution of high magnetic fields and Joule heating of multilayer inductor has been investigated. It was found that non homogeneity of multilayer inductor does not exceed 1% limit in 50 mm^3 what is acceptable for the magnetoresistive sensors calibration.
3. The structure, magnetic field distribution and Joule heating of planar and multilayer micro inductors are investigated. Multilayer micro inductor has better field homogeneity and it less overheated comparing with planar one due to less values of required current to generate the equivalent magnetic flux density.
4. Microsecond high magnetic field shaped pulse generator consisting of capacitor bank, MOSFET switch and microinductor connected in series with resistive ballast is able to generate magnetic field repetitive square shaped pulses up to 5 T. The integration of the cuvette into multilayer microinductor insures contactless biological experimentation.

3

Application of the Microsecond High Magnetic Field Shaped Pulse Generators

In this chapter the application possibilities of the created high magnetic field shaped pulse generators will be presented and analysed. Using developed microsecond high magnetic field square shaped pulse generator, treatment of the biological objects in high-pulsed magnetic fields will be presented as well. The express calibration experimental results using microsecond magnetic field asymmetric shaped pulse generator will be provided. The following experiments were made with MOSFET and SCR based microsecond magnetic field generator using different pulsed inductor structures to ensure the optimal generated magnetic field pulse characteristics.

Four scientific publications were published on the section topic (Grainys, Novickij, Švedienė 2014; Grainys, Novickij, Stirke 2012)

3.1. Calibration of Magnetoresistive Magnetic Field Sensors

The use of high-pulsed magnetic fields in medicine, military, science or industry has increased rapidly in last few decades. One of the biggest problems is the measurement of such high and rapidly changing magnetic fields. Recently the new CMR-B-Scalar magnetoresistive sensors were developed in the Center for Physical Sciences and Technology (FTMC), which can measure magnetic fields up to 100 T without knowing the magnetic field direction. As it was mentioned the CMR sensors have nonlinear resistance vs. magnetic field dependence, moreover, they are sensitive to temperature changes. Due to these reasons manufactured sensors must be calibrated. The calibrations must be made in wide range of magnetic field and temperatures (these ranges depends from field of sensor's using). For this purpose the special microsecond high magnetic field asymmetric shaped pulse generation system with strict pulsed magnetic field characteristics was developed.

In this section the use of developed microsecond pulsed magnetic field generator based on SCR thyristor switches for CMR-B-Scalar magnetic field sensor's calibration will be presented. The calibration results of sensors will be analyzed.

The calibration of magnetic field sensors was made in pulsed magnetic field by the simultaneously recording of pulses of magnetic field and response of CMR sensor. By assigning of magnetic field value measured at given time to the response value of sensor the calibration curves were created. This method of calibration is possible if the calibrated sensor has no hysteresis effect and is enough quick acting.

The principal circuit of magnetic field generator for these calibrations was the same like on Figure 2.8. The crowbar circuit was used to generate the asymmetrical shape of magnetic field pulse with short rise time and long fall time. This shape of pulse is preference for more exactly sensor's calibration. The inductive inductor of 10 windings and 4 layers with inductance of 15.5 μH was selected. The 5.4 mF capacitor banks were charged to 720 V with resulting total energy of 1.4 kJ. At this charging voltage magnetic field with amplitude up to 13 T in the volume of 50 mm^3 was generated. The cross section of inductive inductor and simulation results of magnetic field distribution is presented on Figure 3.1. It can be see, that in the center of inductor the inhomogeneity of magnetic field doesn't exceed of 1%. At the same figure the calibrated ant reference magnetic field sensors are showed. They were positioned in the center of inductor close one to the other. The calibrated loop sensor was used as reference magnetic field sensor. Loop sensor is often used for measurement of pulsed magnetic field. The output signal of them is proportional to the derivative

of changing of magnetic field. To obtain the true shape of magnetic field the passive integrators are some time used. However, when the shape of magnetic pulse is not sinusoid, using of this integrator can lead to big errors. Therefore, for CMR sensors calibration it was used loop sensor without passive integrator. Integrating of signal obtained from loop sensor was made by the computer.

Due to calibration the resistance changing of CMR sensor was converted to the voltage changing across sensor. For this the potentiometer circuit of measurement was used. The schematic diagram of it is showed on Figure 3.1. As can be seen, the calibrated sensor was connected in series with ballast resistor R_1 (R_1 = 6.4 kΩ) and 2.4 V supply source. For measuring and recording of output signals of loop sensor and CMR sensor the oscilloscope Tektronix DPO4034 was used. The Table 3.1 represents the generated pulse parameters and the parameters of the inductive coil, used in the calibration experiment.

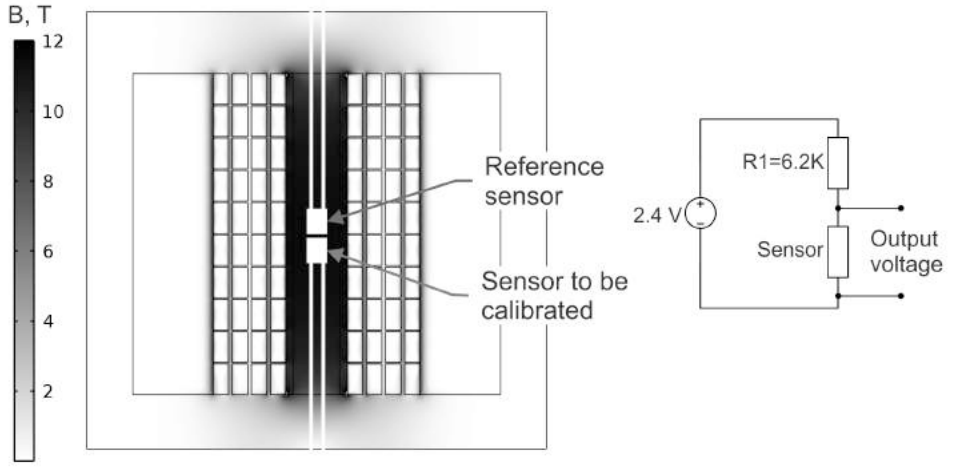

Fig. 3.1. Schematic diagram of the 15.5 μH inductive load and the placement of the manganite and loop sensor inside the inductor

The calibration procedure can be explained by analyse of Figure 3.2. On this figure the output voltage across sensor Figure 3.2 (a) and integrated signal from loop sensor Figure 3.2 (b) are showed.

As it was mentioned before the CMR-B-Scalar sensor is magnetoresistive sensor which resistance decrease by increasing magnetic flux density. Before the starting of pulsed magnetic field (B_0 = 0 T) the output voltage U_0 across CMR sensor depend only from the environment temperature. This voltage in future is used for selection of calibration curves, which will be used for recalculation of CMR output signal to magnetic field value.

Table 3.1. The parameters used for manganite magnetic field sensor calibration

Parameter	Denotation	Value
Pulse width	Δt	900 μs
Rise time	dB_r/dt	$5 \cdot 10^4$ T/s
Fall time	dB_f/dt	$8 \cdot 10^3$ T/s
Capacitor charge voltage	U	720 V
Pulse current	I	12.4 kA
Magnetic field amplitude	B	13 T
Number of inductor windings	n	10
Number of inductor layers	m	4
Inductor inductance	L	15.5 μH

At starting of pulse of magnetic field, the resistance of sensor as well as the voltage drop across its will decrease. As it can see, the front of magnetic pulse is sharper than his back part (the rise time of the pulse is equal to 400 μs, the fall time equals to 600 μs). Therefore, using of back part of pulse allows reducing calibration errors. Moreover, as was mentioned above, the resistance changing of CMR sensor vs. magnetic field is not linear. At low magnetic field this changing is less than at high one (see Figure 1.12). Therefore it is very important for calibration to use a slowly changed magnetic field in the range of low value. Exactly such pulse shape can be obtained using generator with crowbar diode. It allows making the express calibration of sensors, when all magnetic field values from 0 to 15 T was measured during the pulse.

As it was said the magnetoresistance of the used sensor depends on the temperature. For this reason the calibration procedure is done in temperature range from 0 °C to 45 °C each time increasing temperature by 3 °C. All data is storage to the computer. After the finish of calibration the MATLAB software package was used for processing these data. This program for given temperature assigned corresponding output voltage of sensor at zero magnetic field (U_0). Then, for each time point, for each value of the magnetic field program assigned the change in voltage drop across the sensor. So for each temperature it was created the dependence of voltage changes across the CMR sensor vs. magnetic field value. The database of the corresponding calibration curves is showed in Figure 3.3. This database was used by computer program designed in FTMC for measuring of magnetic field by using of CMR-B-Scalar sensors. During measuring, the computer program selects the corresponding curve by approximation the initial voltage U_0 and from selected curve the magnetic flux density was assigned to correspondent voltage across the CMR sensor.

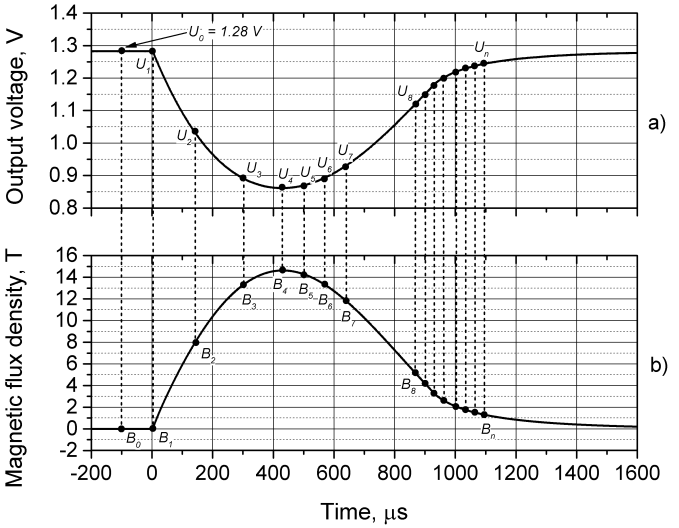

Fig. 3.2. Calibration curves a) response signal of the manganite magnetic field sensor b) magnetic field measured with loop sensor

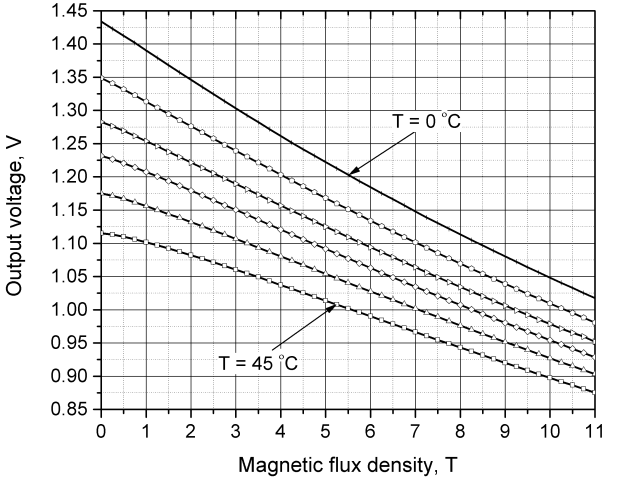

Fig. 3.3. The CMR-B-Scalar magnetic field sensor response in different temperature (The measurements were taken by incresing room temperature by 3 °C)

Result of the measured generated magnetic flux density with calibrated CMR-B-Scalar magnetoresistive sensor is presented on the Figure 3.4. The

5.4 mF capacitor banks were charged to 100 V, 500 V, 1000 V and 1400 V. The peak amplitudes of the generated magnetic field as shown in the Figure 3.4 a) reach 2.5 T, 8 T, 13.5 T and 19 T respectively. The change rate of the magnetic flux density *dB/dt* is equal to $5 \cdot 10^4$ T/s in the front side of the pulse and $8 \cdot 10^3$ T/s in the backside of the pulse. The calibration of the magnetoresistive magnetic field sensors in high magnetic fields ranges are done in the peak amplitude point a) and the calibration in low magnetic field ranges are done in back side of the pulse b) where change rate of the magnetic flux density is lowest.

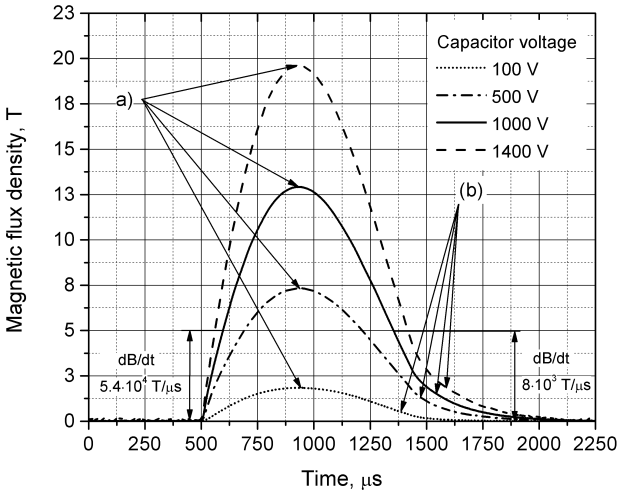

Fig. 3.4. Generated magnetic field pulse used for calibration of the CMR-B-Scalar magnetic field sensors

The developed microsecond magnetic field generator using SCR thyristors capable to generated magnetic field pulses up to 20 T is fully compatible for calibration of the magnetic field sensors due to the special shape of the generated magnetic field. And it is applicable for express calibration of the sensors.

3.2. Treatment of the Biological Objects in Pulsed Magnetic Fields

Application of pulsed power technology in biomedical field for treatment of biological objects such as cells or microorganisms has shown potential in the

past decades. However, application of pulsed magnetic field in this area is very limited due to the technological challenges influenced by the sensitivity of the biological cells to negative factors such as contamination, temperature, sample handling. The high magnetic field square shaped pulse generator was specifically designed for the investigation of the biological objects in high-pulsed magnetic fields. The applicability of the developed high magnetic field square shaped pulse generator in the biomedical area has been evaluated with the human Jurkat T lymphoblasts cells that are used for study acute T cell leukaemia. Also pathogenic fungi *Aspergillus fumigatus* and *Trychophyton rubrum* were investigated. Jurkat T cells are typical for study of the cancer cell susceptibility to drugs or radiation. The *A. fumigatus* and *T. rubrum* are a common case for human mycoses, therefore constant research of new antifungal techniques is performed.

The generated microsecond magnetic field square shaped pulse parameters as well as required pulse characteristics for the treatment are presented in the Table 3.2.

Table 3.2. The pulse characteristics and required parameters for investigation of biological objects in pulsed magnetic field

Parameter	Denotation	Value	Required value
Pulse width	Δt	2 μs – 16 μs	>1 μs
Rise time	t_r	1 μs – 6 μs	$t_r \to 0$
Pulse current	I	500 A	$I \to \infty$
Magnetic field amplitude	B	3–5 T	$B \to \infty$
Pulse repetition rate	f_r	35 Hz	>10 Hz
Number of windings	n	5	–
Number of inductor layers	m	6	–
Inductors effective volume	V_{coil}	2–3 μl	>1 μl

The required values of the treatment have been selected based on several presumptions: 1) the rise time of the pulse must be as low as possible to induce high electric field; 2) a trade-off between the maximum current, peak magnetic field, pulse width and the generated Joule heating must be found; 3) the pulses must be repetitive and the overall treatment time must be as low as possible; 4) the inductors effective volume should be sufficient for analysis of the magnetic field effects on the biological objects. All of the parameter requirements have been matched in the developed magnetic field square shaped pulse generator.

The inductor that has been selected for the treatment features a 6 layer and 5 windings structure and a total inductance of 1.6 μH. The photograph of the inductor and the schematic of the structure are presented in Figure 3.5.

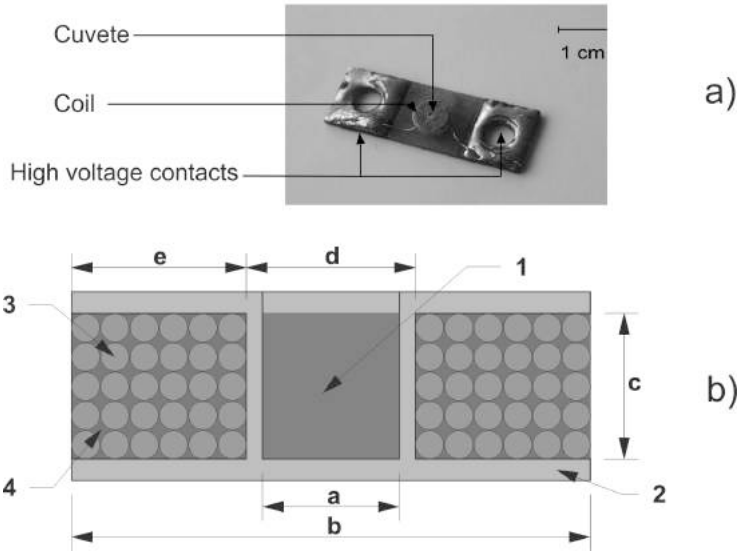

Fig. 3.5. Multilayer inductor for biological application a) the photograph of the inductor and b) the schematicof the inductor structure (Grainys, Novickij, Švedienė 2014)*

As it can be seen from the Figure 3.5 the inductor features a compact design. A plastic container has been integrated inside the effective volume of the inductor. The total volume dedicated for the biological cell medium is equal to 3 μl. The high voltage contacts (see Figure 3.5 a)) were connected to the microsecond pulsed power generator.

One of the major limitations experienced in this area is the Joule heating generated in the inductor windings when the repetitive high-pulsed current is flowing. Therefore, the temperature influence on the biological objects has been evaluated. The temperature rise inside the cuvette has been measured when 200 and 400 magnetic field pulses (5 T, 3 μs) have been generated. Also for comparison purposes active air-cooling has been introduced in the experiments. The change of the temperature during the magnetic field treatment is presented in Figure 3.6. As it can be seen in Figure 3.6 the temperature scale has been divided into temperature ranges applicable for the biological objects.

*The reference is given in the list of publications by the author on the topic of the dissertation

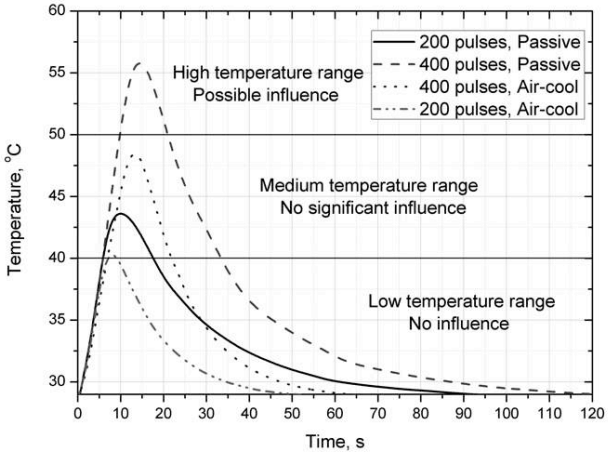

Fig. 3.6. Temperature increase in the cuvette during the magnetic field treatment (Grainys, Novickij, Švedienė 2014)*

The safe operation ranges have been acquired based on the experimental results of the cell viability change due to the thermal stress experienced. The summary is shown in Figure 3.7.

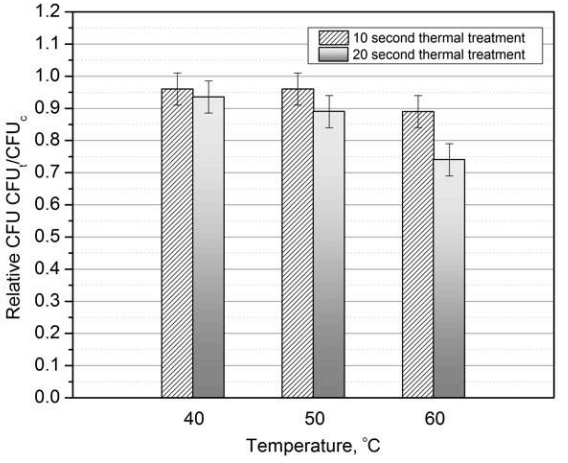

Fig. 3.7. Colony forming unit dependance on the shock temperature (Grainys, Novickij, Švedienė 2014)*

*The reference is given in the list of publications by the author on the topic of the dissertation

The *A. fumigatus* and *T. rubrum* species were affected by the short 10 s and 20 s thermal stress that is experienced during the pulsed magnetic field treatment (200 pulses and 400 pulses, respectively). The number of colony forming units (CFU) has been evaluated after the thermal treatment, where CFU_t is the number of colony forming units in the sample after the treatment and CFU_C is the number of colony forming units in the control sample. As it can be seen in Figure 3.7 it was confirmed that there is very low influence on the vitality of the selected fungus when the temperature is in the range of 40 °C. Also only 11% loss of the cells viability was observed when temperature of 60 °C was applied. Lower temperatures influence is not so significant and vitality loss rates are in the range of 5–11%, which also includes the specimen stress experienced during handling.

It was confirmed that even though the investigated pathogenic fungi have a wide range of habitat temperature, long-term temperatures above human body temperature may negatively affect the treatment. However, that does not include short thermal stress and controlled exposure is acceptable. If the temperature exceeds the applicable temperature ranges for biological experiments the influence on the outcome of the experiments is inevitable. This situation could be observed when 400 magnetic field pulses are generated and no active cooling is used. In other cases the inductor is applicable for investigation of biological cells in pulsed magnetic field. Application of 200 magnetic field pulses using the developed magnetic field square shaped pulse generator and the fabricated inductive coil is acceptable.

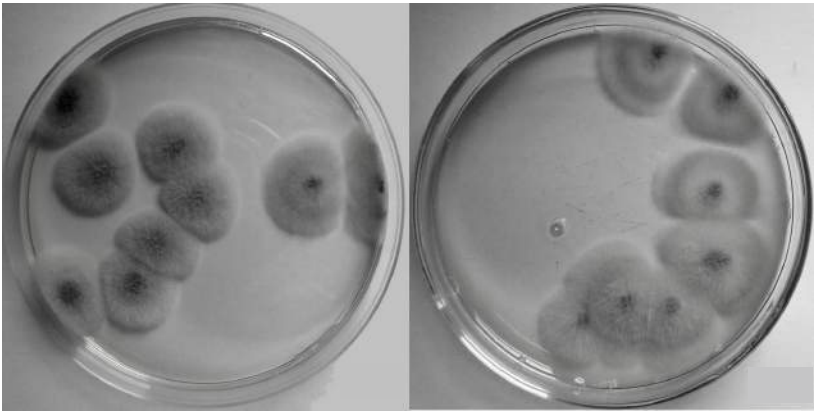

a) b)

Fig. 3.8. Image of *A. fumigatus* cells a) control sample and b) cells after the treatment

During the pulsed magnetic field treatment the fungi cells have been subjected to 5 T pulsed magnetic field with repetitive frequency of 35 Hz. The

total number of pulses did not exceed 200. The cells have been put in distilled water with a total number of $10–15 \cdot 10^3$ cells per µl. All cell samples treated using pulsed magnetic field were immediately examined using light microscopy. Light microscopy photomicrographs were made with a digital camera Nikon DS-Fil mounted on a Nikon eclipse CiS Interference Contrast Light microscope at magnifications up to ×800 (Nikon corporation, Japan). During the light microscopy examination the treated cell morphology (changes and damage of cell wall and cytoplasmic organization, structure and placement of organelles and lipid globules, protoplast turgor) of 100 individual cells was evaluated. Later the cells have been put into petri dishes and after incubation for several days the difference in the colony viability between the control colony and the colony after treatment has been evaluated. The photographs of the control colony and the colony after the treatment of the *A. fumigatus* are shown in Figure 3.8. High intensity microsecond pulsed magnetic field treatment resulted in the 20% vitality loss of the selected specimen. Similar tendency was observed in the T. rubrum case. A reduction in vitality of 23% was observed when the same intensity treatment was applied.

It must be also mentioned that the generated electric field is not sufficient for permeabilization of the biological cells like in the traditional electroporation technique. Nevertheless, it has been confirmed that the repetitive pulsed magnetic field in the range of 5 T has an influence on the vitality of complex pathogenic microorganisms.

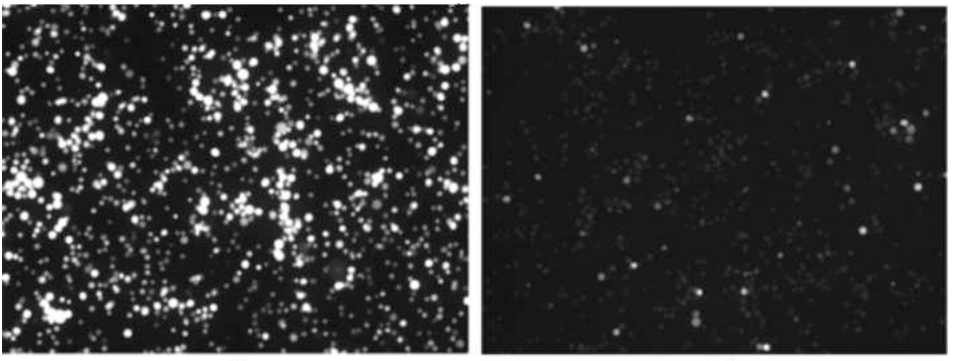

Fig. 3.9. Image of Jurkat T cells a) control sample b) after the treatment (Grainys, Novickij, Stirke 2012)[*]

[*]The reference is given in the list of publications by the author on the topic of the dissertation

In the Jurkat T cells case the analysis was performed using a dye marker. When cell suspension reached about $2 \cdot 10^6$ viable cells/ml the cells were harvested and re-suspended in a fresh medium (without serum) to $2–5 \cdot 10^7$ viable cells/ml. For dye release assays, cells were gently rinsed (3 times) with RPMI-1640 medium and then 100 μM calcein blue AM (excitation/emission maxima of ~322/435 nm) (Life Technologies Corp. CA) was added. Further incubation at room temperature for 20 minutes was performed. After that cells were ready for pulse treatment. The cells in the control sample and after the treatment are presented in Figure 3.9.

As it can be seen in Figure 3.9 the release of the dye marker could be observed in the majority of cells. The chosen implementation of the high power magnetic field square shaped pulse generator allowed to achieve considerable efficiency. The effect is similar to electroporation when the membrane of biological cells is permeabilized and the release of ions, dyes or any other molecules becomes possible. In this case the treatment intensity was high enough to cause the permeabilization of more than 95% of the biological cells.

The experiments showed that the developed microsecond high magnetic field system based on MOSFET switches could be used to investigate the biological effects of the pulsed magnetic field. The possibility to change pulsed magnetic field amplitude, repetition rate and number of applied pulses significantly expands the boundaries of the investigation. The developed novel magnetic field generator does not limit experiments with only one variable parameter.

3.3. Conclusions for the Chapter 3

1. The developed pulsed magnetic field facility with multilayer pulsed inductor generates magnetic fields over 10 T with field inhomogeneity less than 1% in 50 mm^3 area, which is acceptable for express calibration of magnetoresistive sensors.
2. Magnetoresistive sensors calibration by application of asymmetric pulses of rise time of 200 μs and 800 μs decay time and amplitude of 10 T allow the calibration of magnetoresistive sensors with error of ±10% by one pulse registration avoiding the influence of the Joule heating on the calibration accuracy.
3. The developed pulsed magnetic field facilities with MOSFET switch are able to generate square shaped repetitive up to 35 Hz microsecond 3–25 μs in duration and amplitude of 5 T pulsed magnetic field pulses

using multilayer microinductor with integrated 3 μl cuvette for contactless biological experimentation.

4. Repetitive square scraped high magnetic field pulses are capable to initiate reversible and irreversible changes of biological object structure. The vitality of the affected fungus *A. fumigatus* and *T. rubrum* species is decreased about 20%. Repetitive microsecond 3–25 μs duration and amplitude of 5 T pulsed magnetic field pulses are capable to initiate reversible and irreversible changes of biological object structure.

General Conclusions

1. Developed compact flexibly integrated into laboratory facilities high magnetic field pulse generator. The investigation of the generation technologies and transient processes was done. It was decided to generate the pulses by discharging a capacitor bank with high power thyristor switch through the inductor. In order to obtain the asymmetrically shaped pulse magnetic field the crowbar circuit was implemented. The generator can generate asymmetric magnetic field pulses over 10 T.
2. The distribution of high magnetic fields and Joule heating of multilayer and planar inductors was investigated. It was found that the planar inductor design can be used in experiments where homogeneity of the generated magnetic field is not required, while in the calibration experiments the multilayer inductor must be used, which ensure inhomogeneity of the magnetic field within the range of ±1%.
3. The developed high magnetic filed generator with crowbar circuit generates asymmetric magnetic field pulses with rise time of 200 μs and 800 μs decay time and amplitude over 10 T allows the express calibration of magnetoresistive sensors by one pulse registration method avoiding heating influence on calibration accuracy. The calibration of the manganite La-Sr-Mn-O sensors were done. It was found that

calibration error does not exceed ±10%, which is acceptable for high-pulsed magnetic field sensors metrology.

4. In order to generate repetitive microsecond magnetic field pulses magnetic field facility consisting of capacitor bank, MOSFET switch and multilayer inductor was developed and investigated. In order to reduce transient processes and form square pulses the ballast resistor was connected in series with the inductor. Such generator with inductive-resistive load can generate repetitive square magnetic field pulses up to 5 T.
5. Developed microinducor creates magnetic field pulses with fast rise and decay time, which is important for the contactless biological experimentation, because the maximum induced electric field is one of the factors influenced on biological objects is proportional to the magnetic field derivative. Developed multilayer microinductor with integrated cuvette is applicable for contactless biological experimentation.
6. Repetitive up to 35 Hz square microsecond duration 3–25 μs, up to 5 T magnetic field pulses can initiate changes in the structure of biological objects. In experiments with *Aspergillus fumigatus* and *Trychophyton rubrum* the cell viability before and after magnetic field application was investigated. Research has shown that after the magnetic field pulses was applied the cell viability decreased by 20±10% for both types of pathogenic fungus.

References

Akiyama, H.; Sakugawa, T.; Namihira, T.; Takaki, K.; Minamitani, Y.; Shimomura, N. 2007. Industrial Applications of Pulsed Power Technology. *Dielectrics and Electrical Insulation, IEEE Transactions on*. 5(14): 1051–1064.

Altgilbers, L.L.; Baird, J.; Freeman B.L.; Lynch C.S.; Shkuratov S.I. 2010. *Explosive Pulsed Power*. Imperial College Press. ISBN 978-1-84816-323-2. 596.

Arena, C.B.; Sano, M.B.; Rylander, M.N.; Davalos, R.V. 2011. Theoretical considerations of tissue electroporation with high frequency bipolar pulses', *IEEE Trans. Biomed. Eng*. 58(5): 1474–1482.

Aubert, G.; Debray, F.; Dumas, J.; Joss, W.; Krämer, S.; Martinez, G.; Mossang, E.; Petmezakis, P.; Sala, P. 2006. High magnetic field facility in Grenoble. *Journal of Physics: Conference Series*. 51(1): 659–662.

Bae, J.H.; Jang, Y.S.; Ha, D.W. 2014. Design and Analysis of a Conduction-Cooled Superconducting Magnet for 30 kW Class Gyrotron. *Applied Superconductivity, IEEE Transactions on*. 3(24): 1–4.

Balevičius, S.; Žurauskienė, N.; Stankevič, V.; Keršulis, S.; Abrutis, A.; Plaušinaitienė, V. 2010. Electrical Conductivity of Thin Polycrystalline $La_{0.83}Sr_{0.17}Mn_{O3}$ Films in Pulsed High Electric and Magnetic Fields. *J Journal of Low Temperature Physics*. 159(1): 68–71.

Baliga, B.J. 2008. *Fundamentals of Power Semiconductor Devices*. New York: Springer Science. ISBN 978-0-387-47313-0. 1072.

Baliga, B.J. 2010. *Advanced Power MOSFET Concepts*. New York: Springer. ISBN 978-1-4419-5917-1. 550.

Batti, A.F.; Mansur, A.K.; Fadhil A. Abood F.A. 2008. Electromagnetic Thermal Coupled Analysis of a Linear Induction Furnace with Rotational Symmetry. *Journal of Engineering and Development*. 1(12): 53–65.

Bluhm, H. 2006. *Pulse Power Systems: Principals and Applications*. Springer: ISBN 978-3540261377. 326.

Bongseong Kim; Kwang-Cheol Ko; Hotta, E. 2011. Study of Switching Characteristics of Static Induction Thyristor for Pulsed Power Applications. *Plasma Science, IEEE Transactions on*. 3(39): 901–905.

Buttram, M. 2002. Some future directions for repetitive pulsed power. *Plasma Science, IEEE Transactions on.* 1(30): 262–266.

Cahill, K. 2010. Cell-penetrating peptides, electroporation and drug delivery. *IET Syst. Biol*. 4(6): 367–378.

Campbell, L.; Boenig, H.J.; Rickel, D.G.; Schillig, J.B.; Sims, J.; Schneider-Muntau, H.J. 1996. Status of the NHMFL 60 tesla quasi-continuous magnet. *IEEE Trans. Magn.* 32(4): 245–2457.

Carroll, E.I. 1999. Power Electronics for Very High Power Applications. *Power Engineering Journal*. 13(2): 81–87.

Castagno, S.; Curry, R.D.; Loree, E. 2006. Analysis and Comparison of a Fast Turn-On Series IGBT Stack and High-Voltage-Rated Commercial IGBTS. *Plasma Science, IEEE Transactions on*. 5(34): 1692–1696.

Chengxiang, L.; Chenguo, Y.; Caixin, S.; Fei, G.; Wei, Z.; Zhengai, X. 2011. Dependence on electric field intensities of cell biological effects induced by microsecond pulsed electric fields. *IEEE Trans. Dielectr. Electr. Insul*. 18(6): 2083–2088.

Committee to Assess the Current Status and Future Direction of High Magnetic Field Science in the United States. 2013. *High Magnetic Field Science and Its Application in the United States: Current Status and Future Directions*. The National Academies Press. ISBN 978-0-309-28634-3, 232 p.

Das, M.K.; Capell, C.; Grider, D.E.; Raju, R.; Schutten, M.; Nasadoski, J.; Leslie, S.; Ostop, J.; Hefner, A. 2011. 10 kV, 120 A SiC half H-bridge power MOSFET modules suitable for high frequency, medium voltage applications. *Energy Conversion Congress and Exposition (ECCE), 2011 IEEE*. 2689–2692.

Davalos, R.V.; Mir, L.M.; Rubinsky, B. 2005. Tissue ablation with irreversible electroporation. *Ann. Biomed. Eng*. 33(2): 223–231.

Dev, S.B.; Rabussay, D.P.; Widera, G.; Hofmann, G.A. 2000. Medical applications of electroporation. *IEEE Trans. Plasma Sci.* 28(1): 206–223.

Devaux, M.; Debray, F.; Fleiter, J.; Fazilleau, P.; Lecrevisse, T.; Pes, C.; Rey, J.M.; Rifflet, J.M.; Sorbi, M.; Stenvall, A.; Tixador, P.; Volpini, G. 2012. HTS Insert Magnet Design Study. *Applied Superconductivity, IEEE Transactions on*. 3(22).

Ding, H.; Hu, J.; Liu, W.; Xu, Y.; Jiang, C.; Ding, T.; Li, L.; Duan, X.; Pan, Y. 2012. Design of a 135 MW Power Supply for a 50 T Pulsed Magnet. *Applied Superconductivity, IEEE Transactions on*. 3(24).

Dongdong Wang; Liu, Kefu; Jian Qiu. 2012. Investigation on the performance of thyristors for pulsed power applications. *Dielectrics and Electrical Insulation, IEEE Transactions on*. 2(19): 623–631.

Fowler, C.M.; Altgilbers, L.L. 2003. Magnetic Flux Compression Generators: a Tutorial and Survey. *Electromagnetic Phenomena*. 3(11): 305–357.

Garcia, A.; Carrascoa, J.A.; Sotoa, J.F.; Magantob, F.; Moro, C. 2001. A method for calculating the magnetic field produced by a coil of any shape. *Sensors and Actuators A*. 91: 230–232.

Goussev, G.; Sung-Roc Jang; Hong-Je Ryoo; Geun-Hie Rim. 2012. Comparative Study of MOSFET and IGBT for High Repetitive Pulsed Power Modulators. *Plasma Science, IEEE Transactions on*. 10(40): 2561–2568.

Grover, F. W. 2004. *Inductance Calculations.* Dover Publications. ISBN 978-0-48647-440-3. 304.

Han, X. T.; Li, L.; Ding, H. F.; Peng, T.; Xia, Z. C.; Chen, J. 2008. The pulsed high magnetic field facility at HUST, Wuhan, China and associated magnets. *IEEE Trans. Appl. Supercond*. 2(18): 596–599.

Hartmann, W.; Fleck, R.; Graba, R.; Hergt, M. 2013. Characterization of commercial IGBT modules for pulsed power applications. *Pulsed Power Conference (PPC), 2013 19th IEEE*. 1–4.

Herlach, F. 1985. *Strong and Ultrastrong Magnetic Fields and Their Applications*. New Jersey: Springer, Secaucus. ISBN-13 978-0-387-13504-5, 362 p.

Herlach, F. 2006. The Generation and Use of Pulsed Magnetic Fields. *Megagauss magnetic field generation and related topics, 2006 ieee international conference on*, 1–12.

Herlach, F.; Knoepfel, H. 1965. Megagauss Fields Generated in Explosive-Driven Flux Compression Devices. *Review of Scientific Instruments*. 36(8): 1088–1095.

Herlach, F.; Miura N. 2001. *High Magnetic Fields: Science and Technology. Vol.1: Magnet Technology and Experimental Techniques*. World Scientific Publishing. ISBN 981-238-976-8, 326 p.

Herlach, F.; Miura, N. 2006. *High Magnetic Fields: Science and Technology*, World Scientific: ISBN: 978-981-02-4698-3, 936 p.

Idehara, T.; Tsuchiya, H.; Watanabe, O.; Agusu, La.; Mitsudo, S. 2006. The First Experiment of a THz gyrotron with a pulse magnet. *International Journal of Infrared and Millimeter Waves*. 3(27): 319–331.

Ivorra, A. 2010. Tissue electroporation as a bioelectric phenomenon: basic concepts. *Series in Biomedical Engineering*. Springer. ISBN 978-3-642-05420-4 23-61. 23–61 pp.

Jang, S.R.; Ahn, S.H.; Ryoo, H.J.; Rim, G.H. 2010. A comparative study of the gate driver circuits for series stacking of semiconductor switches. *Power Modulator and High Voltage Conference (IPMHVC), 2010 IEEE International*. 322–326.

Kazimierczuk, M.K. 2009. *High-Frequency Magnetic Components*. Wiley. ISBN: 978-0470714539, 508 p.

Kotnik, T.; Kramar, P.; Pucihar, G.; Miklavcic, D.; Tarek, M. 2012. Cell membrane electroporation – part 1: the phenomenon. *IEEE Electr. Insul. Mag.* 28(5): 14–23.

Larsson, A.; Yap, D.; Au, J.; Carlsson, T.E. 2013. Laser-triggering of spark gap switches. *Pulsed Power Conference (PPC), 2013 19th IEEE*. 1–5.

Lee Li; Huang Li; Cai Li; Xiangdong Qi; Fuchang Lin. 2011. Analysis on Electrode Replacement of Spark-Gap Switches With Graphite Electrodes. *Plasma Science, IEEE Transactions on*. 39(9): 1874–1880.

Lee, W.G.; Demirci, U.; Khademhosseini, A. 2009. Microscale electroporation: challenges and perspectives for clinical applications. *Integr. Biol.* 3(1): 242–251.

Lenz, J.; Edelstein, Alan S. 2006. Magnetic sensors and their applications," *Sensors Journal, IEEE*. 6(3): 631–649.

Levy, L. P.; Berthier, C.; Martinez, G. 2002. *High Magnetic Fields: Applications in Condensed Matter Physics and Spectroscopy, Series: Lecture Notes in Physics 595*. Springer. ISBN-13 978-3-540-43979-0, 493 p.

Li, K.; Liu, J.J.; Xiao, G. C.; Wang, Z.A. 2006. Novel load ripple voltage- controlled parallel DC active power filters for high performance magnet power supplies. *IEEE Trans. Nucl. Sci.* 53(3): 1530–1539.

Liebfried, O.; Loffler, M.; Schneider, M.; Balevicius, S.; Stankevic, V.; Zurauskiene, N.; Abrutis, A.; Plausinaitiene, V. 2009. B-Scalar Measurements by CMR-Based Sensors of Highly Inhomogeneous Transient Magnetic Fields. *Magnetics, IEEE Transactions on*. 45(12): 5301–5306.

Ling Dai; Cheng Su; Fuchang Lin; Qin Zhang; Hanbin Dong; Xiangyu Shi. 2012. Research on a miniaturized pulsed inductor applied in PPS. *Electromagnetic Launch Technology (EML), 16th International Symposium on*. 1–6.

Liu, W.W.; Herlach. F.; Ding, H.F.; Duan, X.Z.; Li,L. 2011. A novel control strategy for the power supply to achieve the 45 T/600 ms flat-top field. *Przeglad Elektrotechniczny*. 11(87): 285–289.

Lopez, T.; Alarcon, E. 2012. Power MOSFET technology roadmap toward high power density voltage regulators for next-generation computer processors. *IEEE Trans. Power Electron*. 27(4): 2193–2203.

Mankowski, J.; Kristiansen, M. 2000. A review of short pulse generator technology. *Plasma Science, IEEE Transactions on*. 28(1): 102–108.

Maor, E.; Ivorra, A.; Leor, J.; Rubinsky, B. 2008. Irreversible electroporation attenuated neointimal formation after angioplasty. *IEEE Trans. Biomed. Eng.* 55(9): 2268–2274.

Marszalek, P.; Liu, D.S.; Tsong, T.Y. 1990. Schwan equation and trans-membrane potential induced by alternating electric field. *Biophys. J.* 58(4): 1053–1058.

Miller, J.R.; Bird, M.D.; Bole, S.; Bonito-Oliva, A.; Eyssa, Y.; Kenney, W.; Painter, T.A.; Schneider-Muntau, H.J.; Summers, L.T.; van Sciver, S.W.; Welton, S.; Wood, R. J.; Williams, J.E.C.; Bobrov, E.; Iwasa, Y.; Leupold, M.; Stejskal, V.; Weggel, R., 1994. An overview of the 45 T hybrid magnet system for the new National High Magnetic Field Laboratory. 4(30): 1563–1571.

Mitra, S.; Roy, A.; Sharma, A.; Chakravarthy, D. 2012. Compact inductive energy storage pulse power system. Rev Sci Instrum. 83(5): 054703.

Molloy, S.; Boyi Yang; Shuming Xu; Korec, J.; Jun Wang; Lopez, O.; Jauregui, D.; Kocon, C.; Herbsommer, J.; Daum, G.; Haian Lin; Pearce, C.; Noquil, J.; Shen, J. 2011. NexFET generation 2, new way to power. *Electron Devices Meeting (IEDM). 2011 IEEE International.* 5–7.

Muhammad, R. 2011. Power Electronics Handbook (3 edition). Butterworth-Heinemann. ISBN: 978-0-12-382036-5

Naayagi, R. T.; Shuttleworth, R.; Forsyth, A.J. 2001. Investigating the effect of snubber capacitor on high power IGBT turn-off. *Electrical Energy Systems (ICEES), 2011 1st International Conference on.* 50–55.

Narsetti, R.; Curry, R.D.; McDonald, K.F.; Nichols, L.M.; Clevenger, T. 2005. Application of Pulsed Electric Fields and Magnetic Pulse Compressor Technology for Water Sterilization. *Pulsed Power Conference, 2005 IEEE*. 1282–1285.

Neuber, A.; Dickens, J.C. 2004. Magnetic flux compression Generators. *Proceedings of the IEEE*. 92(7): 1205–1215.

Novickij, J.; Kačianauskas, R.; Filipavičius, V.; Balevičius, S.; Žurauskienė, N., Tolutis, R. 2004. Inductors for High Magnetic Field Generation. *Electronics and Electrical Engineering*. 7(56): 19–24.

Novickij, J.; Kačianauskas, R.; Kačeniauskas, A.; Balevičius, S.; Žurauskienė, N.; Stankevič V. 2004. Axial Magnetic Field Measurements of Pulsed Solenoids. *Electronics and Electrical Engineering*. 2(51): 15–19.

Ortenberg, M.; Herlach, F. 1996. Pulsed magnets for strong and ultrastrong fields. *Magnetics, IEEE Transactions on*. 32(4): 2438–2443.

Paul, A.; Ferl, R.; Meisel, M. 2006. High magnetic field induced changes of gene expression in Arabidopsis. *BioMagnetic Research and Technology*. 4(7): 1–10.

Peng, T.; Herlach, F.; T.; Vanacken, J. 2006. Elements of pulsed magnet design. *J. of Physics: Conf. Series*. 51: 599–602.

Podlesak, T.F.; Thomas, R.L.; Simon, F.M. 2005. Preliminary Evaluation of Super GTOS in Pulse Application. *Plasma Science, IEEE Transactions on*. 4(33): 1235–1239.

Praeg , W.F. 1970. A high-current low-pass filter for magnet power supplies. *Trans. Ind. Elec. and Control Instrum.* 17(1): 16–22.

Ramezani, E.; Spahn, E.; Bruderer, G. 1997. A novel high current rate SCR for pulse power applications" *11th IEEE International Pulsed Power Conference*, 1997.

Ramezani, E.; Spahn, E.; Bruderer. G. 1994. High Voltage Thyristor Switch for Pulse Power Applications. *10th IEEE International Pulsed Power Conference*, 1994.

Ramos, A.; Suzuki, D.O.H.; Marques, J.L.B. 2006. Numerical study of the electrical conductivity and polarization in a suspension of spherical cells. *Bioelectrochemistry*, 68: 213–217.

Rashid, M.H. 2006. *Power Electronics Circuits, Devices and Applications", 3rd Ed*. Upper saddle, NJ: Pearson Prentice Hall.

Ribeiro, P.F.; Johnson, B.K.; Crow, M.L.; Arsoy, A.; Liu, Y. 2001. Energy storage systems for advanced power applications. *Proceedings of the IEEE*. 89(12): 1744–1756.

Ripka, P. 2001. *Magnetic Sensors and Magnetometers*. New York: Artech House Publishers. ISBN 978-1580530576, 516 p.

Sanders, H.; Glidden, S., 2004. High power solid state switch module. *Power Modulator Symposium. Conference Record of the Twenty-Sixth International*. 563–566.

Schillig , J. B.; Boenig, H. J.; Rogers J. D.; Sims J. R. 1994. Design of a 400 MW power supply for a 60 T pulsed magnet. *IEEE Trans. Magn.* 30(4): 1770–1773.

Schneider, M.; Schneider, R.; Stankevic, V.; Balevicius, S.; Zurauskiene, N. 2007. Highly Local Measurements of Strong Transient Magnetic Fields During Railgun Experiments Using CMR-Based Sensors. *Magnetics, IEEE Transactions on.* 43(1): 370–375.

Shirong Hao; Youcheng Wu; Lidong Geng; Yu Yang; Weiping Xie; Minhua Wang; Nanchuan Zhang; Yingmin Dai. 2013. Inductive-energy-storage pulsed power source based on electro-exploding wire opening switch. *Pulsed Power Conference (PPC), 2013 19th IEEE*. 1–4.

Stankevič, T.; Medišauskas, L.; Stankevič, V.; Balevičius, S.; Žurauskienė, N. Liebfried, O.; Schneider, M. 2014. Pulsed Magnetic Field Measurement System Based on CMR-B-Scalar Sensors for Railgun Investigation. *Scientific Instrument*. (To be published in 2014).

Stankevic, V.; Žurauskienė, N.; Balevicius, S.; Keršulis, S.; Schneider, M.; Liebfried, O.; Plausinaitiene, V.; Abrutis, A. 2011. B-Scalar Sensor Using CMR Effect in Thin

Polycrystalline Manganite Films. *Plasma Science, IEEE Transactions on*, 39(1): 411–416.

Sterzelmeier, K.; Spahn, E.; Gauthier-Blum, C.; Brommer, V.; Sinniger, L.; Grasser, B. 2008. 50 kJ Ultra-Compact Pulsed-Power Supply Unit for Active Protection Launcher Systems. *Electromagnetic Launch Technology, 2008 14th Symposium on.* 1–5.

Stokes, J. 1992. *70 Years of Radio Tubes and Valves: A Guide for Electronic Engineers, Historians and Collectors*. Vestal Press, NY. ISBN 1886606110, 263 p.

Tatarov, I.; Panda, A.; Petkov, D. 2011. Effect of magnetic fields on tumor growth and viability. *Comput. Med.* 61(4): 339–345.

Teissie, J.; Golzio, M.; Rols, M.P. 2005. Mechanisms of cell membrane electropermeabilization: minireview of our present (lack of?) knowledge. *Biochim. Biophys. Acta*. 1724(3): 270–280.

Tsunoda, K.; Maeyama, M.; Hotta, E.; Shimizu, N. 2001. Switching properties of series connected static induction thyristor stack. *Pulsed Power Plasma Science*. 2: 1786–1789.

Vanacken, J.; Tao Peng; Herlach, F. 2006. Experimental and Theoretical Analysis of the Heat Distribution in Pulsed Magnets. *Applied Superconductivity, IEEE Transactions on.* 16(2): 1689–1691.

Washizu, M. 2008. Polarisation and membrane voltage of ellipsoidal particle with a constant membrane thickness: a series expansion approach. *IET Nanobiotechnol.* 2(3): 62–71.

Welleman, A.; Fleischmann, W. 2003. Solid state switches in bipolar (thyristor) and BIMOS (IGBT) technology for repetitive pulse applications. *Pulsed Power Conference, 2003. Digest of Technical Papers. PPC-2003. 14th IEEE International*. 1: 353–356.

Welleman, A.; Ramezani, E.; Waldmeyer, J.; Gekenidis, S. 1999. Semiconductor components up to 12 kV and 150 kA for closing switches *12th IEEE International Pulsed Power Conference*. 2: 1268–1271.

Werst, M.D.; Ingram, S.K.; Wehrlen, D.J.; Weldon, W.F. 1994. High magnetic field generation using single-turn coils. *Magnetics, IEEE Transactions on.* 30(4): 2550–2553.

Williams, P.; Marketos, P.; Crowther, L.J.; Jiles, D. 2012. New designs for deep brain transcranial magnetic stimulation. *IEEE Trans. Magn*. 48(3): 1171–1178.

Winands, G. J. J.; Liu, Z.; Pemen, A. J. M.; Van Heesch, E. J. M.; Yan, K. 2005. Long lifetime, triggered, spark-gap switch for repetitive pulsed power applications. *Review of Scientific Instruments*. 76(8): 85107-1–085107-6.

Witte, H.; Gaganov, A.; Kozova. 2006. Pulsed magnets – Advances in coil design using finite element analysis. *IEEE Transactions on Applied Auperconductivity*, 2(16): 1680–1683.

Yun Xu; Rui Yang; Yingmeng Xiang; Hongfa Ding; Tonghai Ding; Liang Li. 2012. Design of a Novel Pulsed Power System for Repetitive Pulsed High Magnetic Fields. *Applied Superconductivity, IEEE Transactions on*. 3(22): 5400104.

Zhang, Q.; Agarwal, A.; Capell, C.; Cheng, L.; O'Loughlin, M.; Burk, A.; Palmour, J.; Temple, V.; Ogunniyi, A.; O'Brien, H.; Scozzie, C.J. 2011. SiC super GTO thyristor technology development: Present status and future perspective. *Pulsed Power Conference (PPC), 2011 IEEE*. 1530–1535.

Zorngiebel, V.; Hecquard, M.; Spahn, E.; Welleman, A.; Scharnholz, S. 2011. Modular 50 kV IGBT Switch for Pulsed-Power Applications. *Plasma Science, IEEE Transactions on*. 1(39): 364–367.

Zorngiebel, V.; Spahn, E.; Buderer, G.; Welleman, A.; Fleischmann, W. 2008. Compact High Voltage IGBT Switch for Pulsed Power Applications. *14th Symposium on Electromagnetic Launch Technology*. 1–5.

Žurauskienė, N.; Balevičius, S.; Cimmperman, P.; A Stankevič, V.; A Keršulis, S.; Novickij, J.; Abrutis, A.; Plaušinaitienė, V. 2010. Colossal Magnetoresistance Properties of La0.83Sr0.17MnO3 Thin Films Grown by MOCVD on Lucalox Substrate. *J Low Temp Phys*. 159: 64–67.

Žurauskienė, N.; Balevičius, S.; Stankevič, V.; Paršeliūnas, J.; Keršulis, S.; Abrutis, A.; Plaušinaitienė, V. 2009. Influence of Sr content on CMR effect in polycrystalline La1-xSrxMnO3 thin films. *Acta Physica Polonica A. Proceedings of the 2nd Euro-Asian Pulsed Power Conference*. 115(6): 1136–1138.

The List of Scientific Author's Publications on the Subject of the Dissertation

Papers in the reviewed scientific periodical publications

Grainys, A.; Novickij, J. 2010. The investigation of 3D magnetic field distribution in multilayer coils. *Electronics and Electrical Engineering*. No. 7(103): 9–12. Kaunas: Technologija. ISSN 1392–1215 (Thomson Reuters Web of Science).

Grainys, A.; Novickij, J. 2011. Investigation of microcoils for high magnetic field generation. *Electronics and Electrical Engineering*. No. 3(109): 63–66. Kaunas: Technologija. ISSN 1392–1215 (Thomson Reuters Web of Science).

Grainys, A.; Novickij, J.; Novickij, V.; Lučinskis, A.; Zapolskis, P. 2013. Compact microsecond pulsed magnetic field generator for application in bioelectronics. *Electronics and Electrical Engineering*. No. 8(19): 25–28. Kaunas: Technologija. ISSN 1392–1215 (Thomson Reuters Web of Science).

Grainys, A.; Novickij, J.; Novickij, V. 2013. Finite element method analysis of microfluidic channel with integrated dielectrophoresis electrodes for biological cell permeabilization and manipulation. *Measurement Science Review*. No. 3(13): 152–156. Warsaw: Versita. ISSN 1335–8871 (Thomson Reuters Web of Science).

Grainys, A.; Novickij, V.; Švedienė, J.; Novickij, J.; Markovskaja, S. 2014. Joule heating influence on the vitality of fungi in pulsed magnetic fields during magnetic permeabilization. *Journal of Thermal Analysis and Calorimetry*. Amsterdam : Springer Netherlands. ISSN 1388–6150 (Thomson Reuters Web of Science).

In the other editions

Grainys, A. 2012. Mikrosekundinės trukmės magnetinių impulsų generatorius. *Science – future of Lithuania: Electronics and Electrical Engineering*. T. 4, Nr.1: 63–66. Vilnius: Technika. ISSN 2029–2341 (IndexCopernicus).

Grainys, A.; Novickij, J.; Novickij, V.; Stirke, A.; Kašėta, V. 2012. High power facilities for electroporation of biological cells in pulsed magnetic fields. *In proceedings of the 19th international conference on microwaves, radar and wireless communication MIKON-2012*. Vol. 2: 508–511. New York: IEEE. ISBN 9781457714351 (IEEE/IEE).

Summary in Lithuanian

Įvadas

Problemos formulavimas

Per paskutinį dešimtmetį magnetinių laukų taikymo aktualumas medžiagotyroje, biomedicinos moksluose ir kitose taikomųjų mokslų šakose pastebimai padidėjo. Ypatingo dėmesio sulaukia tyrimai stipriuose magnetiniuose laukuose. Šiems tyrimams atlikti būtini magnetiniai laukai viršijantys 2 T ribą. Tam tikslui kuriamos sudėtingos didelės galios sistemos, kurios reikalauja pastovaus aušinimo ir atskiro didelės galios maitinimo įvado. Vienas iš pagrindinių tokių sistemų trūkumų yra stacionarumas dėl didelių sistemos gabaritų, svorio, priklausomybės nuo periferinių įrenginių bei energijos šaltinio. Kaip alternatyva stacionarioms magnetinio lauko sistemoms gali būti kompaktiškos magnetinio lauko sistemos, kurias galima būtų saugiai ir greitai transportuoti ir integruoti į jau egzistuojančius eksperimentinius stendus. Daugelyje atvejų kompaktiškos impulsinių magnetinių laukų generavimo sistemos gali pakeisti stacionarius magnetinio lauko šaltinius, jei generuojamo magnetinio lauko tūris neviršija 1 cm^3.

Nepaisant stiprių magnetinių laukų generavimo principo paprastumo, formuotų impulsų magnetinio lauko generatorių kūrimas yra sudėtingas tarpdisciplininis uždavinys, kurį sprendžiant susiduriama su pereinamaisiais vyksmais elektrinėse grandinėse, elektromechaninių jėgų poveikiais induktoriuose bei įšilimo efektais. Stipraus magnetinio lauko sistemos yra galingas įrankis taikomojoje fizikoje, medžiagotyroje ir biotechnologijoje. Magnetinio lauko poveikis priklauso nuo

generuojamo impulso formos, pasikartojimo dažnio ir kitų parametrų. Magnetinio lauko formuotų impulsų sistemos gali būti pritaikytos magnetinio lauko jutiklių kalibravimui. Biotechnologijos ir biomedicinos moksluose svarbu maksimaliai sumažinti eksperimentinių įrankių poveikį tyrimo objektams, dažnai susiduriama su biologinio objekto kontaminacija. Magnetinių laukų taikymas šioje srityje užtikrina bekontaktę tyrimo metodiką.

Disertacijoje sprendžiama mokslinė problema – stiprių impulsinių magnetinių laukų generatorių, skirtų magnetorezistyvinių jutiklių kalibravimui ir biologinių objektų bekontaktiniam tyrimui, kūrimas.

Darbo aktualumas

Stiprių magnetinių laukų generavimas reikalauja didelio kiekio energijos ir brangių aušinimo įrenginių. Dėl šių priežasčių šios sistemos yra stacionarios ir negali būti integruojamos į kitas eksperimentines sistemas arba stendus. Kompaktiškų stiprių magnetinio lauko sistemų kūrimas ir tyrimas yra svarbi užduotis, reikalaujanti tarpdisciplininio bendradarbiavimo, naujų technologijų ir metodų. Todėl stiprių magnetinių formuotų impulsų generatorių kūrimas ir tyrimas yra aktuali elektronikos ir elektros inžinerijos mokslinė problema.

Magnetinio lauko jutikliai yra jautrūs technologinėms sąlygoms, medžiagos struktūrai, temperatūrai. Dėl jautrio temperatūrai manganitiniai magnetinio lauko jutikliai kurių parametrai nepriklauso nuo magnetinio srauto krypties privalo būti kalibruojami vienu impulsu. Dėl skirtingo jautrio magnetiniam laukui jutikliai turi būti kalibruojami su asimetrinės formos impulsais. Todėl stiprių magnetinių laukų formuotų impulsų generatoriai gali būti pritaikyti magnetinio lauko magnetorezistyvinių jutiklių kalibravimui.

Stiprių magnetinių laukų technologija leidžia sukurti bekontaktį poveikį biologiniams objektams. Poveikio intensyvumas priklauso nuo lauko stiprio, impulso ilgio, pasikartojimo dažnio. Kompaktiški mikrosekundinės trukmės magnetinio lauko stačiakampės formos impulsų generatoriai gali tapti nauju įrankiu skirtu tirti biologinius objektus sterilioje aplinkoje.

Tyrimų objektas

Stiprių magnetinių laukų formuotų impulsų generatoriai, magnetorezistyvinių jutiklių kalibravimui ir biologinių objektų tyrimams.

Darbo tikslas

Mokslinio darbo tikslas – sukurti ir ištirti stiprių magnetinių laukų formuotų impulsų generatorius magnetorezistyvinių magnetinio lauko jutiklių kalibravimui ir biologinių objektų tyrimams.

Darbo uždaviniai

Darbo tikslui įgyvendinti ir mokslinei problemai spręsti darbe buvo iškelti šie uždaviniai:

1. Sukurti stiprių magnetinių laukų formuotų impulsų generatorių prototipus ir ištirti pereinamuosius vyksmus.

2. Sukurti daugiasluoksnius ir planarius impulsinius induktorius, nustatyti magnetinio lauko pasiskirstymą, įvertinti jo nehomogeniškumą ir apvijų įšilimo procesus.
3. Atlikti magnetorezistyvinių magnetinio lauko jutiklių kalibravimo tyrimus, naudojant stipraus virš 10 T magnetinio lauko asimetrinės formos impulsų generatoriu.
4. Atlikti biologinių objektų tyrimus, naudojant stipraus iki 5 T magnetinio lauko stačiakampės formos pasikartojančių mikrosekundinių impulsų generatoriu.

Tyrimų metodika

Šiame darbe buvo taikomi analitiniai, skaitiniai ir eksperimentiniai metodai. Panaudojant PSPICE programinį paketą, skaitiniai metodai buvo taikomi tirti pereinamuosius vyksmus stipraus magnetinio lauko formuotų impulsų generatoriuose. Naudojant COMSOL programinį paketą, baigtinių elementų metodu atlikta induktorių įšilimo bei magnetinio lauko pasiskirstymo analizė. Sukurti impulsiniai magnetinio lauko generatoriai buvo ištirti eksperimentiškai magnetorezistyvinių jutiklių kalibravimo ir biologinių objektų tyrimuose, impulsiniuose magnetiniuose laukuose.

Darbo mokslinis naujumas

Darbo mokslinis naujumas pagrįstas šiais rezultatais:

1. Sukurtas kompaktiškas stiprių virš 10 T magnetinių laukų asimetrinės formos impulsų generatorius, generuojantis magnetinio lauko impulsus, kurių priekinis frontas siekia 200 μs, o galinis 800 μs. Generatorius gali būti pritaikytas magnetorezistyvinių magnetinio lauko jutiklių kalibravimui, naudojant vieno impulso kalibravimo metodiką, tokiu būdu išvengiant induktoriaus įšilimo poveikio kalibravimo tikslumui.
2. Sukurtas daugiasluoksnis impulsinis induktorius, generuojantis virš 10 T magnetinį lauką su magnetinio lauko nehomogeniškumu mažesniu nei 1 % 50 mm^3 tūryje, leidžia atlikti magnetorezistyvinių magnetinio lauko jutiklių kalibravimą su ±10 % rezultatų neapibrėžtimi.
3. Sukurtas stiprių iki 5 T magnetinių laukų stačiakampės formos pasikartojančių mikrosekundinių impulsų generatorius su kontroliuojamu impulso ilgiu, amplitude, pasikartojimo dažniu. Nustatyta, kad toks generatorius gali būti naudojamas biologinių objektų tyrimams stipriuose impulsiniuose magnetiniuose laukuose.
4. Nustatyta, kad impulsiniai daugiasluoksniai induktoriai su integruota kiuvete, generuojantys iki 5 T stačiakampės formos magnetinio lauko pasikartojančius mikrosekundinius impulsus, leidžia atlikti bekontakčius biologinių objektų tyrimus magnetiniuose laukuose, išvengiant biologinių objektų kontaminacijos.

Darbo rezultatų praktinė reikšmė

Sukurtas stipraus virš 10 T magnetinio lauko asimetrinės formos impulsų generatorius, susidedantis iš SCR tiristorinio rakto ir trumpiklio grandinės yra tinkamas magnetorezistyvinių magnetinio lauko jutiklių kalibravimui stipriuose impulsiniuose

laukuose. Generatorius buvo pritaikytas manganitinių jutiklių kalibravimui Mokslo, inovacijų ir technologijų agentūros MITA finansuojamame aukštųjų technologijų plėtros programos projekte „Magnetinio lauko matuoklio elektros energetikos sistemoms sukūrimas – MAGEPS" Nr. 31–V149.

Sukurtas kompaktiškas stiprių iki 5 T magnetinių laukų stačiakampės formos impulsų generatorius su kontroliuojamais impulsų parametrais yra tinkamas naudoti grįžtamiems ir negrįžtamiems biologinių objektų struktūros pokyčiams stipriuose magnetiniuose laukuose. Generatorius sėkmingai pritaikytas tarpdisciplinuose tyrimuose kartu su Gamtos tyrimų centro (Vilnius, Lietuva) mokslininkais, tiriant stipraus impulsinio magnetinio lauko įtaką patogeniniams grybams.

Ginamieji teiginiai

1. Sukurtas impulsinis magnetinio lauko formuotų impulsų generatorius, susidedantis iš kondensatoriaus baterijos, SCR tiristorinio rakto ir daugiasluoksnio induktoriumiaus, sujungto lygiagrečiai su trumpikliu, gali generuoti asimetrinės formos virš 10 T amplitudės ir 1 % ašinio magnetinio lauko nehomogeneškumu impulsus, taikytinus magnetorezistyvinių magnetinio lauko jutiklių kalibravimui.
2. Asimetrinės formos virš 10 T magnetinio lauko impulsas, kurio priekinis frontas 200 μs, o galinis 800 μs leidžia atlikti magnetorezistyvinių magnetinio lauko jutiklių kalibravimą su ±10 % rezultatų neapibrėžtimi vieno impulso metu, išvengiant jutiklio įšilimo.
3. Impulsinis magnetinio lauko iki 5 T stačiakampės formos pasikartojančių iki 35 Hz mikrosekundinių impulsų generatorius, susidedantis iš kondensatorių baterijos, MOSFET raktų ir daugiasluoksnio mikroinduktoriaus su integruota kiuvete užtikrimą bekontakčius biotechnologinius tyrimus.
4. Stipraus magnetinio lauko iki 5 T stačiakampės formos ir 3–25 μs impulsai įtakoja biologinių objektų struktūrą ir gyvybingumą ir, priklausomai nuo pasikartojamumo dažnio, inicijuoja grįžtamus arba negrįžtamus procesus.

Darbo rezultatų aprobavimas

Disertacijos tema paskelbti 7 moksliniai straipsniai: 5 – Thompson Reuters ISI Web of Science duomenų bazės recenzuojamuose mokslo žurnaluose su citavimo indeksu, 2 – kituose recenzuojamuose mokslo leidiniuose (IndexCopernicus ir IEEE/IEE). Disertacijos rezultatai buvo pristatyti 7 Lietuvos ir tarptautinėse mokslinėse konferencijose:

- Tarptautinėje mokslinėje konferencijoje "Electronics 2011". 2011. Kaunas, Lietuva;
- Mokslinėje konferencijoje "Science – future of Lithuania: Electronics and electrical engineering". 2011. Vilnius, Lietuva;
- Tarptautinėje mokslinėje konferencijoje "MIKON – 2012". 2012. Varšuva, Lenkija.

- Mokslinėje konferencijoje “Science – future of Lithuania: Electronics and electrical engineering”. 2012. Vilnius, Lietuva;
- 9-oje tarptautinėje mokslinėje konferencijoje, “Measurement 2013”. 2013, Smolenice castle, Slovakija;
- Mokslinėje konferencijoje “Science – future of Lithuania: electronics and electrical engineering”. 2013. Vilnius, Lietuva;
- 2-oje tarptautinėje mokslinėje konferencijoje Thermal Analysis and Calorimetry “CEEC-TAC2”. 2013. Vilnius, Lietuva.

Disertacijos struktūra

Disertaciją sudaro įvadas, trys skyriai, bendrosios išvados, literatūros šaltinių sąrašas, autoriaus publikacijų disertacijos tema sąrašas, santrauka lietuvių kalba. Darbo apimtis – 111 puslapių neskaitant priedų, tekste yra 28 formulės, 52 paveikslai ir 8 lentelės. Rašant disertaciją buvo panaudoti 97 literatūros šaltiniai.

1. Stiprių impulsinių magnetinių laukų generavimo apžvalga

Per paskutinį dešimtmetį magnetinių laukų taikymo aktualumas medžiagotyroje, biomedicinos moksluose ir kitose taikomųjų mokslų šakose pastebimai padidėjo. Šiose srityse taikomi magnetiniai laukai viršija 10 T ribą. Tokių stiprių magnetinių laukų generavimui kuriamos sudėtingos didelės galios sistemos, kurios reikalauja pastovaus aušinimo ir atskiro didelės galios maitinimo įvado. Vienas iš pagrindinių tokių sistemų trūkumų yra stacionarumas dėl didelių sistemos gabaritų, svorio, priklausomybės nuo periferinių įrenginių bei energijos šaltinio. Kaip alternatyva stacionarioms magnetinio lauko sistemoms gali būti kuriamos kompaktiškos stipraus magnetinio lauko specialios formos impulsų generavimo sistemos. Kuriant tokias formuotų impulsų generavimo sistemas būtina spręsti uždavinius susijusius su pereinamaisiais vyksmais elektrinėse grandinėse, elektromechaninių jėgų poveikiais induktoriuose bei įšilimo efektais.

Taip pat skyriuje apžvelgiama magnetoreziztyvinių jutiklių savybės bei jų kalibravimo galimybės stipriuose magnetiniuose laukuose. Atlikus literatūros analizę paaiškėjo, kad magnetoreziztyvinių jutiklių savybės priklauso nuo gamybos technologinių sąlygų, medžiagų struktūros bei temperatūros. Todėl magnetorezistyviniai jutikliai turi būti kalibruojami naudojant stiprius impulsinius magnetinius laukus išvengiant temperatūros poveikio kalibravimo rezultatams. Taip pat skyriuje apžvelgiama stiprių impulsinių magnetinių laukų įtaka biologiniams objektams. Atlikus literatūros analizę paaiškėjo, kad magnetinio lauko poveikis priklauso nuo generuojamo impulso formos, pasikartojimo dažnio ir kitų parametrų. Tiriant biologinius objektus susiduriama su kontaminacijos problemomis. Todėl turi būti sukurtos stiprių magnetinių laukų specialios formos impulsų generavimo sistemos, užtikrinančios biologinių objektų tyrimo galimybes plačiame tyrimų diapazone.

2. Mikrosekundinių stiprių magnetinių laukų formuotų impulsų generatorių kūrimas ir tyrimas

Šiame skyriuje pristatomas sukurtas stiprių virš 10 T magnetinių laukų asimetrinės formos impulsų generatorius. Supaprastinta generatoriaus schema yra pavaizduota S1 paveiksle. Generatorius susideda iš 4 kV maitinimo šaltinio, 5,4 mF, 4 kV kondensatorių bloko, matavimo grandinės, didelės galios (53 kA, 4,2 kV) SCR rakto, trumpiklio, valdymo bloko ir impulsinio induktoriaus.

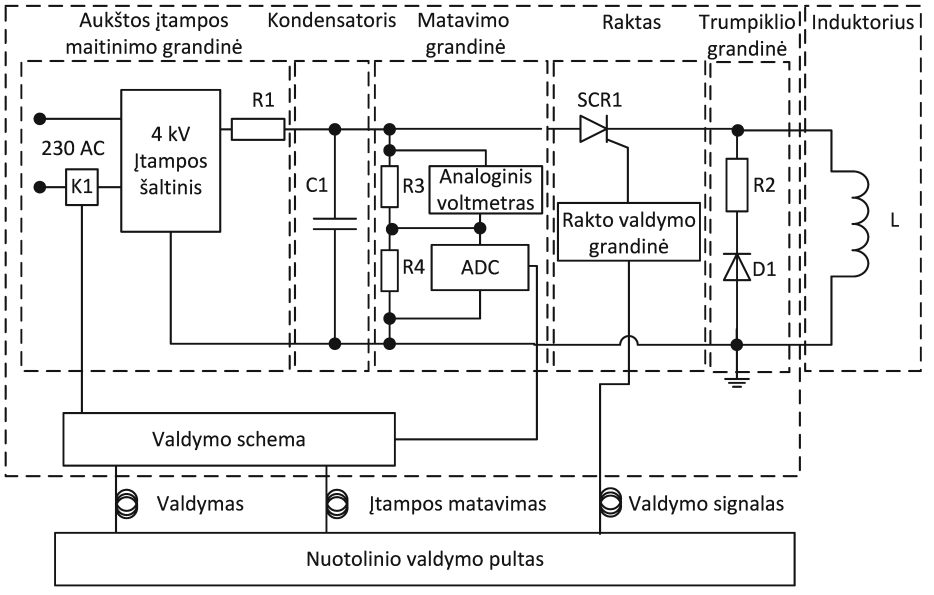

S1 pav. Supaprastinta magnetinio lauko asimetrinės formos impulsų generatoriaus schema

Trumpiklio grandinė, susidedanti iš didelės galios (83 kA, 4 kV) diodo ir 0,2 Ω varžos, kuri yra naudojama sistemos apsaugai nuo viršįtampių ir galinio impulso fronto formavimui. Generatoriaus pakrovimo ir iškrovimo grandinės realizuotos panaudojant relių rinkinį K1 ir K2. Norint galvaniškai atrišti valdymo ir galios grandines, puslaidininkinis SCR raktas yra valdomas naudojant optinį kabelį ir konverterį. Nuotolinis valdymo pultas užtikrina operatoriaus darbo saugą. Iškraunant 5,4 mF kondensatoriaus baterijas per 15,5 μH daugiasluoksnį impulsinį induktorių, generuojami virš 10 T magnetinio lauko asimetrinės formos impulsai. Generatoriaus bendras vaizdas pateiktas S2 paveiksle.

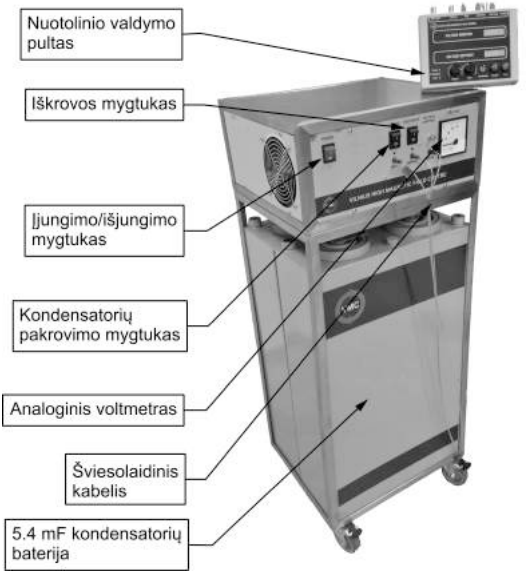

S2 pav. Stipraus, virš 10 T magnetinio lauko asimetrinių impulsų generatoriaus ir nuotolinio valdymo pulto bendrasis vaizdas

Generatoriaus konstrukcija užtikrina sistemos mobilumą ir lankstų integravimą į mokslinių laboratorijų infrastruktūrą. Nuotolinio valdymo pultas jungiamas iki 20 m optiniais kabeliais su pagrindiniu generatoriaus bloku. Sistemos generuojamų magnetinių lauko impulsų forma yra pavaizduota S3 paveiksle.

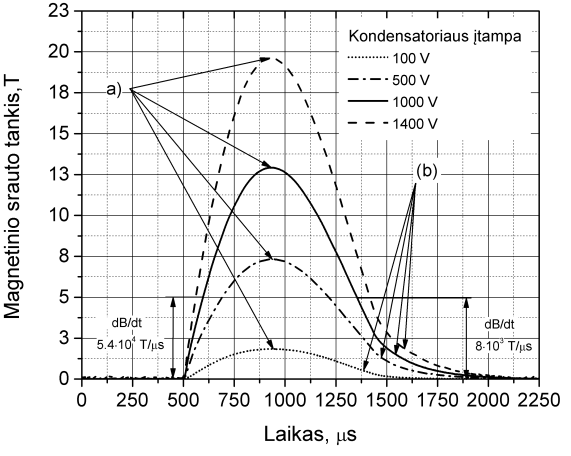

S3 pav. Stipraus magnetinio lauko asimetrinės formos impulsų generatoriaus impulsas

Keičiant kondensatorių baterijos pakrovimo įtampą nuo 100 V iki 1400 V generuojami 2,5–19,6 T magnetinio lauko asimetrinės formos impulsai. Priekinėje impulso dalyje iki 5 T ribos, magnetinio lauko augimo greitis siekia $5{,}4 \cdot 10^4$ T/s, o galinėje – iki $8 \cdot 10^3$ T/s. Stiprių magnetinių lauko ruože jutikliai kalibruojami maksimalios amplitudės taške a), o silpnų magnetinių laukų ruože kalibravimas atliekamas b) atkarpoje, kur magnetinio lauko augimo greitis mažiausias.

Taip pat šiame skyriuje pristatomas sukurtas stiprių, iki 5 T, magnetinių laukų, stačiakampės formos, pasikartojančių mikrosekundinių impulsų generatorius. Impulso amplitudė, trukmė 3–25 μs ir impulso pasikartojamumo dažnis nuo 1 Hz iki 35 Hz gali būti keičiami priklausomai nuo eksperimento užduočių. Supaprastinta generatoriaus schema yra pavaizduota S4 paveiksle. Generatorius susideda iš 2 kV maitinimo šaltinio, 940 μF, 2 kV kondensatorių bloko ir 200 μF, 2 kV kondensatorių bloko, didelės galios (463 A, 1.2 kV) MOSFET raktų, trumpiklio, apsaugos grandinės, valdymo bloko ir impulsinio mikroinduktoriaus.

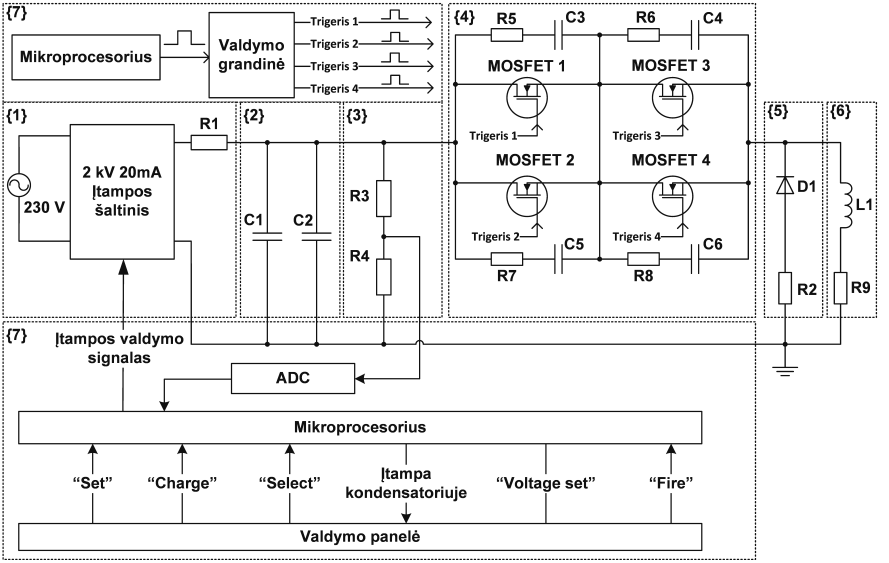

S4 pav. Supaprastinta stipraus magnetinio lauko, iki 5 T, stačiakampės formos mikrosekundinių impulsų generatoriaus schema

Nuosekliai su impulsiniu induktoriumi įjungta balastinė varža R9 siekiant išvengti parazitinių švytavimų. MOSFET raktai sujungti nuosekliai ir lygiagrečiai, siekiant padidinti komutuojamą srovę iki 900 A ir darbinę įtampą iki 2,4 kV. RC grandinė ir trumpiklio grandinė apsaugo MOSFET raktus nuo viršįtampių. Parametrų nustatymas, generatoriaus valdymas ir pakrovimo įtampos matavimas įgyvendintas panaudojant XMEGA128AU mikrovaldiklį. Sukurto generatoriaus bendrasis vaizdas pateiktas S5 paveiksle.

S5 pav. Stiprių magnetinių laukų stačiakampės formos pasikartojančių mikrosekundinių impulsų generatorius

Generatorius yra kompaktiškas, lengvai transportuojamas ir integruojamas į eksperimentinę infrastruktūrą. Generatoriaus grafiniame ekrane atvaizduojami impulsų nustatymo parametrai.

Generatoriaus sukuriami magnetinio lauko impulsai su skirtingais impulsiniais induktoriais yra pavaizduoti S6 paveiksle.

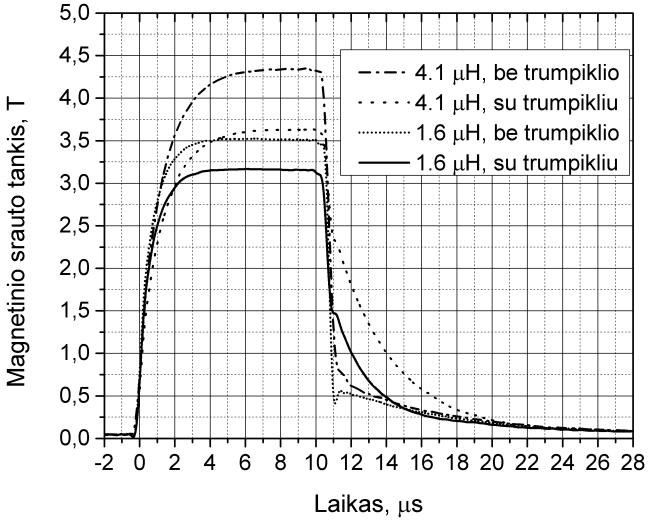

S6 pav. Generuojami magnetinio lauko impulsai su skirtingais impulsiniais induktoriais

Priklausomai nuo trumpiklio parametrų ir impulsinio induktoriaus induktyvumo kinta impulso forma. Biologiniuose tyrimuose yra svarbu pasiekti kuo didesnį lauko augimo greitį *dB/dt*. Todėl toks generatorius yra taikytinas bekontakčiuose tyrimuose biotechnologijoje.

Priklausomai nuo induktoriaus struktūros, keičiasi generuojamo magnetinio lauko stipris, forma ir homogeniškumas. Todėl būtina analizuoti sukurtų daugiasluoksnių ir planarių induktorių konstrukcijas, magnetinio lauko pasiskirstymą bei induktorių įšilimą atsirandantį dėl didelių srovių, tekančių induktorių apvijose.

Medžiagotyroje ir magnetinio lauko jutiklių kalibravimo tyrimuose, reikalingas homogeniškas ir lėtai kintantis magnetinis laukas. Tikslui įgyvendinti sukurtas daugiasluoksnis impulsinis induktorius. Induktoriaus struktūra buvo analizuojama panaudojant COMSOL programinį paketą, taip pat atlikta induktorių įšilimo, bei magnetinio lauko pasiskirstymo analizė. Magnetinio lauko pasiskirstymo daugiasluoksnėje ritėje rezultatai pateikti S7 paveiksle.

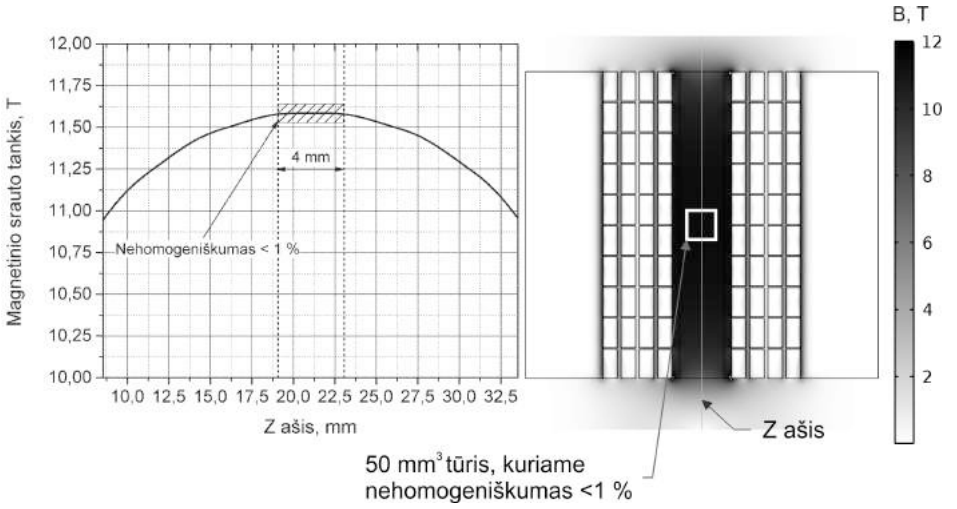

S7 pav. Magnetinio lauko pasiskirstymo daugiasluoksniame induktoriuje

Keturių sluoksnių ir 10 apvijų kiekviename sluoksnyje impulsiniame induktoriuje magnetinio lauko nehomogeniškumas neviršija 1 % 50 mm^3 tūryje. Todėl toks induktorius yra taikytinas magnetorezistyvinių magnetinių jutiklių kalibravimui.

Biotechnologijos tyrimuose svarbu pasiekti kuo didesnį magnetinio lauko augimo greitį ir amplitudę, tačiau nehomogeniškumas gali išlikti 10 % ribose. Taip pat būtina integruoti kiuvetę į induktoriaus konstrukciją, norint išvengti tyrimo objekto kontaminacijos problemų.

Magnetinio lauko pasiskirstymas daugiasluoksniame ir planariame mikroinduktoriuje pateiktas S8 paveiksle.

Planarios konstrukcijos ritė generuoja iki 4 T magnetinį lauką 0,1 µl tūryje, o daugiasluoksnis induktorius – 3 µl tūryje. Dėl didesnio efektinio tūrio, daugiasluoksnis

induktorius lengviau integruojamas į biologinių tyrimų infrastruktūrą. Panaudojant 6 sluoksnių ir 5 apvijų kiekviename sluoksnyje struktūrą, impulsinis generatorius generuoja magnetinio lauko, iki 5 T, stačiakampės formos mikrosekundinius impulsus.

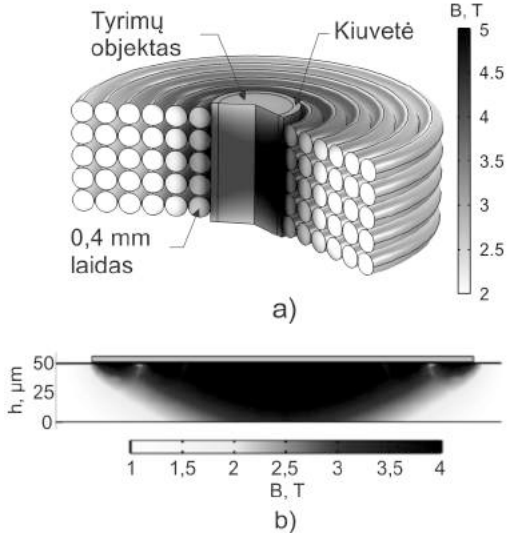

S8 pav. Generuojamas magnetinis laukas a) daugiasluoksniame mikroinduktoriuje b) planariame induktoriuje (Novickij V., Grainys, Novickij J. 2013) *

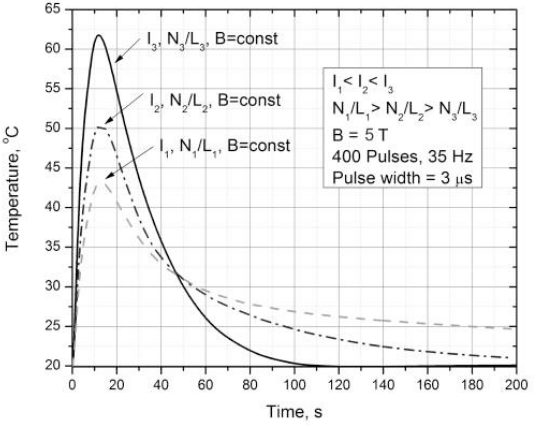

S9 pav. Impulsinio induktoriaus įšilimo proceso dinamika (Grainys, Novickij, Švedienė 2014)*

*Nuoroda pateikta autoriaus mokslinių publikacijų disertacijos tema sąraše

Generuojant stiprius magnetinius laukus induktoriaus apvijose išsiskiria šiluma. Dėl to pasikeičia impulso forma, šiluma įtakoja tyrimo objekto parametrus. Keičiant induktoriaus apvijų ir ilgio santykį N/L buvo vertinama įšilimo proceso dinamika.

Kompiuterinio modeliavimo rezultatai pateikti S9 paveiksle. Didinant N/L santykį, pikinė temperatūros vertė mažėja, o ritės aušinimo procesas pailgėja kaip ir impulso užaugimo laikas. Atsižvelgiant į rezultatus buvo nustatyta, kad maksimalus leidžiamas impulsų kiekis yra iki 200, norint išvengti negatyvaus šiluminio poveikio biologiniams objektams.

3. Stiprių magnetinių laukų formuotų mikrosekundinių impulsų generatorių taikymas

Sukurti stiprių magnetinių laukų formuotų impulsų generatoriai buvo pritaikyti magnetorezistyvinių jutiklių kalibravimo eksperimentuose ir biologinių objektų stipriuose magnetiniuose laukuose tyrimuose.

Magnetorezistyvinio magnetinio lauko jutiklio kalibravimo schema yra pavaizduota S10 paveiksle.

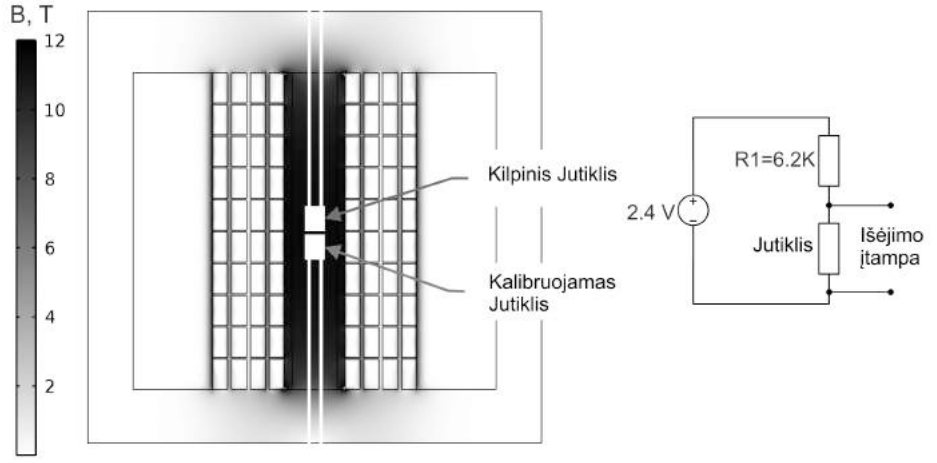

S10 pav. Magnetorezistyvinio magnetinio lauko jutiklio kalibravimo schema

Magnetorezistyvinių magnetinio lauko jutiklių kalibravimui buvo panaudotas stiprių magnetinių laukų asimetrinės formos mikrosekundinių impulsų generatorius su 15,5 μH induktoriumi.

Magnetinio lauko jutiklis buvo patalpintas kartu su kalibruotu kilpiniu jutikliu į ritės centrą, kur magnetinio lauko nehogeniškumas neviršyja 1 %. Įtampos kritimas

*Nuoroda pateikta autoriaus mokslinių publikacijų disertacijos tema sąraše

magnetorezistyviniame magnetinio lauko jutiklyje lyginamas su kalibruoto kilpinio jutiklio įtampa. Įtampos kritimo magnetorezistyviniame magnetinio lauko jutiklyje priklausomybė nuo magnetinio srauto tankio pavaizduota S11 paveiksle. Kadangi magnetorezistyvinių jutiklių magnetovarža kinta ir nuo aplinkos temperatūros, sudarytos kalibracinės kreivės nuo 0 °C iki 45 °C temperatūrų diapazone. Eksperimentiniu metodu buvo nustatyta, kad sukurta asimetrinės formos magnetinių mikrosekundinių impulsų generatorius yra tinkamas naudoti jutiklių kalibravimui su ±10 % neapibrėžtimi.

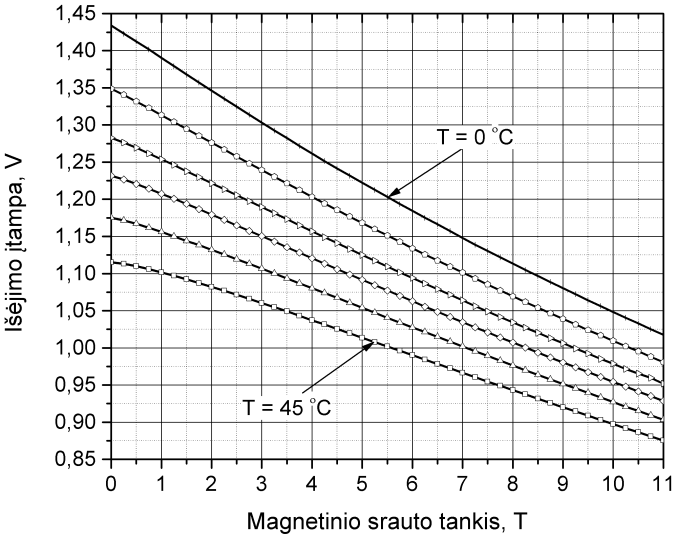

S11 pav. Magnetinio lauko magnetorezistyvinio jutiklio kalibravimo kreivės

Biologinių objektų stipriuose magnetiniuose laukuose tyrimams buvo naudojamas magnetinių laukų stačiakampės formos impulsų generatorius su 1,6 μH mikroinduktoriumi ir integruota kiuvete. Generatorius generavo pasikartojančius 3 μs trukmės 5 T magnetinio lauko impulsus. Žmogaus ląstelės Jurkat T ir patogeniniai mikroorganizmai *Aspergillus fumigatus* ir *Trychophyton rubrum* buvo tiriami kambario temperatūroje. Jurkat T ląstelės pokytis magnetiniame lauke buvo fiksuojamas panaudojant calcein blue AM (~322/435 nm) (Life Technologies Corp. CA) dažą. Jurkat T ląstelės prieš ir po magnetinio lauko poveikio yra pavaizduotos S12 paveiksle.

Nustatyta, kad virš 95 % ląstelių buvo pažeista membrana ir fluorascentinis dažas ištekėjo į terpę.

Eksperimentuose su *Aspergillus fumigatus* ir *Trychophyton rubrum* buvo vertinamas ląstelių gyvybingumas prieš ir po magnetinio lauko poveikį. Tyrimų metu nustatyta, kad po magnetinio lauko poveikio, ląstelių gyvybingumas sumažėja 20±10 % abiems patogeninių tipų grupėms.

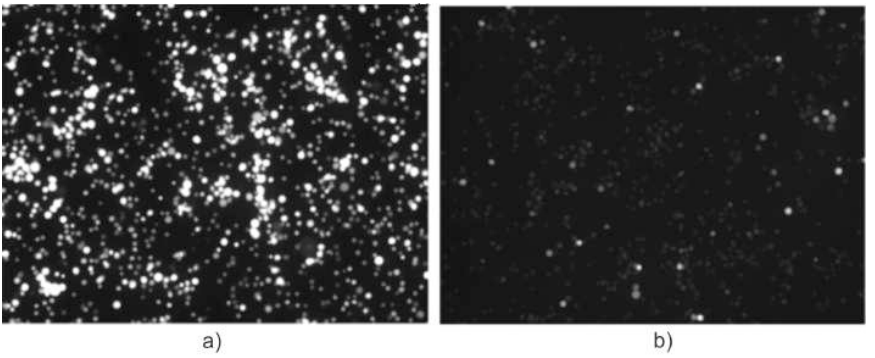

S12 pav. Jurkat T ląstelės a) prieš magnetinio lauko poveikį ir b) po 200 impulsų, 5 T, 3 µs magnetinio lauko poveikio (Grainys, Novickij, Stirke 2012)*

Sukurtas stirprių magnetinių laukų stačiakampės formos mikrosekundinių impulsų generatorius yra tinkamas naudoti biologinių objektų tyrimams stipriuose impulsiniuose magnetiniuose laukuose.

Bendrosios išvados

1. Sukurtas mobilus, lengvai integruojamas į laboratorijos infrastruktūrą stiprių magnetinių laukų generatorius. Ištyrus taikytinas generavimo technologijas ir pereinamuosius vyksmus buvo nutarta generuoti impulsus, iškrovus greitaeigių kondensatorių bateriją su didelės galios tiristoriumi per impulsinį induktoriu. Siekiant gauti asimetrinės formos impulsą, lygiagrečiai su induktoriumi įjungta trumpiklio grandinė. Toks generatorius gali generuoti asimetrinės formos magnetinio lauko impulsus virš 10 T.
2. Ištirtas planarinis ir daugiasluoksnis induktoriai, įvertinti įšilimo procesai ir magnetinio lauko pasiskirstymas. Nustatyta, kad planarinė induktoriaus konstrukcija tinka lauko generavimui, kai nėra svarbus lauko homogeniškumas, tuo tarpu kalibravimo eksperimentuose turi būti naudojamas daugiasluoksnis induktorius, užtikrinantis magnetinio lauko nehomogeniškumą ±1 % ribose.
3. Sukurtas stiprių magnetinių laukų generatorius su trumpiklio grandine, generuojantis asimetrinius impulsus su 200 µs priekiniu frontu, 800 µs galiniu frontu ir virš 10 T amplitude, leidžia kalibruoti magnetorezistivinius jutiklius vieno impulso metu, išvengiant impulsinio induktoriaus įšilimo įtakos kalibravimo tikslumui. Tyrimo metu buvo kalibruojami manganitiniai

* Nuoroda pateikta autoriaus mokslinių publikacijų disertacijos tema sąraše

La-Sr-Mn-O jutikliai. Kalibravimo kreivių neapibrėžtis neviršijo ±10 % procentų, kas yra priimtina impulsinio magnetinio lauko jutiklių metrologijoje.

4. Siekiant generuoti pasikartojančius mikrosekundinius magnetinio lauko impulsus buvo sukurtas ir ištirtas impulsinis generatorius, susidedantys iš kondensatorių baterijos, MOSFET raktų ir mikroinduktoriaus. Maksimaliai leistina komutuojama MOSFET raktų srovė yra pagrindinis maksimalaus generuojamo lauko ribojantis faktorius. Siekiant sumažinti pereinamuosius vyksmus ir suformuoti stačiakampius impulsus, nuosekliai su mikroinduktoriumi buvo jungta balastinė varža. Toks generatorius su induktyvaus bei rezistyvinio pobūdžio apkrova gali generuoti stačiakampės formos pasikartojančius magnetinio lauko impulsus iki 5 T.
5. Sukurti mikroinduktoriai sukuria magnetinio lauko impulsus su stačiais frontais, kas yra svarbu, taikant bekontaktę tyrimo metodiką biotechnologijoje, nes indukuotas maksimalus elektrinis laukas, kaip vienas iš poveikio faktorių yra proporcingas impulsinio magnetinio lauko išvestinei. Toks mikroinduktorius su integruota kiuvete, užtikrina bekontaktę tyrimų metodiką taikytina biotechnologijoje.
6. Pasikartojantys iki 35 Hz stačiakampės formos mikrosekundinės 3–25 μs trukmės, iki 5 T magnetinio lauko impulsai gali sukelti pokyčius biologinių objektų struktūroje. Atlikti *Aspergillus fumigatus* ir *Trychophyton rubrum* eksperimentiniai tyrimai, įvertintas ląstelių gyvybingumas prieš ir po magnetinio lauko poveikio. Tyrimų metu nustatyta, kad po magnetinio lauko poveikio, ląstelių gyvybingumas sumažėja 20±10 % abiems patogeninių tipų grupėms.

Annexes[2]

Annex A. The Coauthors Agreements to Present Publications for the Dissertation Defence
Annex B. Copies of Scientific Publications by the Autor on the Topic of the Dissertation

[2]The annexes are supplied in the enclosed compact disc

Audrius GRAINYS

MICROSECOND HIGH MAGNETIC FIELD
SHAPED PULSE GENERATORS RESEARCH

Doctoral Dissertation

Technological Sciences,
Electrical and Electronic Engineering (01T)

Audrius GRAINYS

MIKROSEKUNDINIŲ STIPRIŲ MAGNETINIŲ LAUKŲ
FORMUOTŲ IMPULSŲ GENERATORIŲ TYRIMAS

Daktaro disertacija

Technologijos mokslai,
elektros ir elektronikos inžinerija (01T)

2014 05 09. 10,25 sp. l. Tiražas 20 egz.
Vilniaus Gedimino technikos universiteto
leidykla „Technika“,
Saulėtekio al. 11, 10223 Vilnius,
http://leidykla.vgtu.lt
Spausdino UAB „Ciklonas“
J. Jasinskio g. 15, 01111 Vilnius.